South Dakota State University

Open PRAIRIE: Open Public Research Access Institutional Repository and Information Exchange

Electronic Theses and Dissertations

2019

Repairable Moment-Resisting Steel Buildings

Heath William Pederson
South Dakota State University

Follow this and additional works at: https://openprairie.sdstate.edu/etd

 Part of the Civil Engineering Commons, and the Statistical, Nonlinear, and Soft Matter Physics Commons

REPAIRABLE MOMENT-RESISTING STEEL BUILDINGS

BY

HEATH WILLIAM PEDERSON

A thesis submitted in partial fulfillment of the requirements for the

Master of Science

Major in Civil Engineering

South Dakota State University

2019

REPAIRABLE MOMENT-RESISTING STEEL BUILDINGS

HEATH WILLIAM PEDERSON

This thesis is approved as a creditable and independent investigation by a candidate for the Master of Science degree and is acceptable for meeting the thesis requirements for this degree. Acceptance of this thesis does not imply that the conclusions reached by the candidate are necessarily the conclusions of the major department.

Mostafa Tazarv, Ph.D., P.E.
Thesis Advisor   Date
Civil and Environmental Engineering

Nadim Wehbe, Ph.D., P.E.
Department Head   Date
Civil and Environmental Engineering

Kinchel C. Doerner, Ph.D.
Dean, Graduate School   Date

ACKNOWLEDGEMENTS

I express sincere gratitude toward my academic advisor Dr. Mostafa Tazarv. I am extremely thankful for the opportunity provided to me through the conduction of research. He has been tremendously helpful throughout this whole experience and I am very honored to be a part of his research group. I have learned many new and innovative ways to think about structural engineering and am excited to use this new creative thinking in future practice.

I would also like to thank Dr. Nadim Wehbe, who has been very instrumental in getting me to the point where I am today. I have learned so much from him both in the classroom and through research, and I am extremely grateful to have had the opportunity to work with him.

I would like to acknowledge my research colleagues who have been very supportive throughout this journey, namely Sandip Rimal, Abdullah Boudaqa, Puskar Dahal, and Matthew LaVoy. I am forever grateful for the help that they have provided me throughout my graduate career.

Finally, I would like to thank my parents, Jeff and Andrea Pederson, who have been lifelong supporters of my pursuit happiness. I would also like to give a special thanks to all my siblings, Matthew Pederson, Hilary Pederson, and Sean Pederson who have helped form me into the person I am today.

TABLE OF CONTENTS

LIST OF ABBREVIATIONS

Abbreviation	Definition
AISC	American Institute of Steel Construction
ASTM	American Society for Testing and Materials
BRB	Buckling Restrained Bracing
BRF	Buckling Restrained Fuse
BRR	Buckling Restrained Reinforcement
FBJ	Flange Bolted Joint
FEA	Finite Element Analysis
FED	Friction Energy Dissipation
FRP	Fiber Reinforced Polymer
ft	Feet
in.	Inch
kip	1000 pounds
ksi	Kip per square inch
Kn	Kilo Newton
m	Meter
MCE	Maximum Considered Earthquake
MPa	Mega Pascal
mm	mille meter
MR	Moment-Resisting
MRF	Moment-Resisting Frame
PVC	Polyvinyl Chloride

PVD	Penguin Vibration Damper
RC	Reinforced Concrete
SDSU	South Dakota State University
SMA	Shape Memory Alloy

LIST OF FIGURES

LIST OF TABLES

ABSTRACT

REPAIRABLE MOMENT-RESISTING STEEL BUILDINGS

HEATH WILLIAM PEDERSON

2019

Current seismic design codes ensure life safety for buildings, but structural members may significantly yield or even fail under strong earthquakes. A new design approach is to implement connections that localize yielding and failure to occur in within structural fuses. A more sophisticated approach is to be able to replace the fuses after the event. The present study was carried out to develop repairable moment-resisting (MR) connections for steel buildings and investigate their seismic performance through nonlinear finite element analyses (FEA). Two details were proposed using buckling restrained fuses (BRFs) and buckling restrained reinforcement (BRR). Test data was collected from the literature on buckling restrained braces (BRBs) and a conventional steel MR joint. FE modeling methods were then proposed and validated against the test data. Subsequently, FE models were developed for the repairable joints using the validated models. For the repairable alternatives using BRFs, it was found that the displacement capacity was twice of that for the conventional joint. However, the initial stiffness of the BRF repairable joints was 34-44% lower than that for the conventional MR joint. A similar trend was observed for the BRR alternatives. Overall, this pilot analytical study confirmed that both proposed repairable details are viable with improved seismic performance. Furthermore, these joints can be quickly repaired after strong

earthquakes by replacement BRF or BRR and thus total replacement of the steel building is prevented.

Chapter 1: Introduction

1.1 Introduction

Steel buildings can exhibit significant ductility under an earthquake if properly

designed. Of different seismic resisting systems, moment-resisting frames (MRFs) provide

lateral strength while also supporting gravity loads. Even though current building codes

ensure life safety, structural members may significantly yield and sometimes failure under

strong earthquakes. In these cases, the repair of damaged members might not be feasible,

and entire structures must be replaced. An emerging design philosophy is to localize the

damage to occur within replaceable components.

1.2 Objectives and scope

The main objective of the present study is to develop new MR joint details for steel

buildings, which allows replacement of damaged members. The use of buckling restrained

fuses (BRFs) and buckling restrained reinforcement (BRR) is emphasized. BRF and BRR

components are designed to yield and take all damage after a severe event, while all other

structural components remain linear elastic. Both BRF and BRR can then be removed and

replaced upon failure.

Nonlinear finite element analyses (FEA) were conducted using two software packages,

ANSYS and OpenSees, to investigate the seismic performance of the proposed detailing.

The following steps were undertaken to achieve the project goal:

1. Design BRF and BRR based on the information in the literature.

2. Develop new repairable joints using BRF and BRR.

3. Conduct FEA on a reference conventional beam-column MR connection and a reference buckling restrained brace (BRB) to validate the modeling procedures.

4. Investigate the seismic performance of the proposed repairable joints through nonlinear FEA.

5. Investigate the seismic performance of multi-story buildings using the proposed detailing.

1.3 Document Organization

Chapter 1 presents an introduction to the research conducted, objectives and scope of the present study. Chapter 2 provides a literature review on BRB component tests, BRR component tests, and detailing of existing repairable steel MR connections. Chapter 3 presents the details of the proposed repairable joints using BRF and BRR. Chapter 4 presents the FEA modeling methods, verifications, and results for both the conventional and new detailing. The summary and conclusions of the present research are discussed in Chapter 5.

Chapter 2: Literature Review

2.1 Introduction

   Steel buildings usually have a lower mass compared to reinforced concrete (RC)

buildings and can exhibit significant ductility under large earthquakes. However, steel

structures that undergo significant nonlinear deformations during a major event such as an

earthquake often experience yielding or failure of structural components and may require a

total replacement. A new design approach is to implement connections that localize the

yielding and failure to occur in fuses. A more sophisticated approach is to be able to

replace these fuses after the event. This chapter summarizes the findings of previous

studies, mainly on repairable or replaceable connections. First, buckling restrained braces

(BRB) and buckling-restrained reinforcement (BRR) are introduced with their behavior

discussed, and then repairable connections proposed by previous researchers are briefly

discussed.

2.2 Previous Studies on Buckling Restrained Bracing

   Lateral braces are usually needed in steel structures to limit the lateral displacements

and meet the design code drift limits. Conventional steel braces usually buckle under large

cyclic actions such as earthquakes. Buckling restrained braces (BRBs) were developed to

prevent brace buckling and to show a symmetric behavior under cyclic loading. BRBs are

designed to yield both in tension and compression and might be replaced after failure.

Extensive research has been conducted to investigate the behavior of BRB as a component or as part of laterally braced frames. The findings of the pioneering studies are summarized. Furthermore, a brief discussion on BRBs with unconventional materials and methods is also presented in this section.

BRBs have been widely used in high seismic regions in structures such as hospitals, stadiums, and multi-story buildings (Surendran et al., 2017). The primary function of BRBs is to increase the lateral stiffness of steel frames with an additional benefit of being replaceable after an event. Unbonded BRBs were first conceptualized and experimentally tested in Tokyo, Japan (Watanabe et al., 1988), and then were commercially produced by Nippon Steel. These braces showed stable and repeatable force-deformation hysteretic behavior with a compressive strength that was equal to the tensile strength. The test specimens consisted of a rectangular steel plate as the yielding core, an encasing steel tube, concrete as a filler material to prevent buckling of the core, and an un-bonding agent between the steel core and concrete to prevent the axial force transfer by the friction. The only parameter varied in this test was the sectional geometry of the encasing tube as shown in Fig 2.1a. All specimens exhibited stable and repeatable force-displacement hysteretic behavior, like that shown in Fig. 2.2, which pertains to Specimen No. 2 in this test. This successful pioneering study has paved the way for numerous component and system performance studies on BRBs. A few studies were selected and reviewed to further discuss the BRB performance.
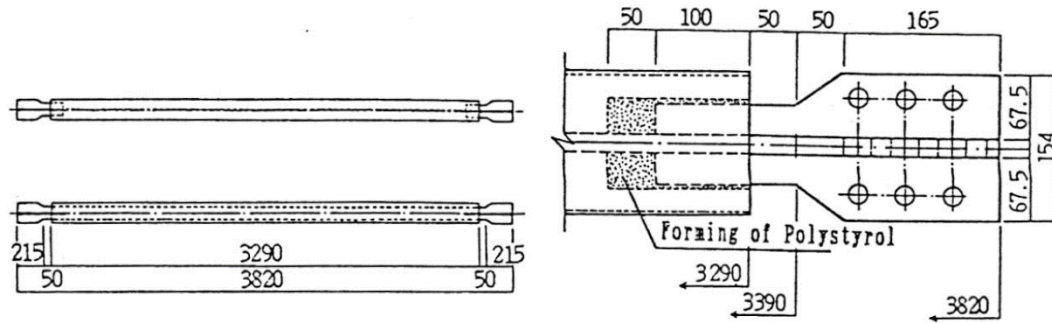
(a) BRB test specimens and end connection details
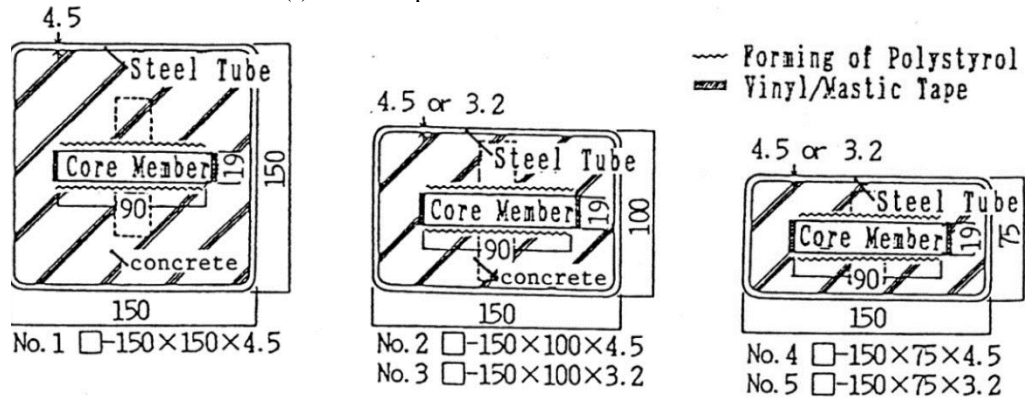
(b) Cross-section of BRB test specimens

Figure 2.1 – Detailing of buckling restrained braces tested by Watanabe et al. (1988)
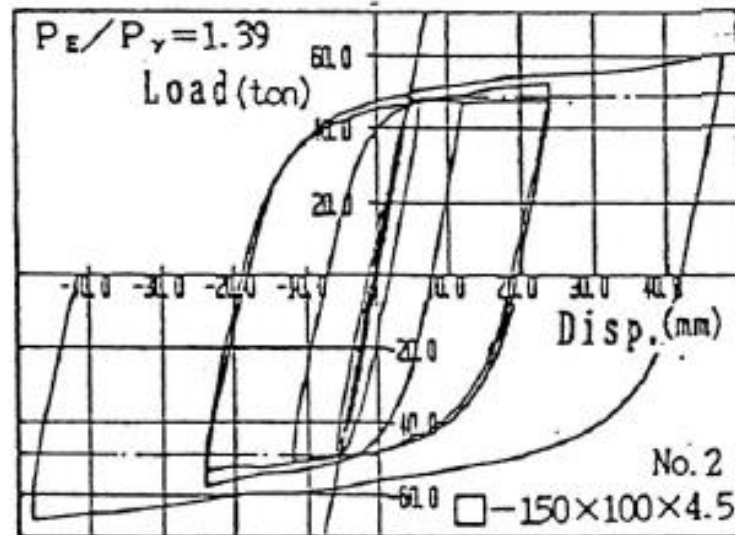
Figure 2.2 – Force-displacement relationship for Specimen No. 2 tested by Watanabe et al. (1988)

Black et al. (2002) performed a two-phase comprehensive testing program on a series

of unbonded BRBs. In the first phase, BRBs were subjected to a standard loading protocol

(Fig. 2.3), followed by additional loading representing large-deformation low-cycle fatigue loads, and simulated earthquake loads. Figure 2.4 shows the BRB test setup. The measured force-displacement hysteresis for Specimen 00-11 is shown in Fig. 2.5. Similar to the aforementioned study, the BRB exhibited stable hysteretic behavior at all displacement amplitudes. Furthermore, the forces and displacements of the inner core relative to the outer tube were separately measured at each end (Fig. 2.6). A nearly identical hysteretic behavior was observed, which verifies that yielding was uniformly distributed over the length of the core. The results from this test further prove that unbonded braces are ductile structural members that exhibit stable force-deformation hysteretic behavior.
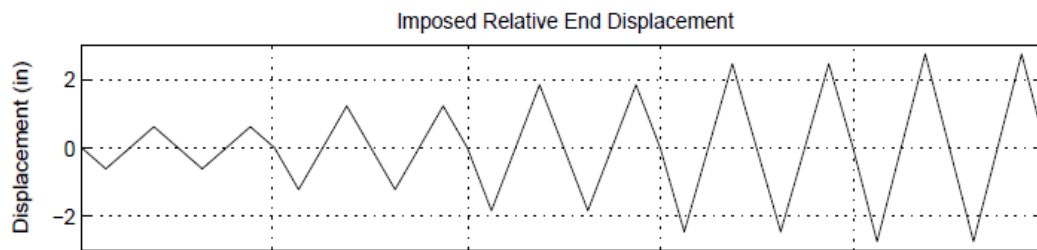
Figure 2.3 – BRB loading protocol tested by Black et al. (2002)
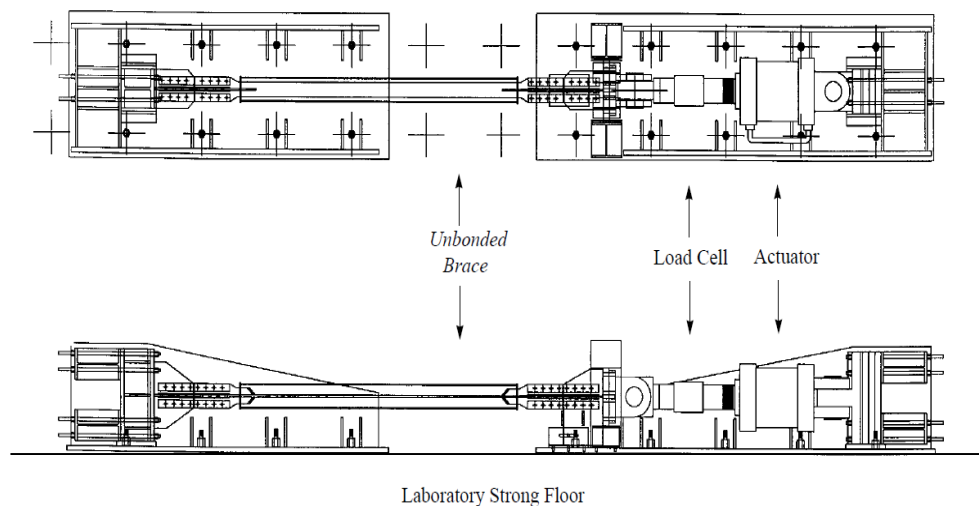
Figure 2.4 – BRB test setup in Black et al. (2002)
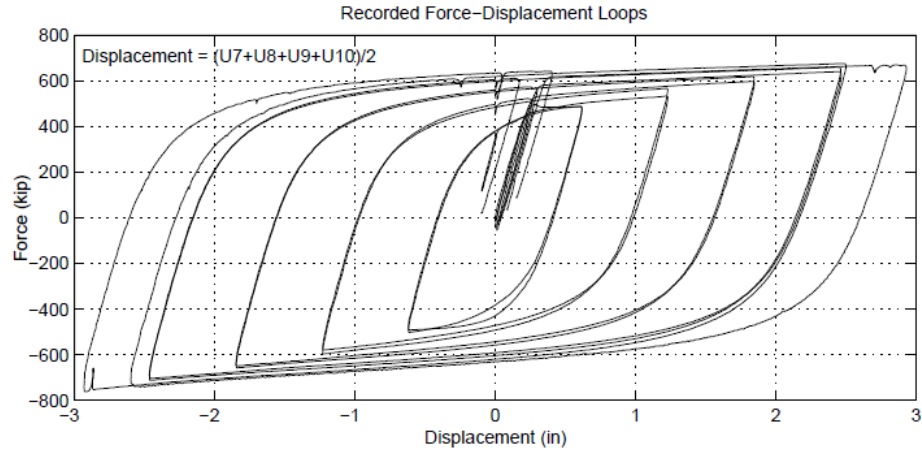
Figure 2.5 – Force-displacement hysteresis for Specimen 00-11 (Black et al. 2002)
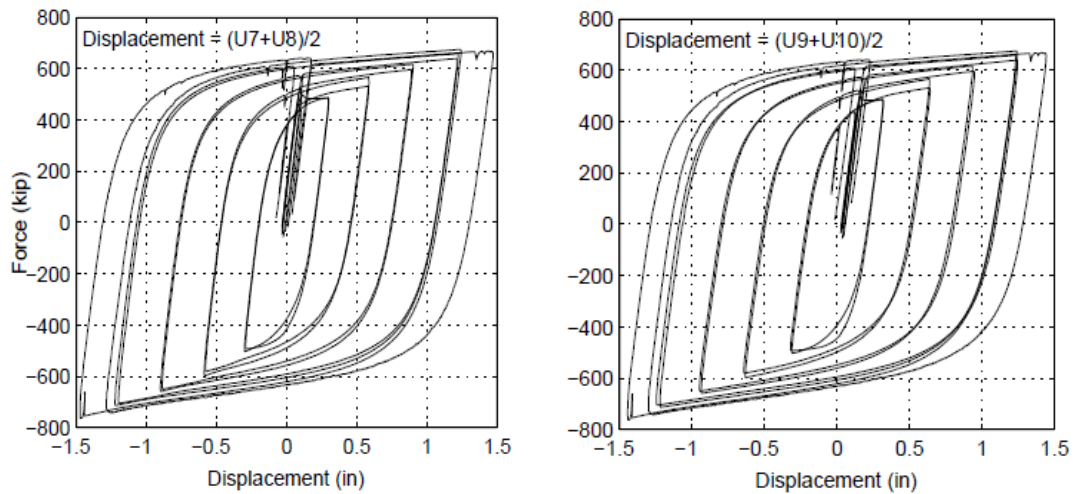
(a) Force-displacement of inner core relative to outer tube (one end)

(b) Force-displacement of inner core relative to outer tube (one end)

Figure 2.6 – Force-displacement hysteresis of inner core relative to outer tube for Specimen 00-11 (Black et al. 2002)

As mentioned previously, the encasing tube for a typical BRB specimen is constructed of structural steel, and it is critical to understand how the encasing tube influences the overall behavior of the BRB. A study by Rahai et al. (2008) experimentally and numerically investigated the behavior of BRBs with the same sectional properties but encased with different materials. The encasing was concrete with no confining tube (Model 1), conventional concrete-filled steel tube (Model 2), concrete-filled Polyvinyl Chloride (PVC) pipes (Model 3), and fiber-reinforced polymer (FRP) confined concrete

(Model 4). Figure 2.7 shows the measured hysteretic behavior of these four models. Model 1, without a confining tube, showed an irregular and unsymmetrical behavior after only a few cycles, which is desirable for a BRB. This behavior was expected since concrete is weak in tension thus concrete cracked after a few cycles and was detached from the steel core. Models 2-4 had similar hysteretic behavior in tension and compression, and Model 2 had the highest energy dissipation capacity (Fig. 2.8). No buckling of the steel core occurred in any of these models, which demonstrated that the encasing with the steel tubes, PVC tubes, and FRP sheets was viable. The BRBs with the concrete-filled steel tube, the concrete-filled PVC pipe, and the FRP confined concrete showed 160%, 110%, and 125% higher force capacity compared to that of Model 1, respectively.
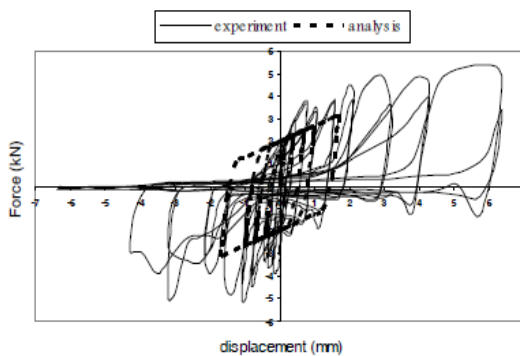
(a) Model 1 experimental and analytical hysteretic response
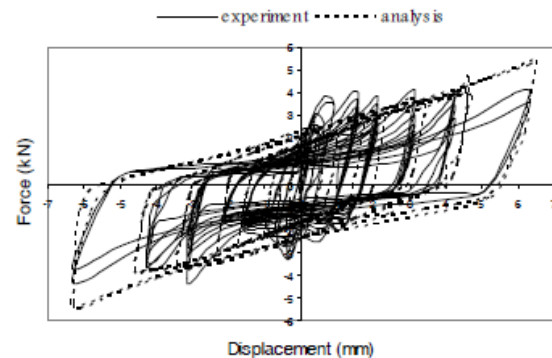
(b) Model 2 experimental and analytical hysteretic response
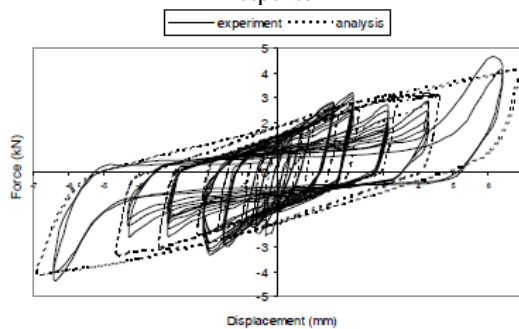
(c) Model 3 experimental and analytical hysteretic response
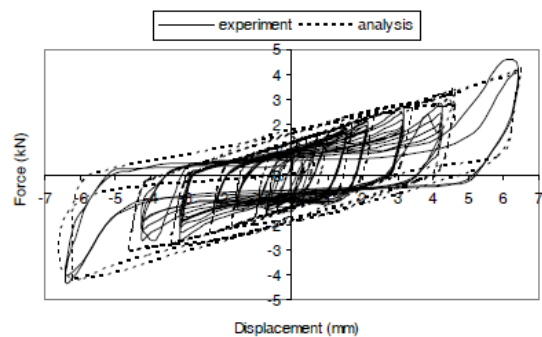
(d) Model 4 experimental and analytical hysteretic response

Figure 2.7 – Force-displacement hysteresis for different BRBs tested by Rahai et al. (2008)
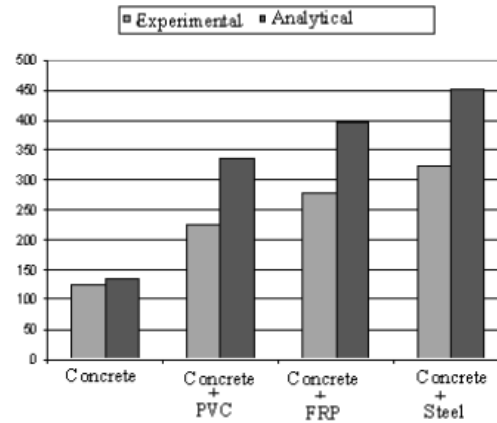
Figure 2.8 – Energy dissipation capacity of BRBs tested by Rahai et al. (2008)

Gheidi et al. (2009) investigated the effect of the filler material on the local and global cyclic behavior of BRBs. This study conducted both uniaxial tests (Specimens 1-3) and frame tests (Specimens 4-5) as shown in Fig. 2.9 and 2.10, respectively. The cores and tubes were made of structural steel, and the filler materials were normal weight concrete, lean concrete with a water to cement ratio equal to one, or compacted aggregates, namely gravel and sand. Figure 2.11 shows the measured force-displacement hysteretic behavior of Specimens 1-3. Specimen 1 demonstrated stable and repeatable hysteretic behavior, with no strength degradation. Specimen 2 buckled in compression, indicating aggregates poor performance to prevent global and local buckling for the steel core. Specimen 3 showed slight variations in force-deformation behavior compared to Specimen 1, in which some local buckling occurred in the transition segment due to the crushing of the lean concrete.
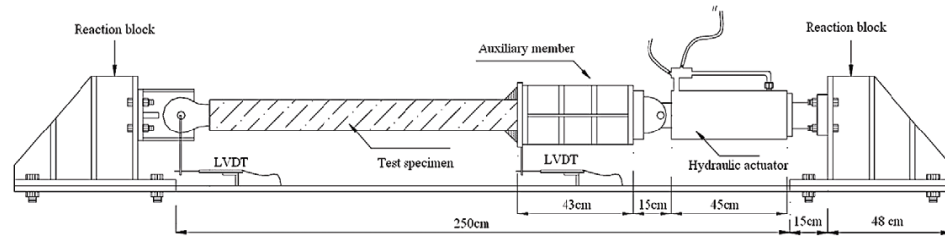
Figure 2.9 – Uniaxial BRB test setup for Specimens 1-3 (Gheidi et al. 2009)
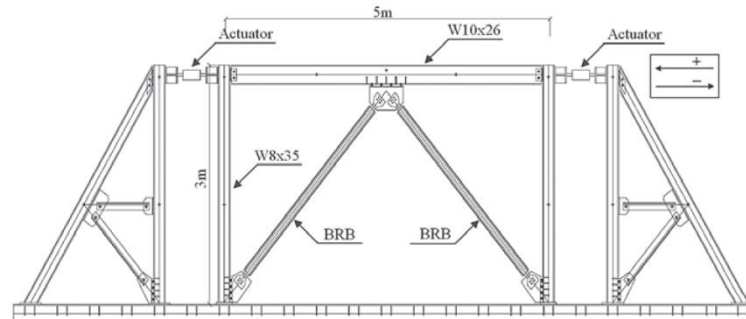
Figure 2.10 – BRB frame test setup for Specimens 4-5 (Gheidi et al. 2009)
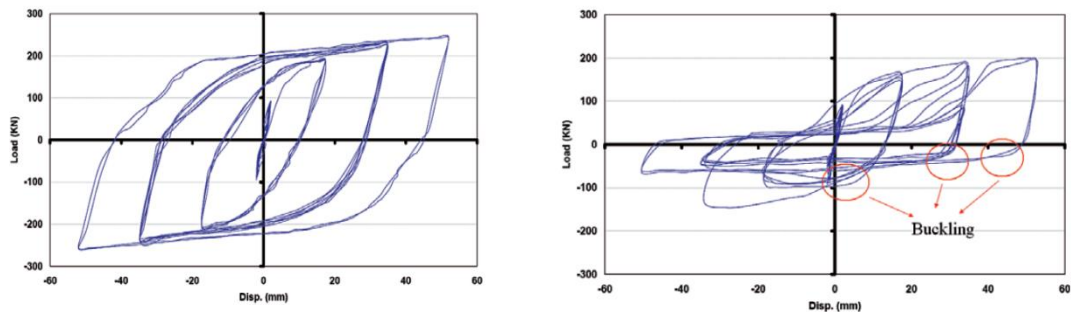
(a) Specimen 1 - Filled w/ normal weight concrete (b) Specimen 2 - Filled w/ aggregates
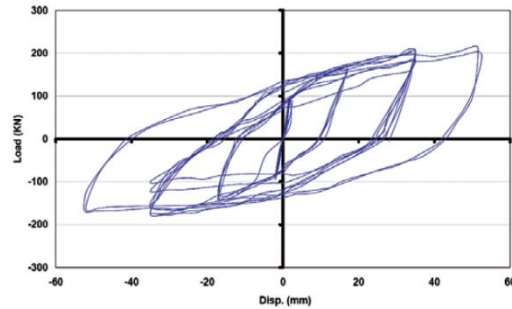
(c) Specimen 3 - Filled w/ lean concrete

Figure 2.11 – Force-displacement hysteresis for BRB Specimens 1-3 tested by Gheidi et al. (2009)

In the frame tests, normal weight concrete (Specimen 4) and aggregates (Specimen 5) were used as the tube filler material. Figure 2.12 shows the measured force-deformation

hysteresis of the two BRB models. Specimen 4 exhibited no strength degradation in compression or tension, whereas Specimen 5 showed significant strength and stiffness degradation. Analytical models were constructed for Specimens 4 and 5 in OpenSees (2006). A reasonable accuracy was observed for Specimen 4.
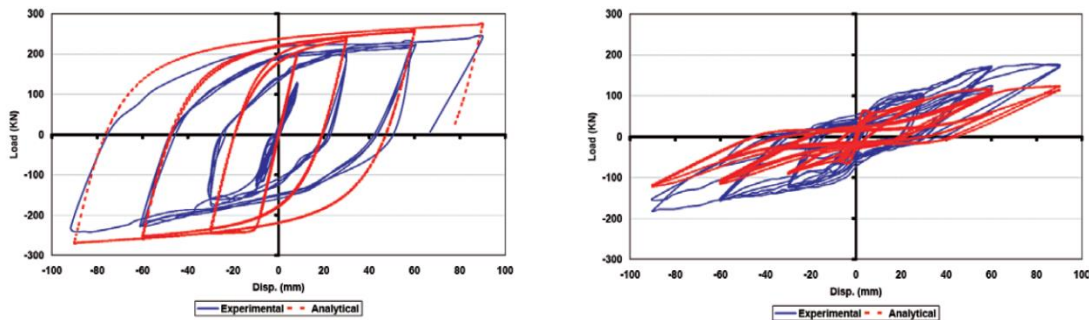
(a) Specimen 4 - Frame with normal weight concrete filled BRBs   (b) Specimen 5 - Frame with aggretate filled BRBs

Figure 2.12 – Force-displacement hysteresis for BRB Specimens 4 and 5 tested by Gheidi et al. (2009)

2.2.1 BRB with Nonconventional Materials and Methods

Miller et al. (2012) investigated the behavior of a new BRB that incorporates pre-tensioned superelastic Ni-Ti SMA rods (Fig. 2.13). This was done to minimize the residual displacements of the BRB. Cyclic tensile tests were performed on five specimens based on the protocol developed by DesRoches et al. (2004). The experimental variables included the duration of heat treatment, and the sequence of machining and annealing. The fifth specimen was of a different material batch than the first four specimens. Figures 2.14 shows the hysteretic response of SC-BRB-1 and SC-BRB-2. Residual elongation of 3.53% was observed in the SC-BRB-1, while the other four specimens exhibited a residual elongation of less than 1%. There was a slight stiffness degradation, but no strength degradation in the specimens. Overall, the study showed a sufficient performance for BRB with smaller residual displacements.
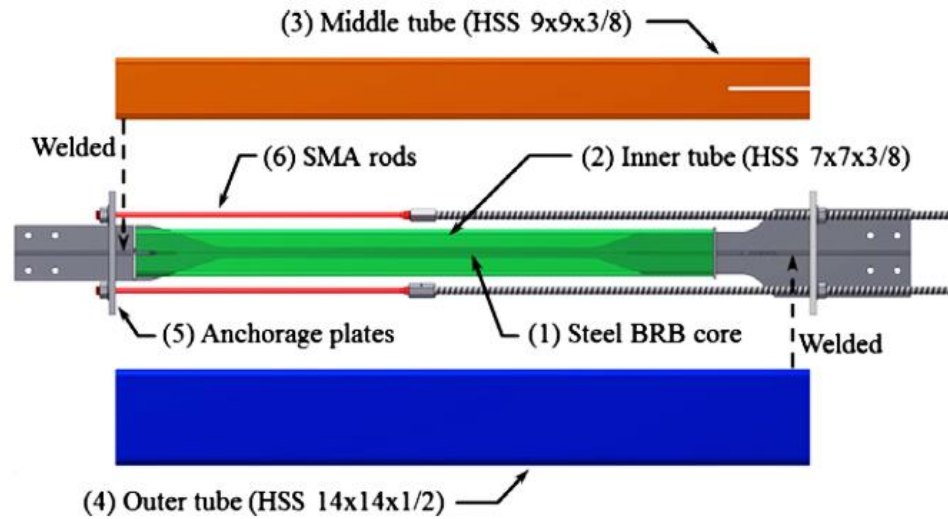
Figure 2.13 – Self-centering BRB components proposed by Miller et al. (2012)

(a) SC-BRB-1 overall response   (b) SC-BRB-1 component response
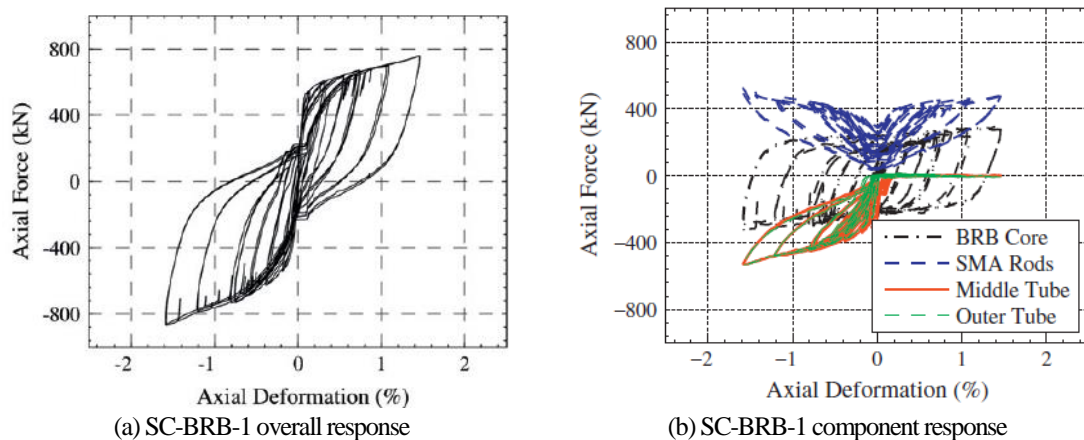
Figure 2.14 - Force-displacement hysteresis of BRBs with SMA Rods (Miller et al., 2012)

Hoveidae et al. (2012) conducted a finite element analysis on a new type of BRB, which is confined with only steel members (Fig. 2.15). Analyses were carried out for 13 BRBs with varying cross sections (Fig. 2.16). Specimens $S1g0_{.5}$, S_5g_2, and S_1g_0 , in which the indices respectively represent the model number and gap amplitude, experienced a sudden strength degradation and buckled as shown in Fig. 2.17. The strength degradation was mainly due to the ratio of "the Euler buckling load" to "the yield strength" being less

than 1.2. When that ratio was greater than 1.2, no buckling was analytically observed, and the braces remained undamaged. It was also found that when there was a gap between the core and restraining steel members some instability occurred leading to higher buckling modes of the core, but the gap did not have any effect on the hysteretic behavior**.**
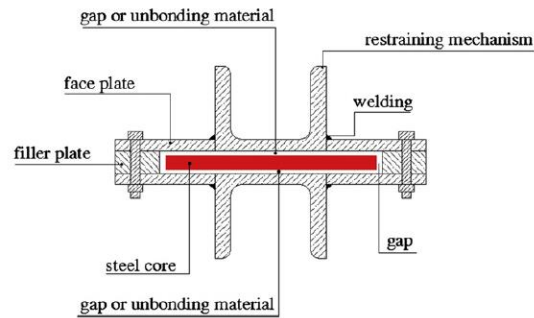
Figure 2.15 - Typical all-steel BRB detailing proposed by Hoveidae et al. (2012)
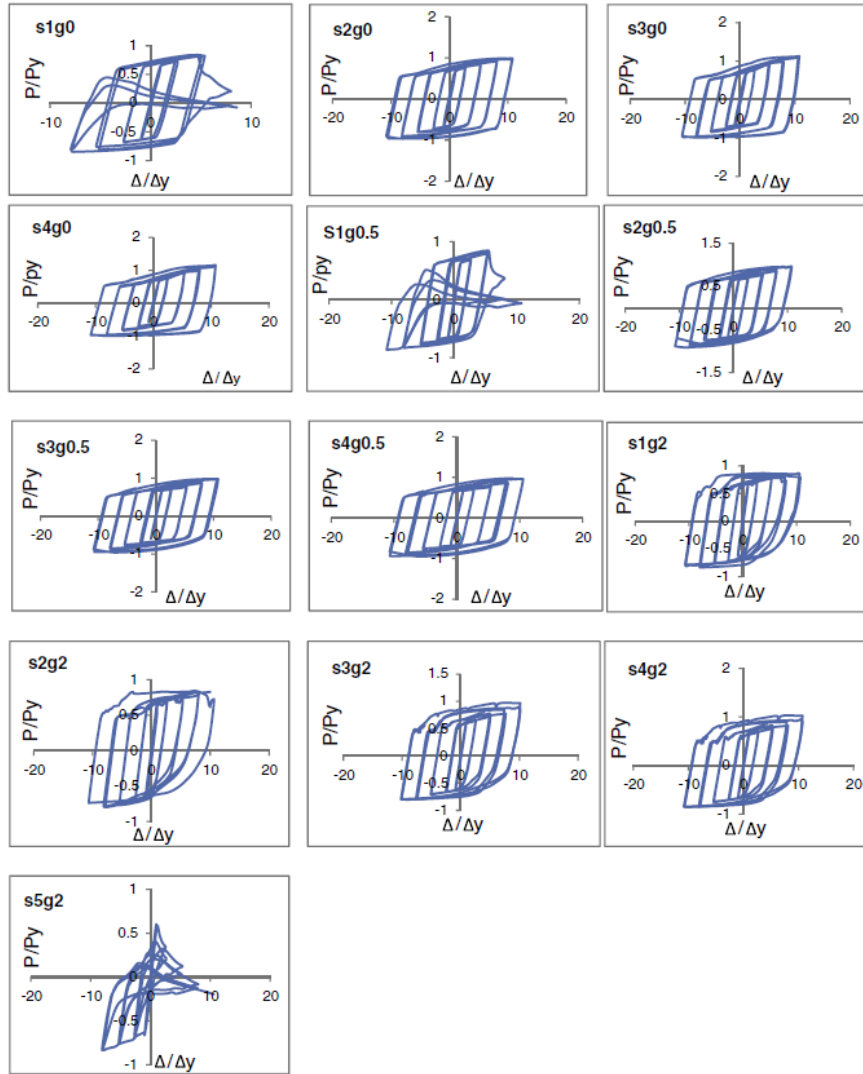
Figure 2.16 - Calculated response for all-steel BRBs proposed by Hoveidae et al. (2012)

(a) Model S_1g_0

(b) Model S_5g_2

(c) Model $S_1g_{0.5}$
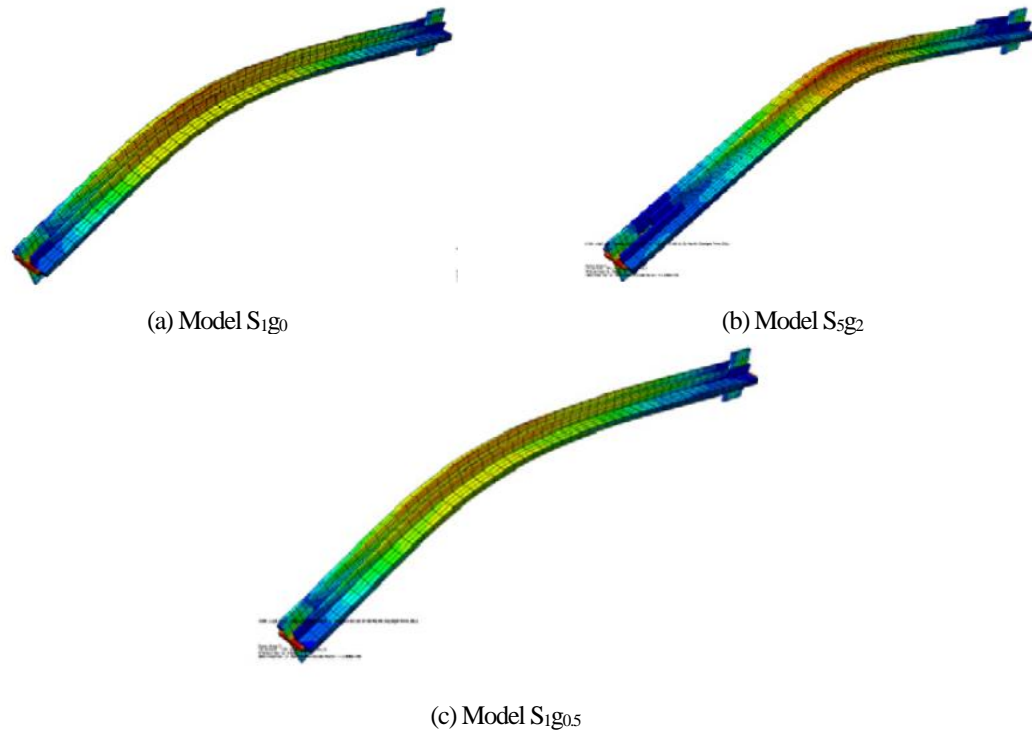
Figure 2.17 - Global buckling of all-steel BRBs (Hoveidae et al., 2012)

As previously mentioned, there has been an extensive research on BRB as either

component or a as part of a subassembly such as a frame (Nishimoto et al., 2004). Several

studies were conducted to determine the hysteretic behavior of BRBs with varying

geometric properties of the core, the buckling restraining mechanism (Takeuchi et al.,

2012), the buckling mechanism of the steel core (Wu et al., 2015), and BRBs with

connection plates welded perpendicular to the steel core (Xu, et al., 2017) as opposed to

being continuous with the core. The results from these studies confirmed that stable and

repeatable force-deformation hysteretic behavior can be achieved for BRBs with large

energy dissipation capacity.

2.3 Previous Studies on Buckling Restrained Reinforcement (BRR)

External energy dissipaters are usually used in rocking structures to decrease

displacement demands. A new type of external energy dissipater was recently emphasized

in the literature in which steel bars are restrained against buckling. These devices are called "buckling restrained reinforcement" (BRR). A few studies have investigated the BRR performance. Boudaqa (2018) investigated the incorporation of BRR as part of a repairable precast beam-column moment-resisting connection. A summary of BRR performance and the behavior of precast joints with BRR is presented in this section.

2.3.1 Study by Sarti et al. (2016)

Sarti et al. (2016) conducted experimental and analytical studies on fuse-type mild steel replaceable dissipaters. The varying parameters included fuse diameter, fuse length, and two different types of filler materials, grout and epoxy. Six specimens with the configuration shown in Fig. 2.18 were subjected to quasi-static, push-pull tests. Figure 2.19 shows the force-deformation hysteretic behavior. It was found that the BRR specimens with a slenderness ratio of 60 could show 9% strain capacities before buckling. Buckling occurred at 9% and 6% strains for BRR with a slenderness ratio of 75 and 90, respectively. It was found that the filler materials had no significant effect on the overall behavior of the BRR. An analytical analysis was then carried out to reproduce the behavior of each specimen. The analyses were able to simulate the yielding point of BRR.
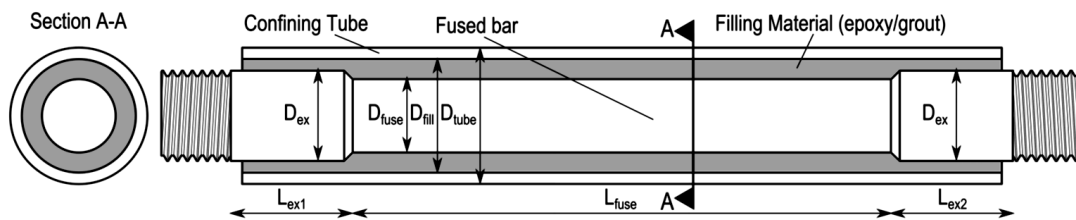
Figure 2.18 - Geometric configuration for dog-bone energy dissipaters (Sarti et al., 2016)
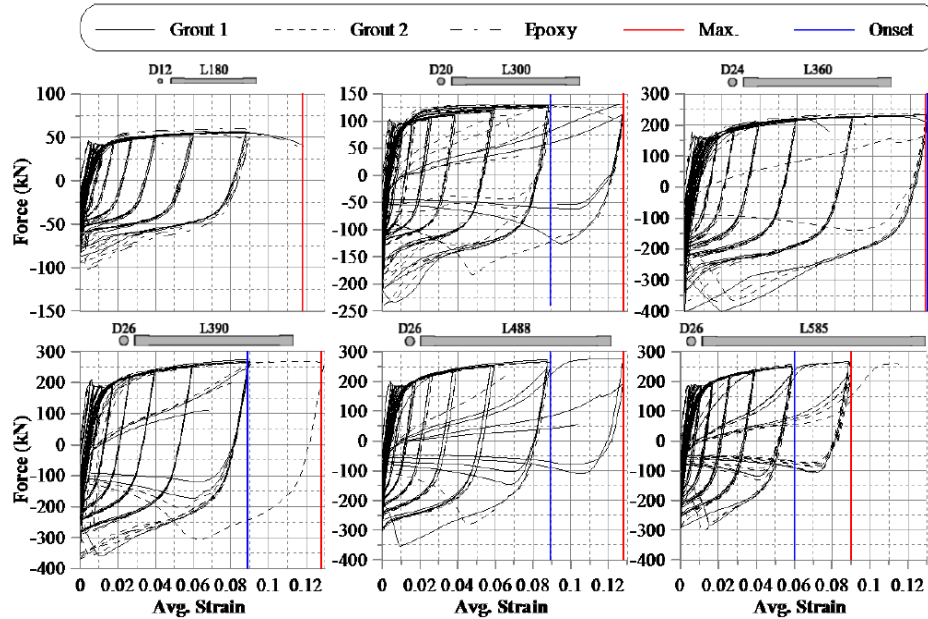
Figure 2.19 - Hysteretic response for BRR specimens tested by Sarti et al. (2016)

2.3.2 Study by Boudaqa et al. (2017)

Boudaqa et al. (2017) carried out an experimental study to establish the mechanical properties and failure mechanism BRR. Sixteen BRR specimens including four deformed reference bars, three deformed reference bars restrained with steel nuts, and nine BRR specimens were tested under uniaxial monotonic compressive loading (Fig. 2.20). One bar was also tested under uniaxial cyclic compressive loads. No. 4 (13-mm) and No. 8 (25-mm) ASTM A706 Grade 60 steel bars were tested. The encasing tube was a Grade 1026 carbon steel, and two different tube diameters with different wall thicknesses were considered in this study. The filler material was a conventional non-shrink grout.

Figure 2.21 shows the measured stress-strain relationships for all specimens and Fig. 2.22 shows the failure mode of the specimens. Upon completion of the test, it was observed that the No. 4 (13-mm) bars buckled at low compressive stresses well below the yield strength. When steel nuts were added to the No. 4 (13-mm) reinforcing bars, the bars

did not buckle up to a compressive strength of 144.7 ksi (997.7 MPa). This was achieved when the gap between the nuts and the face of the steel support did not exceed $0.5d_b$, where d_b is the bar diameter. For the No. 4 (13-mm) BRR specimens, buckling occurred at very large stresses exceeding 200 ksi (1378.9 MPa) when the axial gap between the tube and support did not exceed $0.5d_b$. In summation, it was observed that larger gaps (greater than $0.5d_b$) resulted in lower compressive stresses, and BRR that have tubes with a greater wall thickness show higher stress capacities than thinner tubes. They also proposed a design method for BRR and verified the method using all available BRR test data.
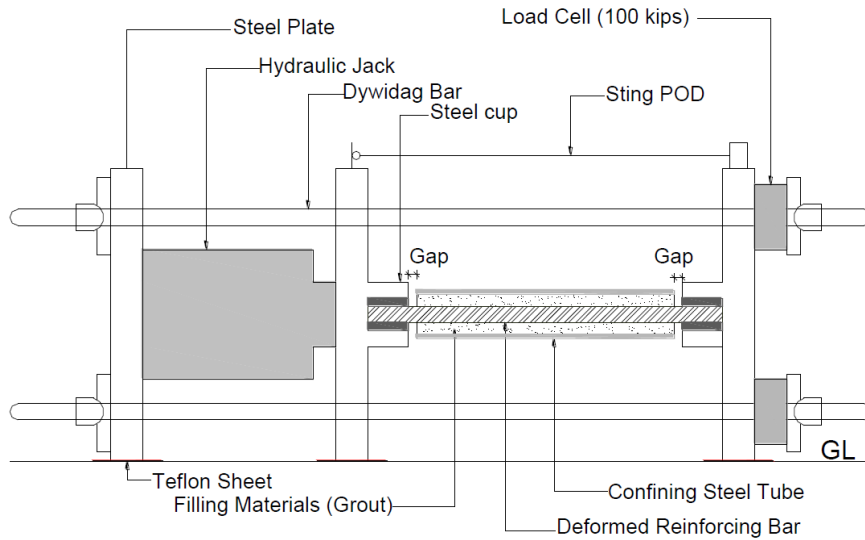
Figure 2.20 – BRR test setup in Boudaqa et al. (2016)
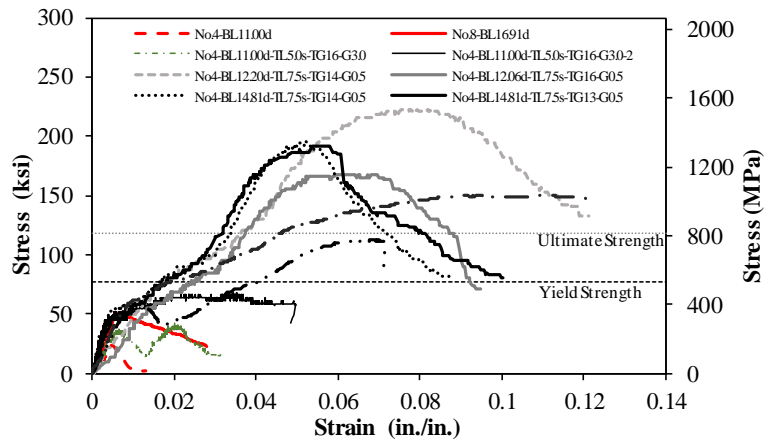
Figure 2.21 – Stress-strain relationships for BRR specimens tested by Boudaqa et al. (2016)

(a) No4-BL11.00d

(b) No4-BL11.00d-Nuts-G0.875

(c) No4-BL11.00d-Nuts-G0.42

(d) No4-BL11.00d-Nuts-G0.20

(e) No4-BL11.00d-TL5.0s-TG18-G3.0

(f) No4-BL10.94d-TL5.0s-TG16-G2.94

(g) No4-BL12.20d-TL7.5s-TG14-G0.5

(h) No4-BL12.28d-TL7.5s-TG16-G0.29

(i) No4-BL14.81d-TL7.5s-TG13-G0.5

(j) No4-BL14.81d-TL7.5s-TG14-G0.5

(k) No8-BL17.00d-TL10.0s-TG11-G1.0

(l) No8-BL14.56d-TL10.0s-TG13-G0.5

(m) No8-BL19.62d-TL15.0s-TG11-G0.5

Figure 2.22 – Failure modes for BRR specimens tested by Boudaqa et al. (2016

2.4 Previous Studies on Nonconventional Steel Joints

Nonconventional joint detailing that can improve the seismic behavior of structures while localizing all failure within specific and possible replaceable structural components has been recently emphasized in the literature. Nonconventional steel joint details proposed in previous studies are reviewed in this section.

2.4.1 Hybrid Joints

Ricles et al. (2002) developed a post-tensioned beam-column connection detail for steel moment-resisting frames to enhance the self-centering capabilities (Fig. 2.23). The cyclic behavior of the new connection was experimentally investigated through nine large-scale subassembly tests. The hybrid moment-resisting connection consisted of post-tensioning steel tendons and bolted top and seat angles. Figure 2.24 shows the measured force-displacement relationships for six specimens. All specimens showed stable and repeatable hysteretic behavior. Large elastic stiffness, sufficient strength, and large ductility were also observed while maintaining a flag-shaped hysteresis. It was reported that most of the energy was dissipated in the angles. Another observation was that since the posttensioning tendons provided self-centering capabilities without any residual deformation, the beam and column remained elastic while the inelastic deformations occurred only in the angles.
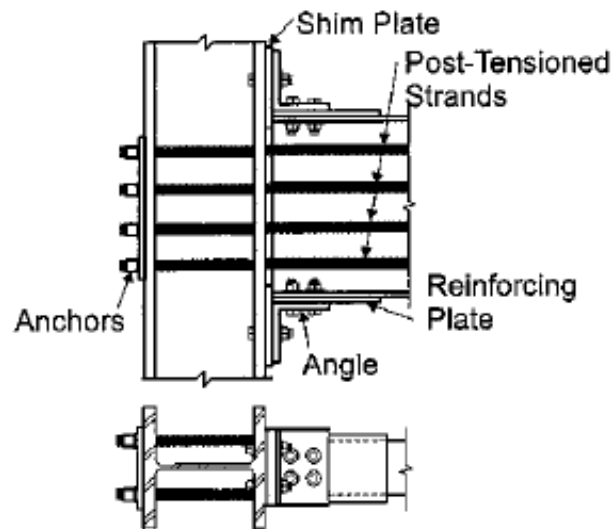
Figure 2.23 – Post-tensioned steel moment-resisting connection detailing (Ricles et al., 2002)

(a) Specimen PC1   (b) Effect of angle g/t ratio

(c) Effect of angle thickness   (d) Effect of post-tensioning forces
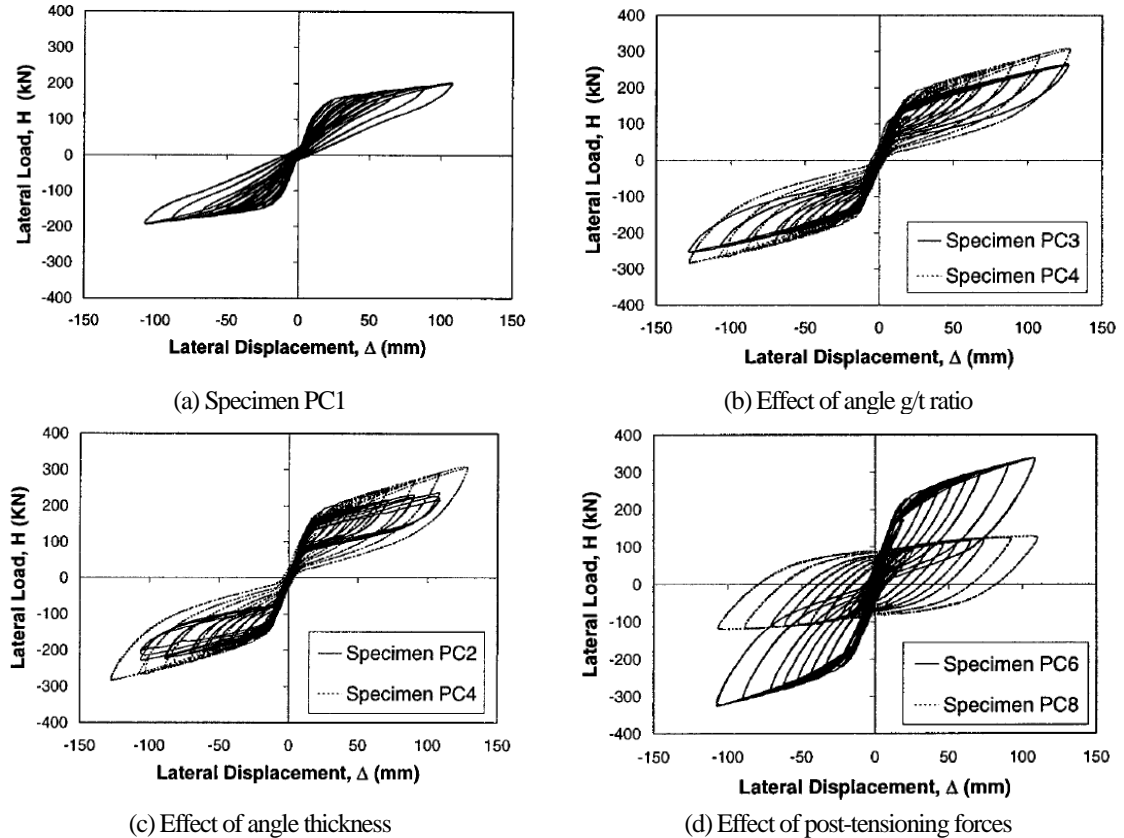
Figure 2.24 – Force-displacement hysteretic behavior for post-tensioned steel moment-resisting connections (Ricles et al., 2002)

Kim et al (2008) proposed and experimentally validated a moment-resisting connection for steel structures that uses post-tensioning tendons to improve the self-centering tendency and friction devices to dissipate energy (Fig. 2.25). Both interior beam-column connections (Fig. 2.26) and exterior connections were tested. Analytical models were developed and validated against the test results. Figure 2.27 shows the detailing for the energy dissipating device for the interior beam-column connection. Three connection tests were carried out on assemblies, one with only the friction energy dissipation devices (FED Specimen) activated, one with loosened FEDs bolts but with tensioned post-tensioning bars (SC Specimen), and finally one with tightened bolts and PT bars tensioned to form the full proposed specimen (SCFR). Figure 2.28 shows the cyclic hysteretic response of the FR

and SC specimens in which the energy dissipation capacity and self-centering capability was clearly demonstrated. Figure 2.29 shows the cyclic response of the interior specimens (INSCFR), which confirmed the validity of this connection at large deformations.
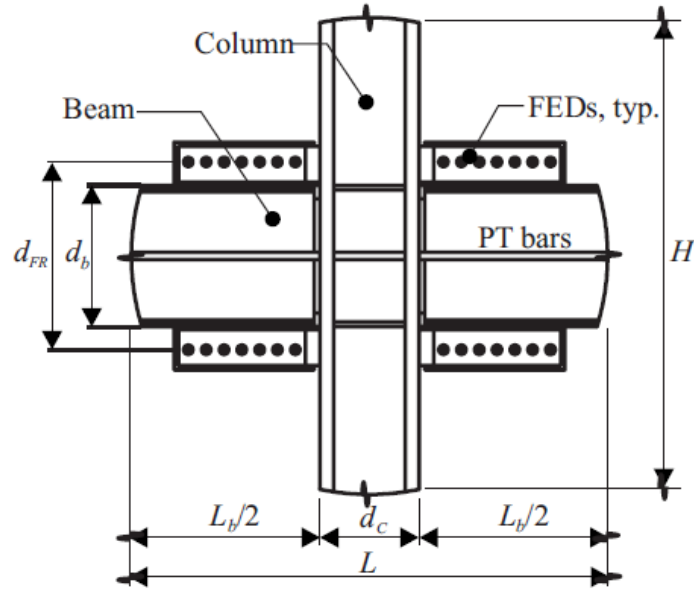
Figure 2.25 – Post-tensioned steel moment-resisting connection detailing (Kim et al. 2008)
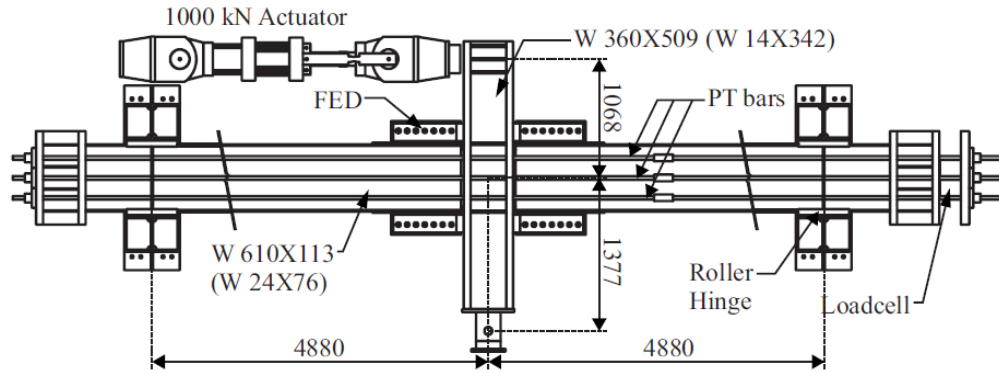
Figure 2.26 - Test setup in Kim et al. (2008)
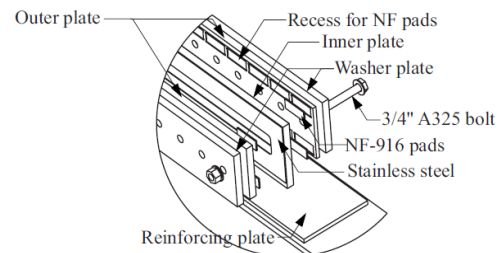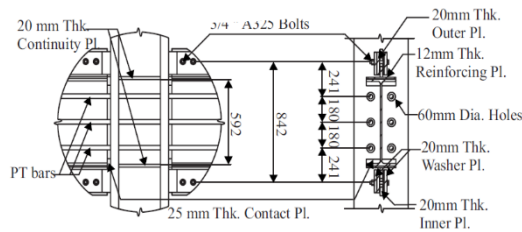
(b)Beam-column interface   (c)Friction energy dissipating device elements

Figure 2.27 - Interior hybrid beam-column connection detailing (Kim et al. 2008)

(a) Exterior FR Specimen

(b) Exterior SC Specimen
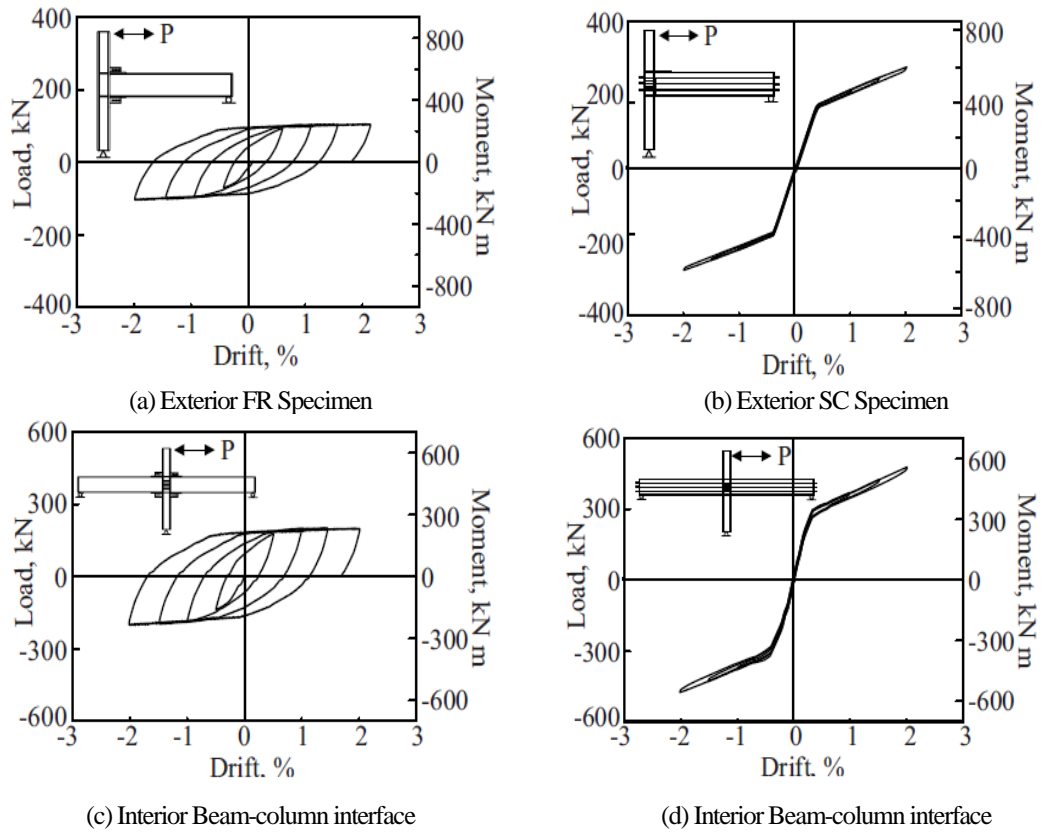
(c) Interior Beam-column interface

(d) Interior Beam-column interface

Figure 2.28 – Hysteretic response of FR and SC hybrid steel joints (Kim et al. 2008)

(a) Test setup

(b) Load versus drift from the first test

(c) PT load variation of first test

(a) Load versus drift of the second test
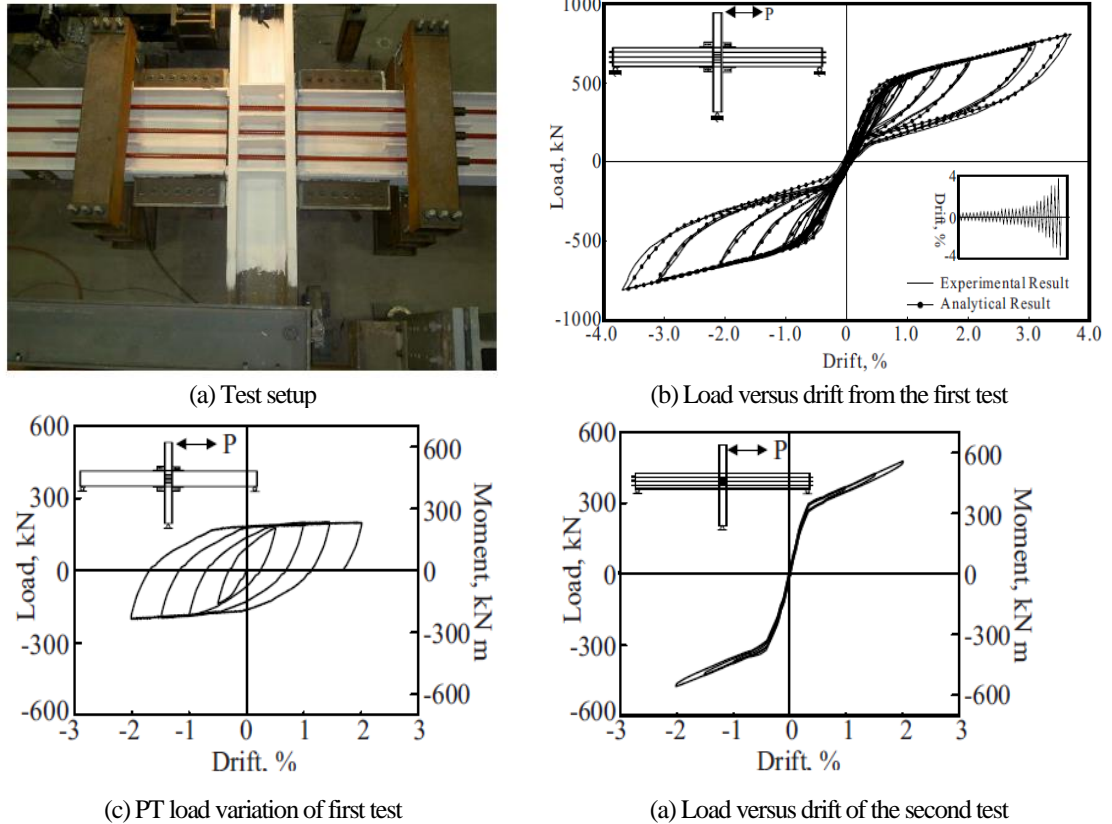
Figure 2.29 – Cyclic response of the INSCFR specimen (Kim et al. 2008)

Several analytical studies have investigated the behavior of hybrid steel connections. For example, Moradi (2016) assessed the lateral load drift response of five post-tensioned beam-column connections that were investigated by Ricles et al. (2002). Wiebe and Christopoulos (2015) also carried out numerical analysis on two-story, six-story, and 12-story building frames incorporating posttensioning bars and strands. Both studies observed negligible residual displacements using the hybrid joints.

2.4.2 Steel Moment-Resisting Joints with Fuses

Clifton et al. (2000) investigated the behavior of three semi-rigid joints in a steel moment-resisting structure that are replaceable after a design level earthquake. It was found that only the flange bolted joint (FBJ) showed satisfactory behavior under cyclic loading, so the discussion will focus explicitly on this alternative. Three FBJ were

developed, including the standard FBJ (Fig. 2.34a), FBJ with brass shims used on the

bottom of the beam flange (Fig. 2.34b), and a FBJ with a sliding bottom flange (not shown

in the figure). Figure 2.31 shows the measured moment-rotation hysteresis for the standard

FBJ. A satisfactory performance was reported using this joint.
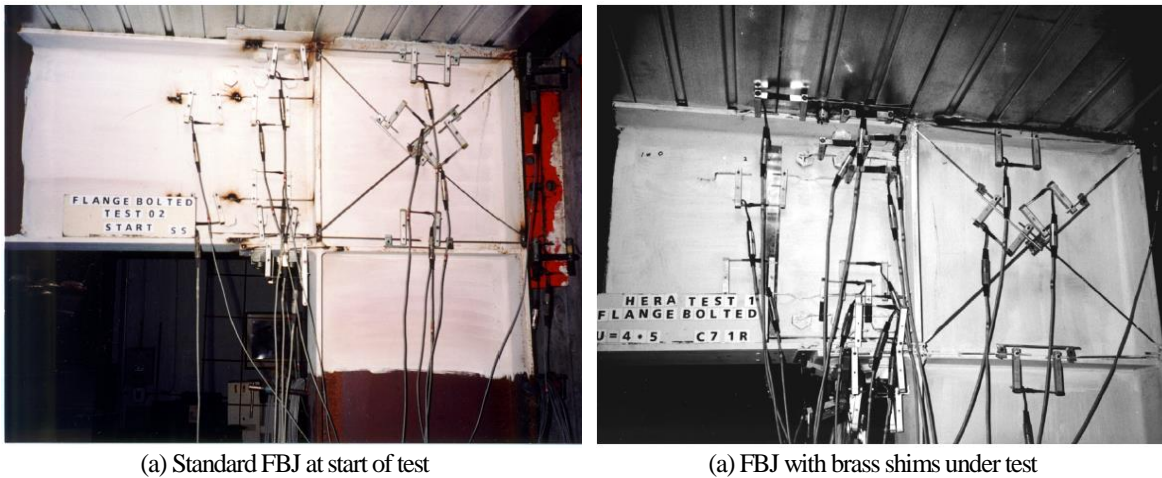
(a) Standard FBJ at start of test   (a) FBJ with brass shims under test

Figure 2.30 – Flange bolted joint connections developed by Clifton et al. (2000)
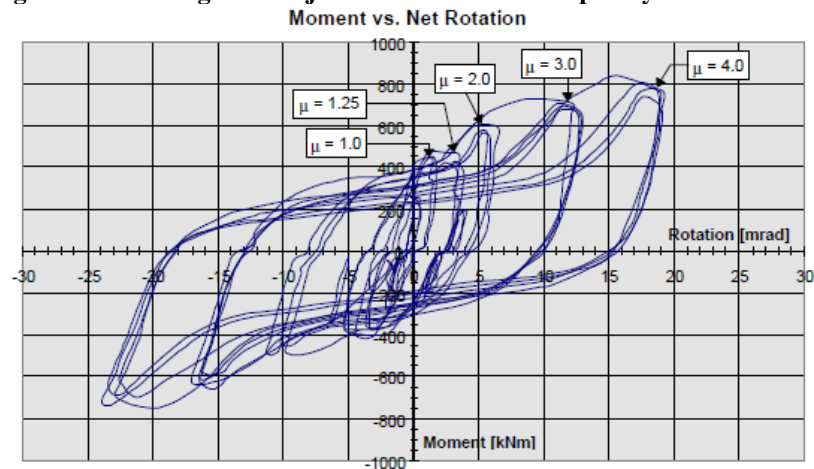
Figure 2.31 – Measured moment-rotation hysteresis for Standard FBJ connection (Clifton et al., 2000)

Kishiki et al. (2006) conducted cyclic tests on a repairable steel moment-resisting

connection (Fig. 2.32 and 2.37) in which the bottom T-stub can be replaced. The yield

strength of the beam-bottom flange damper was designed to be the weak link, and the T-

stub on the top of the beam flange was designed to remain elastic under cyclic

displacements. Two pairs of specimens were tested, with each pair including a bare steel

connection without a concrete slab, and a composite connection which included a concrete

slab. Figure 2.34 shows the measured force-rotation of the conventional welded

connection and the proposed connection. While the two connections had the same strength,

the welded connection failed in a lower rotation with a failure mode of the fracture of the

beam-bottom flange. Lateral buckling failure was reported for the proposed connection but

at a higher rotation. Figure 2.35 shows the crack pattern in the concrete slab after the

testing. The concrete in the conventional connection cracked throughout the entire slab,

while the concrete in the proposed connection cracked near the face of the column.
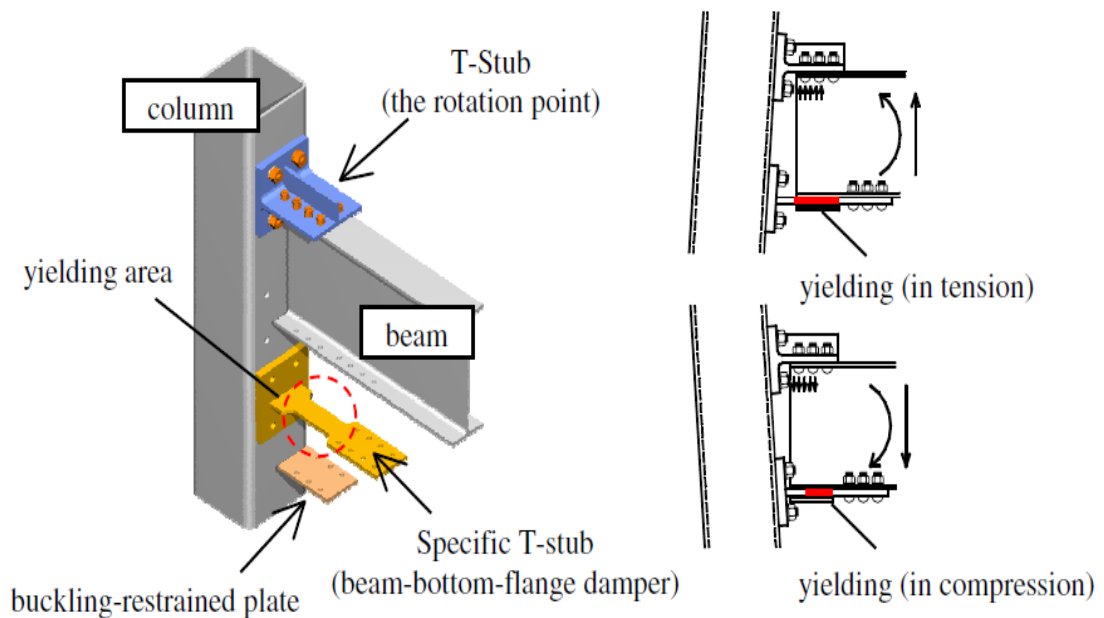
Figure 2.32 — Ductile damage-controlled moment-resisting connection proposed by Kishiki et al. (2006)
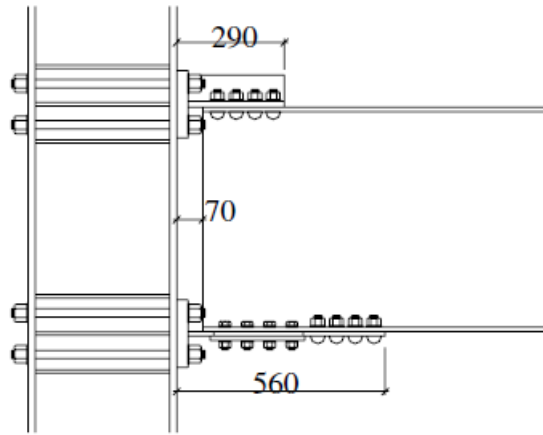
(a) Elevation of proposed connection detailing   (b) Plan view of proposed connection detailing
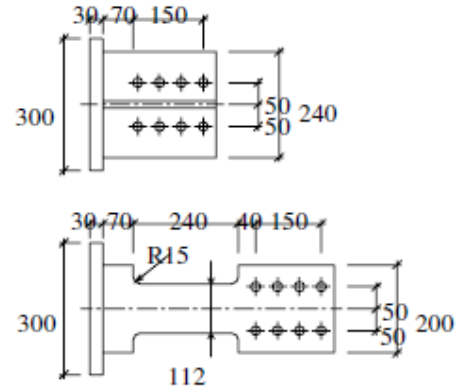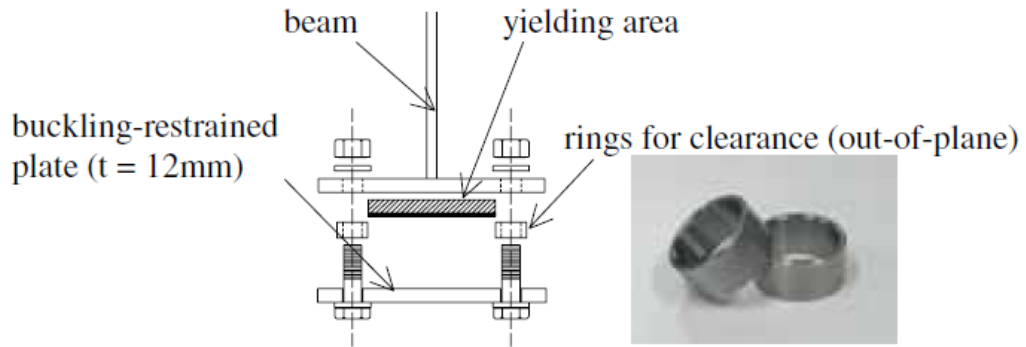
(c) Detailing for the beam-bottom flange damper
Figure 2.33 — Proposed connection detailing (Kishiki et al., 2006)
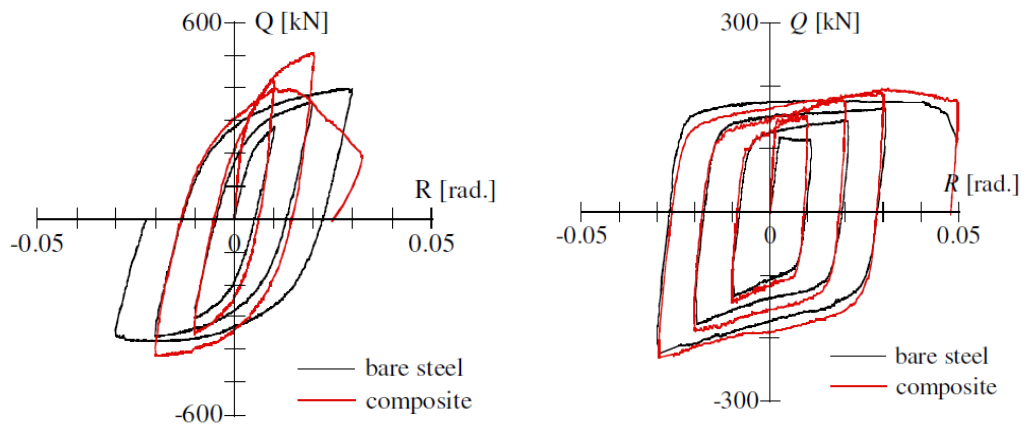
(a) Conventional welded connection   (a) Proposed connection
Figure 2.34 – Force-rotation relationship for damage-controlled connection (Kishiki et al., 2006)
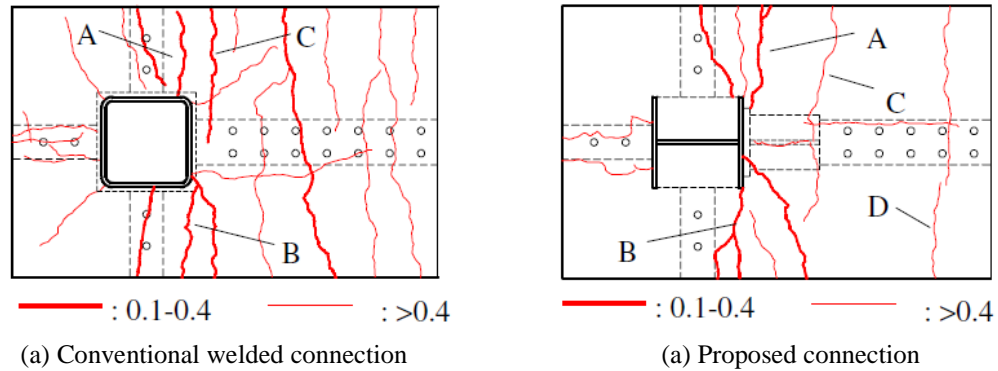
(a) Conventional welded connection　　　　　　(a) Proposed connection

Figure 2.35 – Slab crack pattern in damage-controlled moment-resisting connection (Kishiki et al., 2006)

DesRoches et al. (2009) investigated the seismic performance of a steel moment-resisting connection incorporating shape memory alloy (SMA) to dissipate energy and provide self-centering capability through finite element analysis using OpenSees. Two SMA types were investigated: austenitic superelastic SMA to provide re-centering capability, and martensitic SMA to dissipate energy. Figure 2.36 shows typical stress-strain relationships for these SMA bars. A three-story partially restrained steel moment frame in Los Angeles, CA and a nine-story steel moment frame in Seattle, WA designed by Maison and Kasai (2000) were used in the analyses as the reference frames (PR). Subsequently, SMA bars were used in the beam-column connections as shown in Fig. 2.37. Figure 2.38 and 2.39 show peak drift and residual drift demands for the three- and nine-story frames, respectively. It was found that the martensitic SMA-reinforced three-story frame was more effective, but the reduction in the peak inter-story drift was insignificant, meaning that SMA may not be a cost-effective material to use. However, for both frames, the superelastic SMA system was effective in reducing residual deformation demands. For the nine-story frame, of the SMA-reinforced frame showed an increase in the peak interstory drift demand. It was concluded that neither SMA connection was superior to the

other in reducing seismic demands, so the selection must be based on performance

objectives for that specific frame.
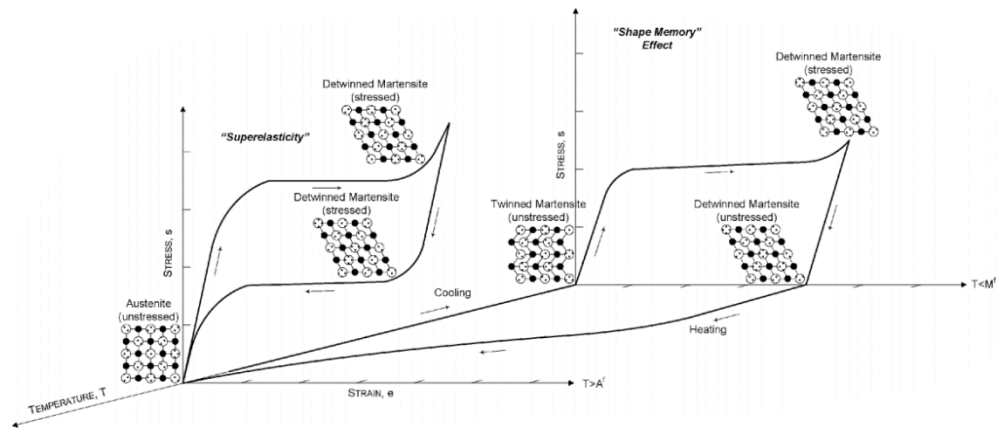
Figure 2.36 — Superelastic and Shape Memory Effect of typical SMA bars (DesRoches et al., 2009)
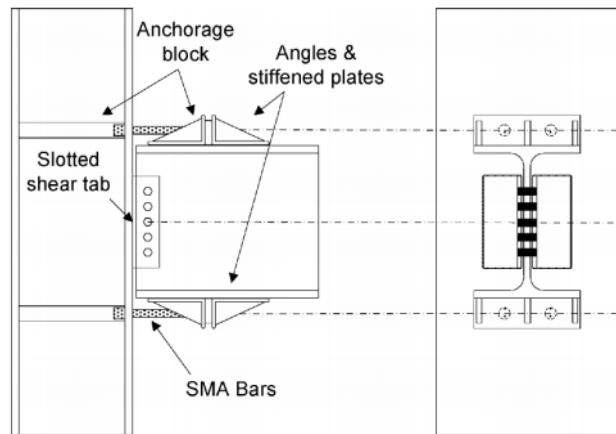
Figure 2.37 – Steel joint connection with SMA bars (DesRoches et al., 2009)
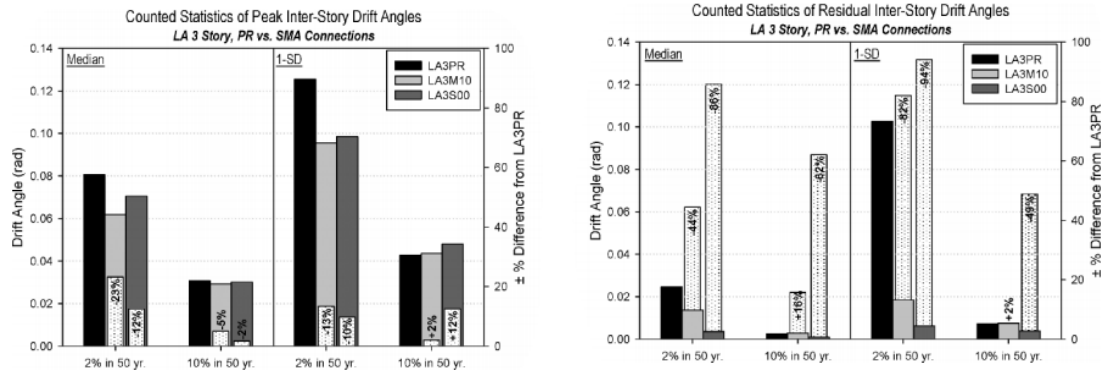
(a) Peak inter-story drift demands   (b) Residual inter-story drift demands

Figure 2.38 – Drift demands for three-story frames (DesRoches et al., 2009)
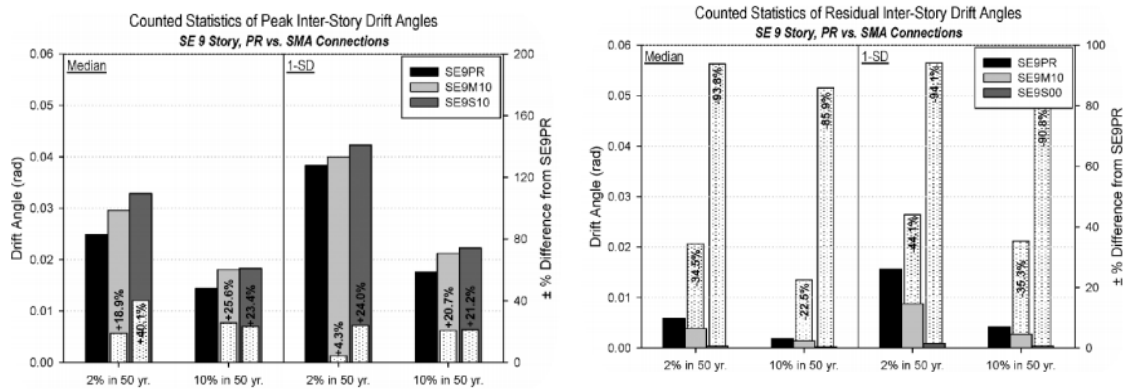
(a) Peak inter-story drift demands   (b) Residual inter-story drift demands

Figure 2.39 – Drift demands for nine-story frames (DesRoches et al., 2009)

Mansour et al. (2011) developed a replaceable shear link to be placed in chevron braces

(Fig. 2.40) and tested the connection under cyclic loads. The test data showed that flexural

loads at the link ends were greater than predicted. Figure 2.41 shows the plastic link

rotations versus the link shear forces for all specimens. The links with the web-bolted

connections showed a pinching in the hysteretic response while were able to exhibit higher

inelastic deformations. It was reported the shear links could be replaced after a residual

drift of 0.5%, which was indicated as the limit where it is more economical to rebuild a

structure than replace it (McCormick et al, 2008).

(a) End-plate connected specimen   (b) Web connected specimen
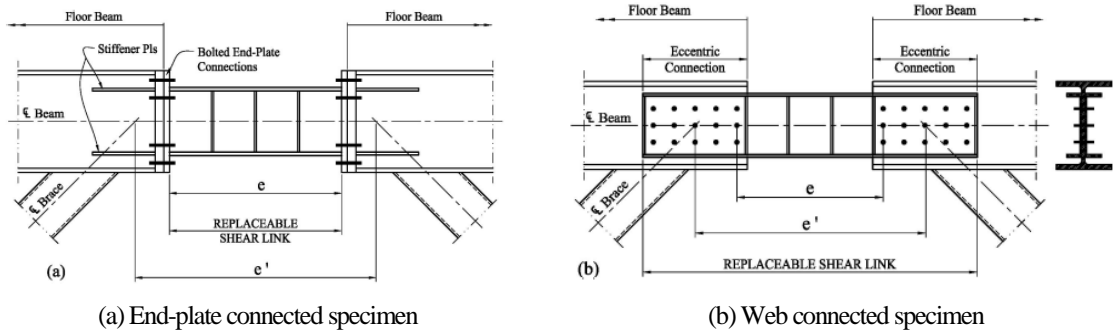
Figure 2.40 – Replaceable shear link details (Mansour et al., 2011)
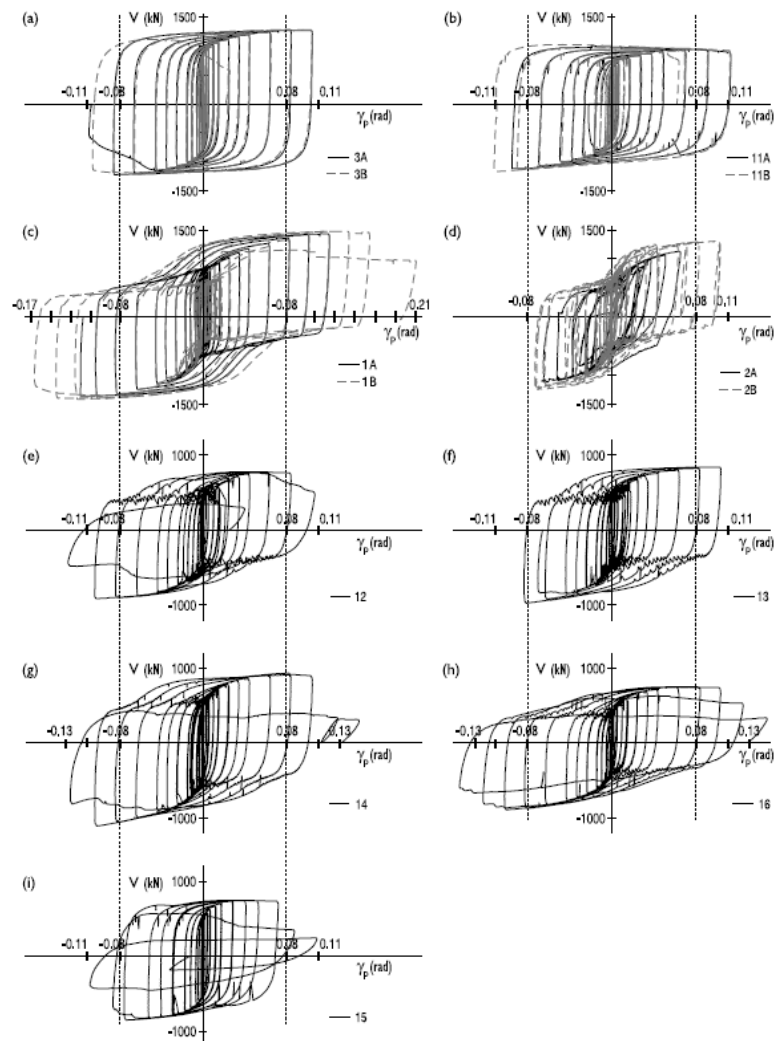
Figure 2.41 — Force-rotation relationships for frames with replaceable shear links (Mansour et al. 2011)

Several experimental and analytical studies have investigated similar replaceable shear link connections and have found consistent results. For example, Okazaki et al. (2006) and Zhang et al. (2013) tested shear links in eccentrically braced frames and diagrid structural frames respectively. Diagrid frames have diagonal grids which carry the gravity loads, and are connected to horizontal members, eliminating the need for vertical columns. The results from both studies showed that shear links provide sufficient seismic performance, largely due to the energy dissipating capacity within these links.

Oktavianus et al. (2015) conducted two finite element case studies on a proposed blind-bolted T-stub connection suitable for steel beam to concrete-filled circular column connections (Fig. 2.42 and 2.43). The blind bolt is a bolt that can be tightened from one side only, with the other side being embedded into the concrete. The energy dissipating device, which was referred to as a buckling restrained fuse (BRF), could be replaced after an event. BRF was included at the bottom flange. Later, Yao et al. (2008) and Yao et al. (2011), performed analytical studies to investigate the seismic performance of 10-story moment-resisting frames incorporating this BRF. Under the design level earthquake and maximum considered earthquake (MCE), the proposed connections showed a residual drift of less than 0.01% and 3.5%, respectively. It was also found that under MCE, the beam, column, and other connection components remained elastic, while all failure was localized to the BRF.
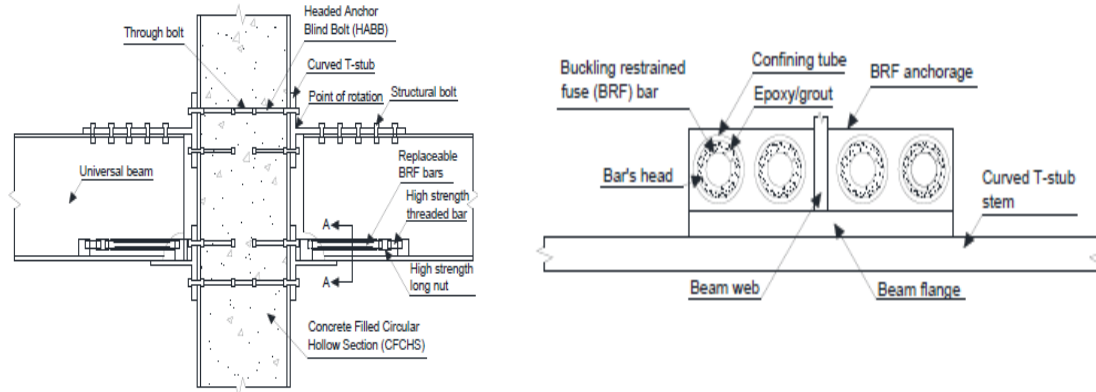
(a) Joint connection detailing   (a) Section view of anchorage method

Figure 2.42 – Repairable connection details proposed by Oktavianus et al. (2015)
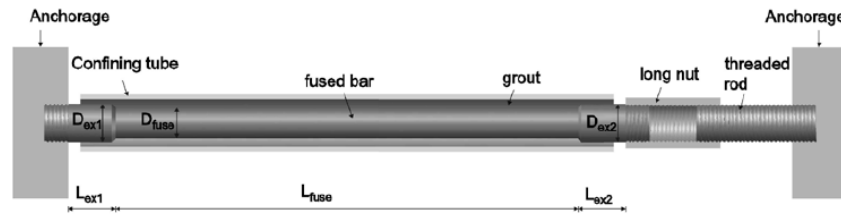
Figure 2.43 — Energy dissipating device proposed by Oktavianus et al. (2015)
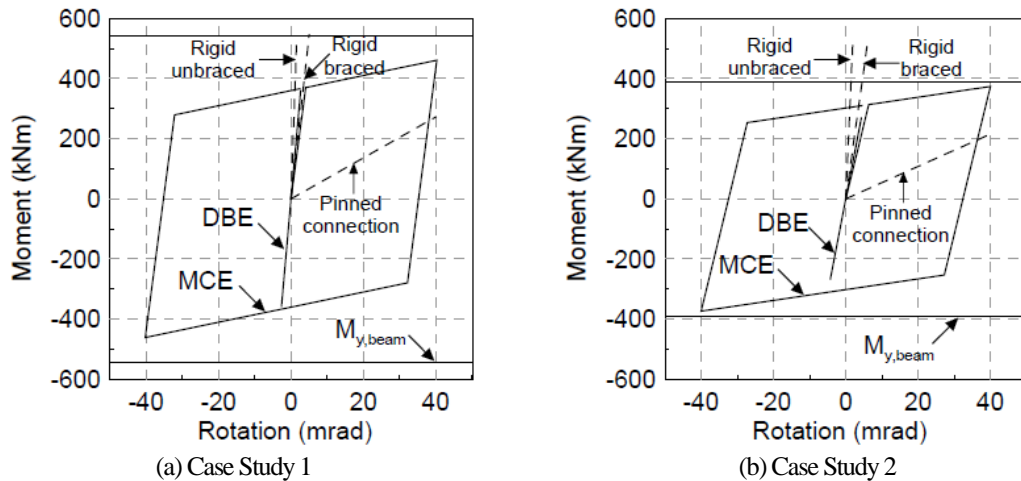
(a) Case Study 1   (b) Case Study 2

Figure 2.44 – Calculated moment-rotation relationships for each case study (Oktavianus et al. (2015)

Shahrooz et al. (2017) tested steel coupling beams with a replaceable fuse (Fig. 2.45) to serve as the primary energy-dissipating components by yielding before all other structural components. Two mid-span fuses were tested under double curvature by moving one wall

pier in the vertical direction (Fig. 2.46). The coupling beam with the central fuse showed

the same behavior as a regular steel coupling beam (Fig. 2.47). It was also reported that the

stiffness before and after the fuse replacement was nearly identical after a 1% chord

rotation. The connection performed in a way that the fuses dissipated most of the energy,

and failure occurred within the fuses, which allowed for replacement of the fuses after

unloading.
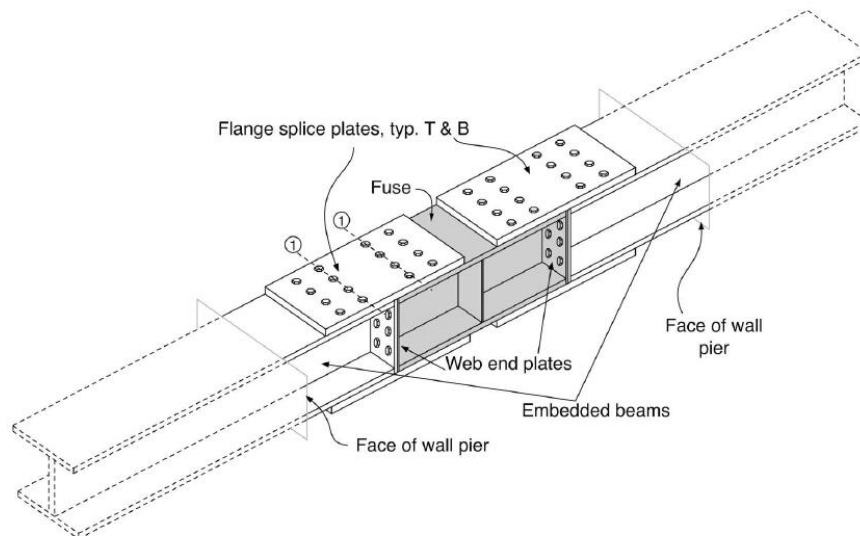
Figure 2.45 – Steel coupling beam with replaceable fuse (Shahrooz et al., 2017)
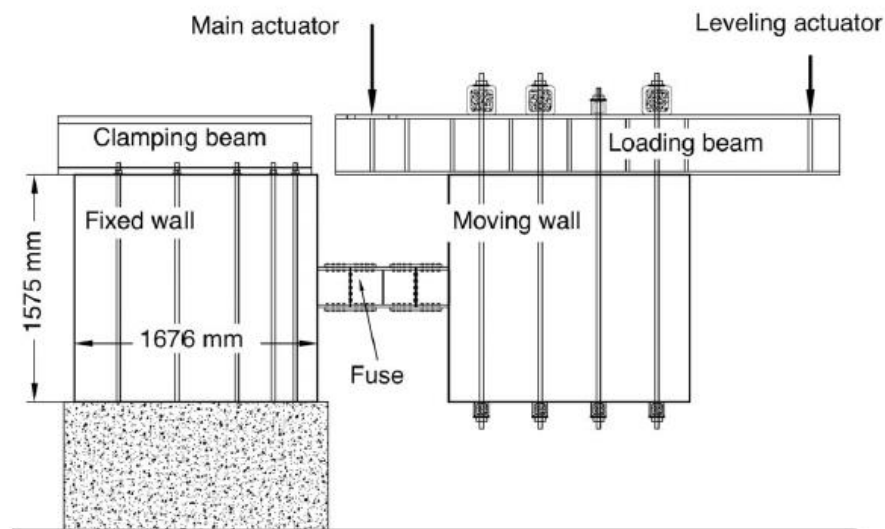
Figure 2.46 – Coupling beam test setup in Shahrooz et al. (2017)
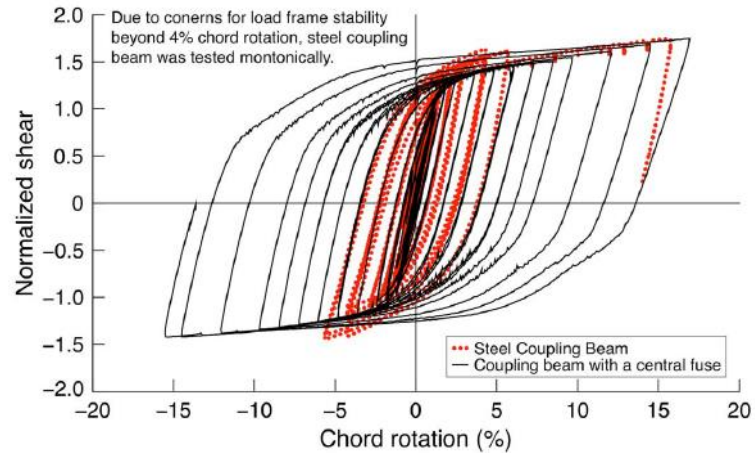
Figure 2.47 – Normalized shear-chord rotation of steel coupling beams in Shahrooz et al. (2017)

Many studies have further experimentally investigated the coupling beam connection type. For example, Ji et al. (2017) conducted cyclic loading tests similar to that of Sharooz et al. (2017) and the general observation was consistent. This type of connection dissipates energy while being replaceable upon fracture of the coupling beam.

He et al. (2018) experimentally investigated the performance of an asymmetrical moment-resisting connection, which localizes the failure within the replaceable angles at the bottom flange of the beam (Fig. 2.48). Three full-scale tests were carried out with different angle configurations. Two sets of angles were prepared for each specimen to evaluate the response of the connection before and after the angles had been ruptured and replaced. Figure 2.49 shows the angles used in Specimens P1, P2, and P3. Cyclic loading was applied at the free end of the beam. Figure 2.50 shows the measured hysteretic response for each specimen, and Fig. 2.51 shows the failure modes for the angles. The results showed that the failure can be localized into the angles while preventing other structural components to yield or fail. Stable hysteretic behavior was observed, and no significant strength degradation was observed when the angles buckled. After angle

replacement, the specimens exhibited an 80% strength reduction at the early stages of the

loading since the bolts slipped, but the specimens with the replaced angles exhibited

satisfactory performance in terms of drift capacity.
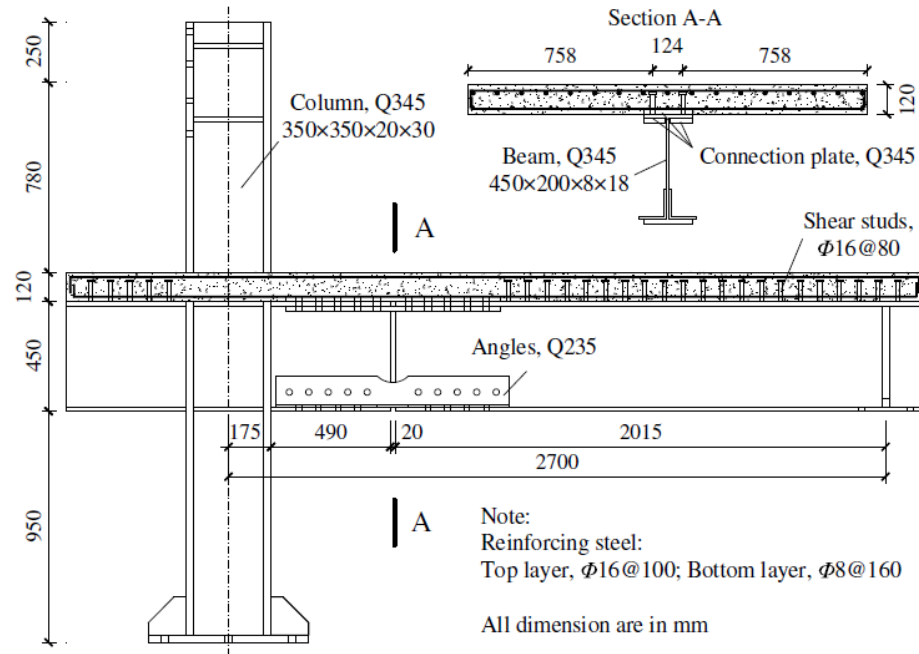
Fig. 3. Details of Specimen P1

Figure 2.48 – Beam-column connection detailing with replaceable Angles (He et al., 2018)
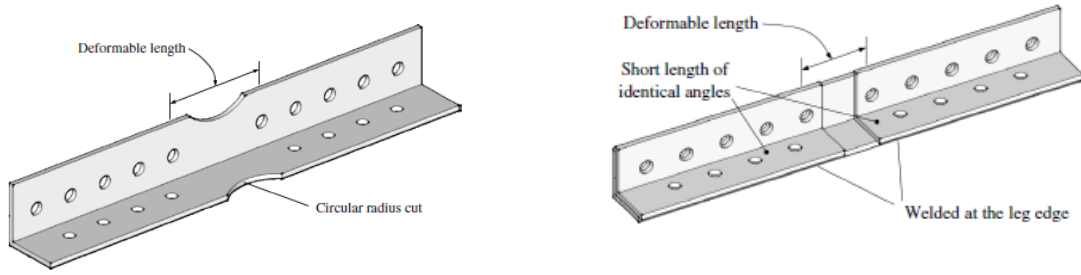
(a) Angle details for P1

(b) Angle details for P2
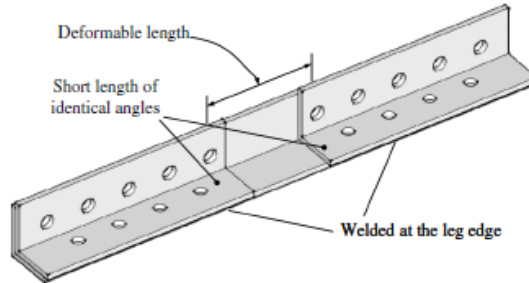
(c) Angle details for P3

Figure 2.49 – Angles as energy dissipating components (He et al., 2018)

(a) P1

(b) P2

(c) P3
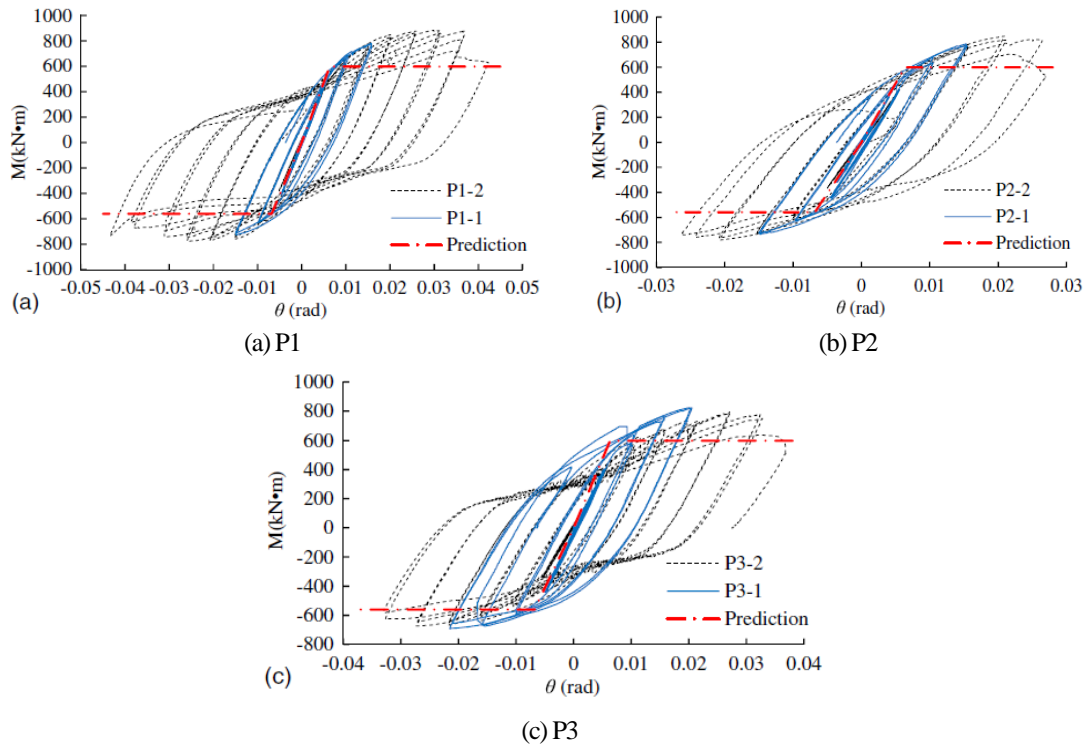
Figure 2.50 – Moment-rotation hysteresis for connections with replaceable angles (He et al., 2018)

(a) Reduced section angle   (b) End-reinforced angle
Figure 2.51 – Failure modes of connections with replaceable angles (He et al., 2018)

Behnamfar et al. (2018) proposed a repairable steel MR connection incorporating rubber and steel bolts as shown in Fig 2.52. The steel bolts were designed to dissipate energy, and the rubber was to restore the system to its original position after removing the bolts. Some tests were performed on the components and the connection including tensile tests on the bolts, cyclic tests on the connection without the steel bolts, and cyclic tests on the connection as a whole. The focus of this discussion is on the connection tests only. Twelve connection specimens were constructed and tested, and the varying parameters included the different bolt material, thickness of the rubber layer, loading rate, and variation of the section shape with varying bolt arrangements. Figure 2.53 shows the configuration of the connection placed in the testing apparatus, before installation of the bolts (Fig. 2.53a), after installation (Fig. 2.53b), and the testing setup (Fig. 2.53c). Figure 2.54 shows the shear force-displacement relationships for some of the tested energy dissipating components. It was concluded that using a thinner rubber layer with steel bolts made of stainless steel is the best alternative for this connection.
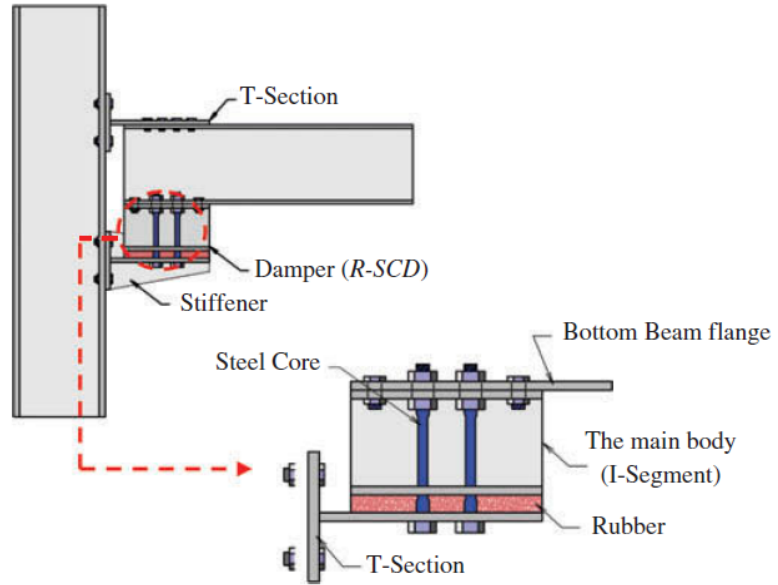
Figure 2.52 – Beam-column connection detailing with replaceable energy dissipaters (Behnamfar et al. 2018)
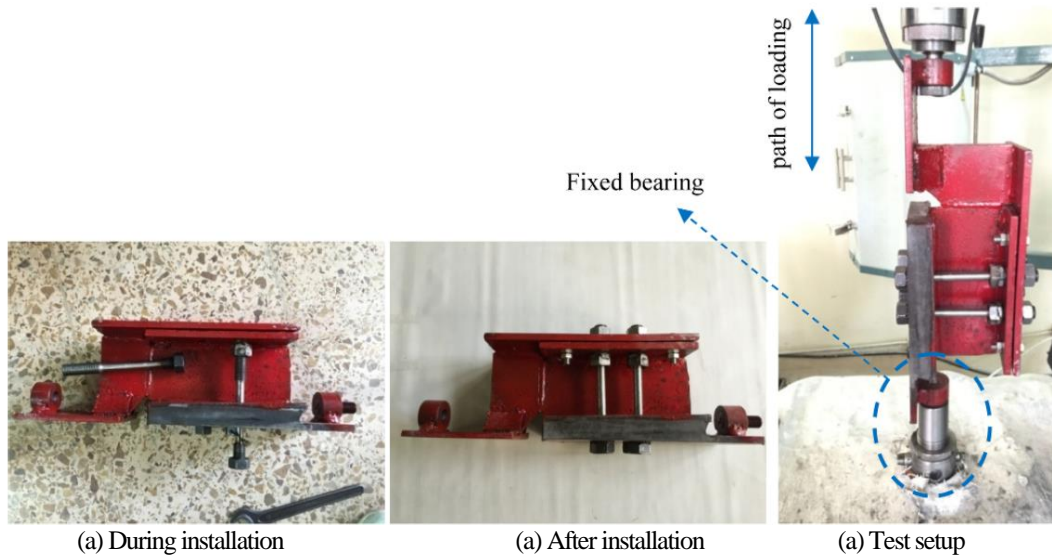
(a) During installation   (a) After installation   (a) Test setup

Figure 2.53 – Replaceable energy dissipater proposed by Behnamfar et al. (2018)
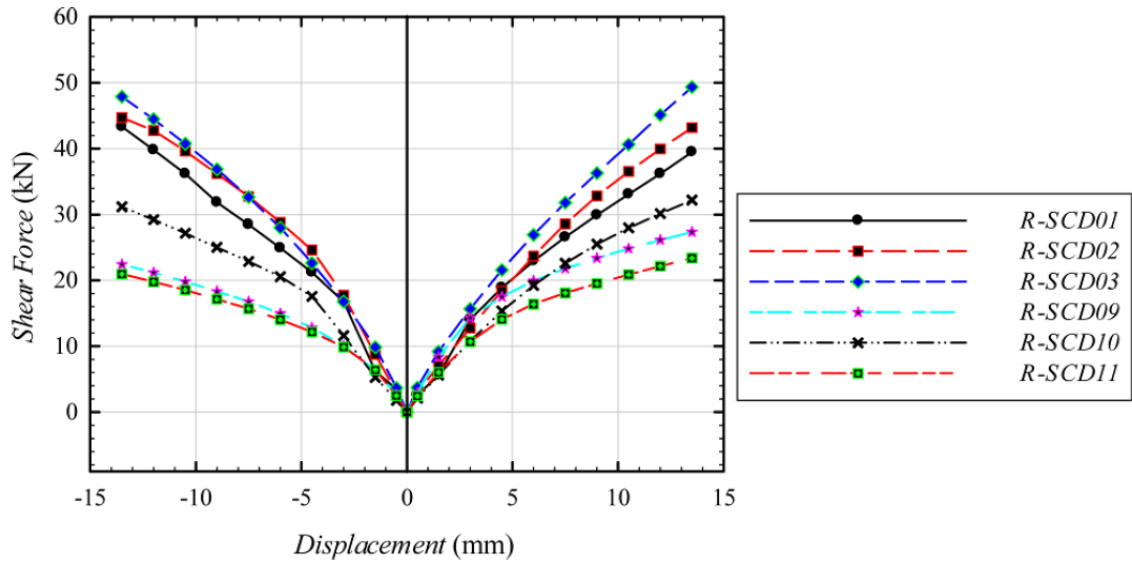
Figure 2.54 – Shear force-displacement envelope for energy dissipater specimens (Behnamfar et al. 2018)

Boudaqa (2018) developed a new precast moment-resisting connection incorporating BRR (Fig. 2-55) to accelerate construction of precast bridges or buildings, to improve the seismic performance, and to be easily repaired after an event by replacing the BRR. A cast-in-place beam-column specimen was tested as the reference, and subsequent tests were conducted on the precast beam-column specimens using dog-bone steel and SMABRR. Two precast beams were constructed (PBC1 and PBC2). PBC2 was designed after testing PBC1 to minimize the cosmetic damage in the precast beam itself. PBC1 was tested before and after replacing the dog-bone steel BRR. PBC2 was first tested with dog-bone steel BRR and then with SMA bars. PBC1 showed cosmetic damage but with the same force-deformation behavior before and after replacing BRR. PBC2 showed insignificant damage up to 14 times the design level earthquakes and exhibited insignificant residual drifts when SMA BRR was used. Overall, the performance of the precast joint can significantly outperform that for conventional joints. The BRR can also be replaced after each test.
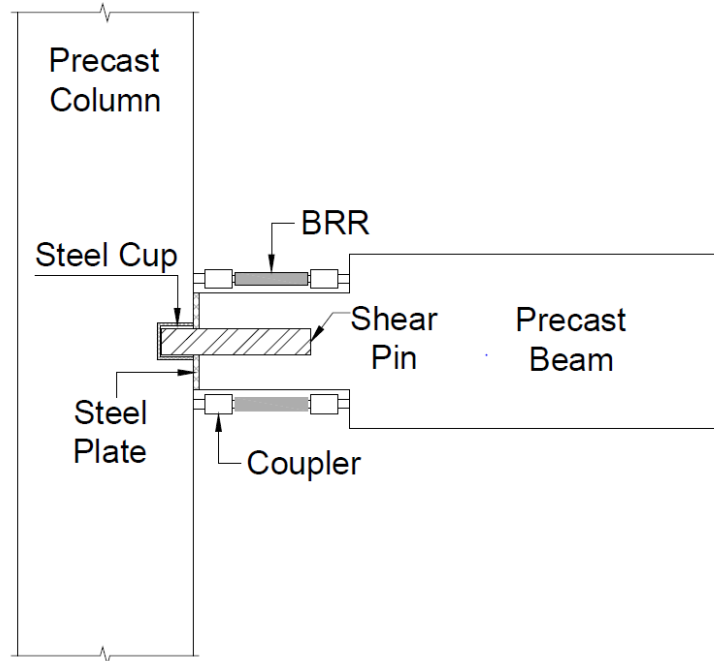
Figure 2.55 – Precast repairable beam-column connection detailing (Boudaqa 2018)
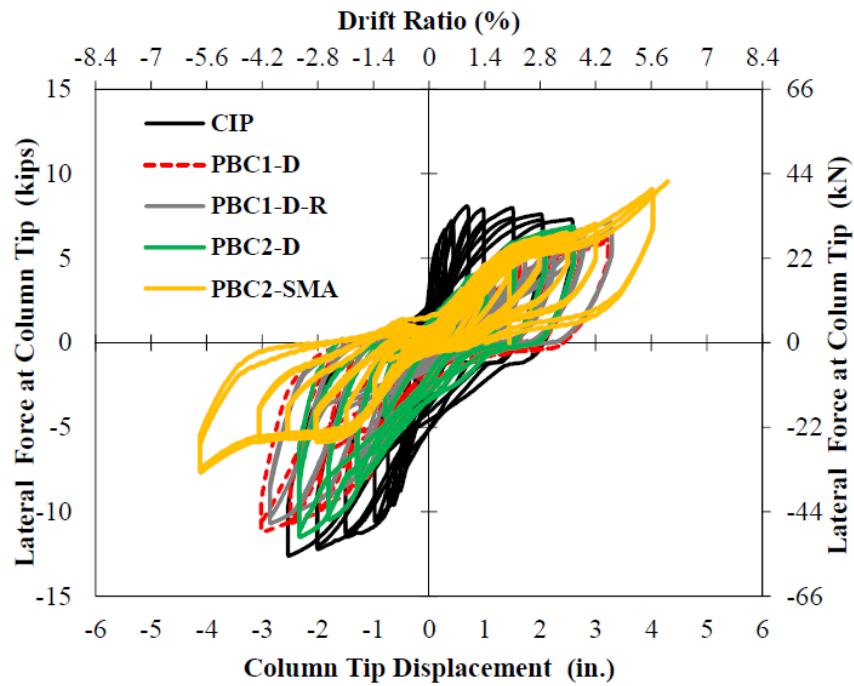
Figure 2.56 – Force-displacement behavior of Specimen PBC1-D (Boudaqa, 2018)

Simpson Strong-Tie (2019) developed a repairable moment-resisting connection that

incorporates replaceable yield links as structural fuses (Fig. 2.57). A design guideline was

proposed. AISC 358-16 currently allows Simpson Strong-Tie frames only as ordinary

moment-resisting systems. The major benefits of this connection are that there is no

welding required, construction is simple, and after a major event such as an earthquake, the

yield links are replaceable. Since all failure is localized to these components, steel beams

and columns will have minimal damage and yielding. The behavior of this connection was

experimental and analytical investigated by the company. Figure 2.58 shows the finite

element model of the connection. The analysis confirmed that all inelastic actions were

localized to the yield link (Fig. 2-59). Figure 2.60 showed the measured and calculated

force-displacement behavior of the test specimen. The full-scale beam-column specimen

exhibited a stable hysteretic behavior, and the OpenSees-calculated force-displacement

relationship closely matched with that obtained from the test.

(a) Two-Piece T-Stub Link   (b) End-Plate Link
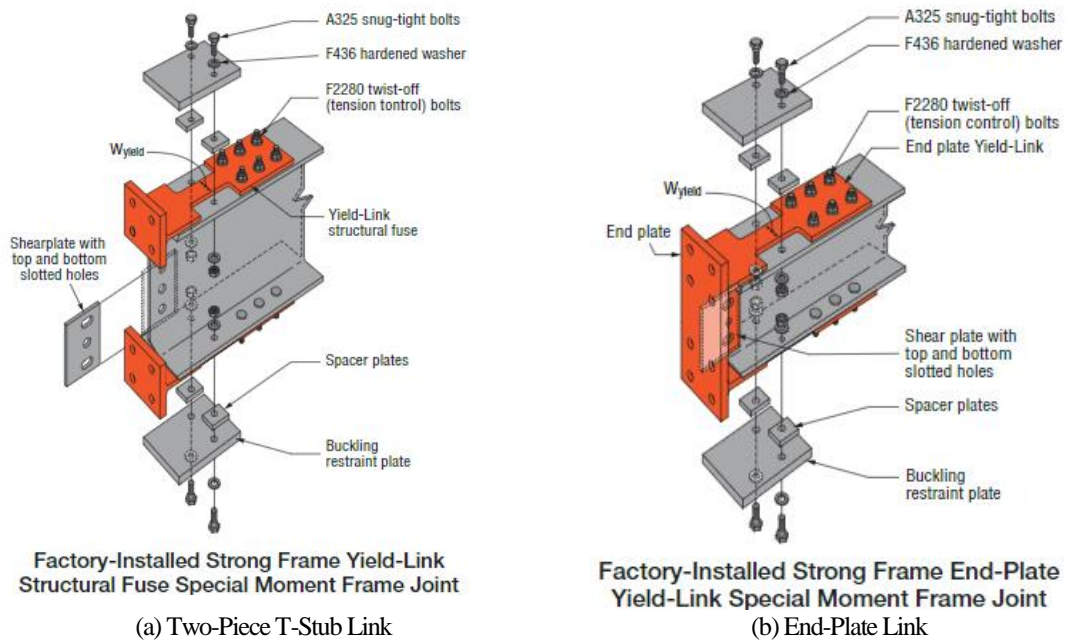
Figure 2.57 – Repairable beam-column connection detailing using yield links (Simpson Strong-Tie, 2019)
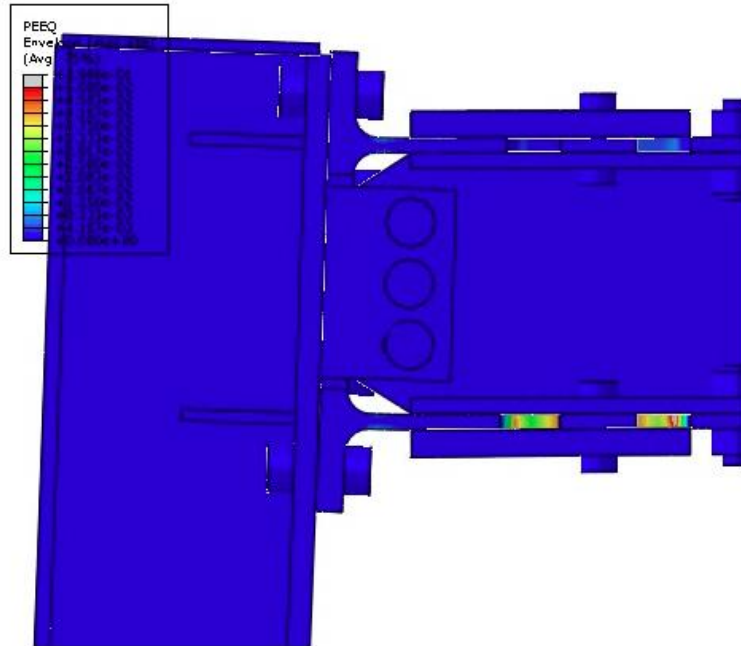
Figure 2.58 – Failure region of beam-column joint with yield link as a structural fuse (Simpson Strong-Tie, 2019)
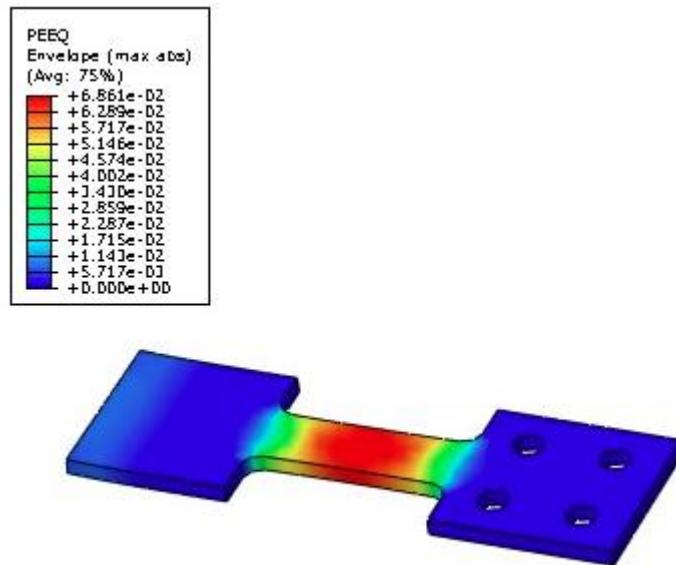
Figure 2.59 – Strain contour for yield links (Simpson Strong-Tie, 2019)
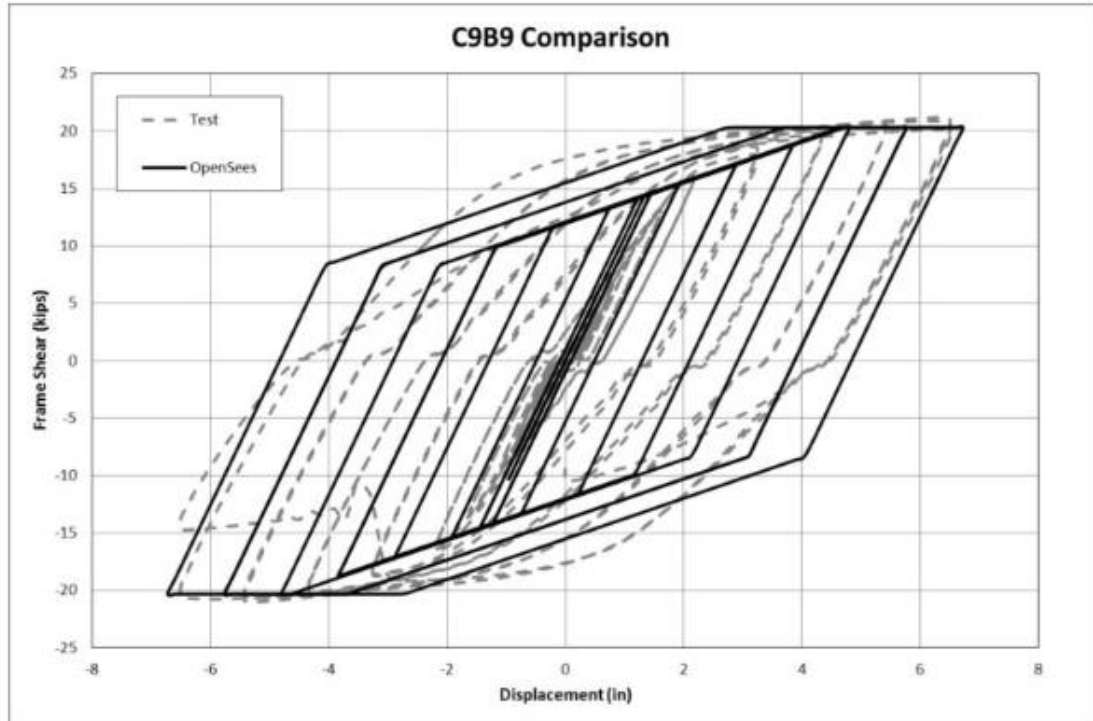
Figure 2.60 – Measured and calculated force-displacement relationships for yield-link joints (Simpson Strong-Tie, 2019)

2.5 Patented Repairable Steel Joints

Several replaceable steel joint details have been patented in the U.S. and other countries. This section presents a short review of patents on replaceable steel moment-resisting joints.

Figure 2.61 shows a shear link with replaceable cover plates (Choi, 2019). All plastic damage due to external loading or displacement is localized within the first and second cover plates (137 and 138 in Fig. 2.61) on the top and bottom of the shear link.
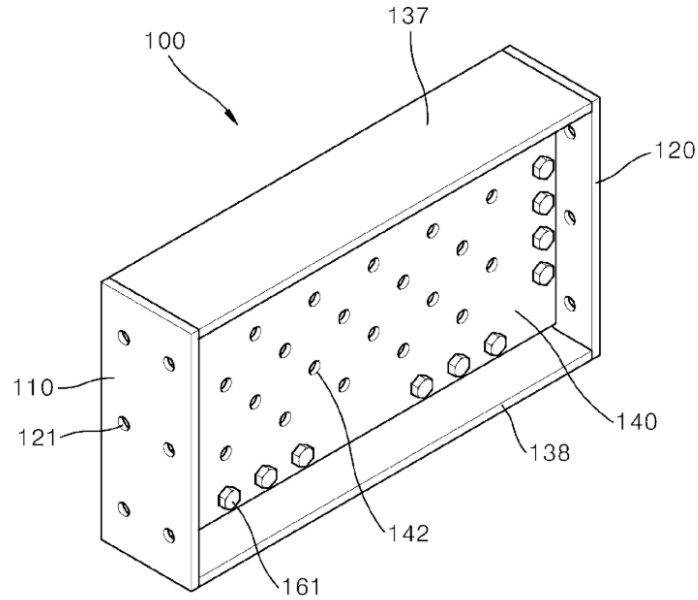
Figure 2.61 – Patented shear link with replaceable cover plates (Choi, 2019)

Figure 2.62 shows a patented replaceable joint connection for steel moment frames. This connection consists of a buckle suppression block attached to the top and bottom flanges of the beam. Each block includes bores through the center of the block and one yield link. The connection has a stable hysteretic behavior, and once the links are damaged upon yielding, they are easily replaced with the structure remaining intact.
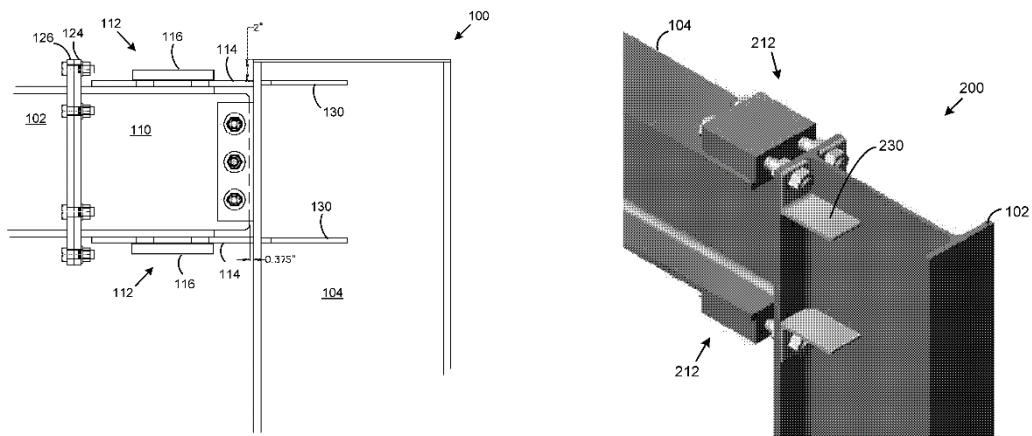
(a) Connection detailing   (b) Connection finite element model
Figure 2.62 – Patented moment frame connection (Hiriyur, 2013)

The moment frame links wall (Fig. 2.63) consists of replaceable yield links with a yield point below that of the moment frame that is designed to take all plastic damage. A casing may be provided around the yielding links to prevent compressive buckling.
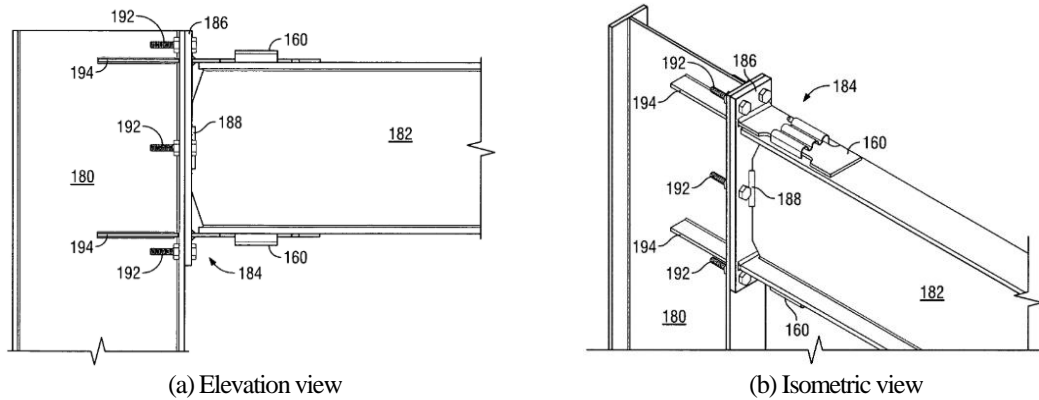
(a) Elevation view   (b) Isometric view

Figure 2.63 – Patented moment frame links wall (Pryor et al., 2011)

Another patented replaceable connection is a beam-column join shown in Fig. 2.64. This connection has a pair of split tees (Fig. 2.64) consisting of a web with a portion having a reduced cross-sectional area to localize all plastic failure.
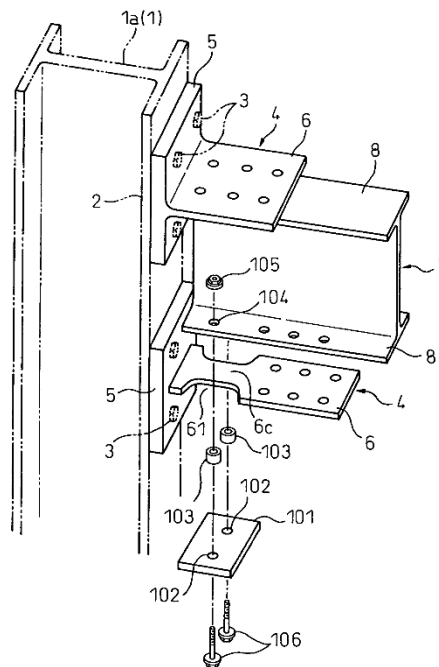
Figure 2.64 – Patented beam-column join structure (United States Patent No. US7497054B2, 2009)

Shown in Fig. 2.65 is another replaceable energy dissipating joint connection. The connection consists of a U-shaped piece, high-strength bolts, and prestressed tendons. Upon failure, the upper and lower prestressed tendons can be removed and replaced as all damaged is mainly concentrated to these components.
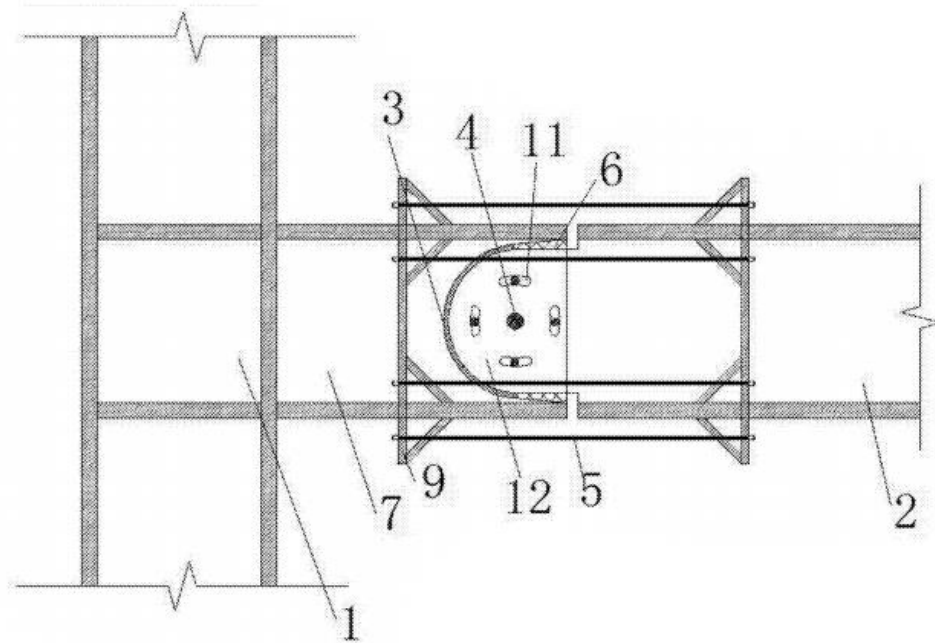
Figure 2.65 – Patented replaceable energy dissipation connecting joint (Takeuchi et al., 2009)

2.6 References

Boudaqa, A., Tazarv, M., and Tuhin, I. (2017). "Ductility without confinement a new

   design and construction approach for RC bridge columns." International Journal of

   Bridge Engineering, pp. 53–77.

Boudaqa, A., (2018). "Repairable precast buildings and bridges," PhD Dissertation, South

   Dakota State University, 249 pp., https://openprairie.sdstate.edu/etd/2467/.

Choi, J. H. (2019). *U.S. Patent No. US10184244B2*. Washington, DC: U.S. Patent and Trademark Office.

Clifton, C. and Butterworth, J. (2000). "Moment-resisting steel framed seismic-resisting systems with semi-rigid connections." The Processing of the 12th World Conference on Earthquake Engineering, Auckland, New Zealand, pp. 1-8.

DesRoches, R., and Ellingwood, B.R. (2010). "Seismic performance of steel frames with shape memory alloy connections, Part I & Part II - Analysis and Seismic Demands." Journal of Earthquake Engineering, Vol. 14, No. 10, pp. 471-486.

DesRoches, R., McCormick, J, Delemont, M. (2004). "Cyclic properties of superelastic shape memory alloy wires and bars." Journal of Structural Engineering, Vol. 130, No. 1, pp. 38-46.

Gheidi, A., Mirtaheri, M., Zandi, A.P., and Alanjari, P. (2009). "Effect of filler material on local and global behaviour of buckling-restrained braces." The Structural Design of Tall and Special Buildings, Vol. 20, No., pp. 700–710.

Badri, H., and Steven, P.E. (2013). "Moment frame connector." *U.S. Patent No. US8375652B2*. Washington, DC: U.S. Patent and Trademark Office.

Hoveidae, N., and Rafezy, B. (2012). "Overall buckling behavior of all-steel buckling restrained braces." Journal of Constructional Steel Research, Vol. 79, pp. 151–158.

Ji, Z, Wang, Y., Ma, Q., Okazaki, T. (2016) "Cyclic behavior of steel coupling beams." Journal of Structural Engineering, Vol. 143, No. 2, 11 pp. 1-11.

Kim, H.J., and Christopoulos, C. (2008). "Friction damped posttensioned self-centering steel moment-resisting frames." Journal of Structural Engineering, Vol. 134, No. 11, pp. 1768–1779.

Kishiki, S., Yamada, S., Suzuki, K., Saeki, E., and Wada, A. (2006). "New ductile moment-resisting connections limiting damage to specific elements at the bottom flange". The 8th U.S. National Conference on Earthquake Engineering, San Francisco, USA, pp. 1-9.

Mansour, N., Christopoulos, C., and Tremblay, R. (2011). "Experimental validation of replaceable shear links for eccentrically braced steel frames." Journal of Structural Engineering, Vol. 137, No. 10, pp. 1141–1152.

Mazzoni S, McKenna F, Scott M, Fenves G. (2006). Open system for earthquake engineering simulation., Berkeley, CA.

McCormick, D., Aburano, H., Ikenaga, M., and Nakashima, M. (2008). "Permissible residual deformation level for building structures considering both safety and human elements." The 14th World Conf. on Earthquake Engineering, Beijing, China, pp. 1-8.

Miller, D.J., Fahnestock, L.A., and Eatherton, M.R. (2012). "Development and experimental validation of a nickel–titanium shape memory alloy self-centering buckling-restrained Brace." Engineering Structures, Vol. 40, pp. 288–298.

Mohammadrezapour, E., and Danesh, F. (2018). "Experimental investigation of bolted link-to-column connections in eccentrically braced frames." Journal of Constructional Steel Research, Vol. 147, pp. 236–246.

Nikoukalam, M., and Dolatshahi, K.M. (2015). "Development of structural shear fuse in moment resisting frames." Journal of Constructional Steel Research, Vol. 114, pp. 349–361.

Nishimoto, K., Nakata, Y., Kimura, I., Aiken, I., Yamada, S. and Wada, A. (2004). "Sub-assembly testing of large buckling-restrained unbonded braces." The 13th World Conference on Earthquake Engineering, Vancouver, B.C., Canada, pp. 1-9.

Oktavianus, Y., and Goldsworthy, H. (2015). "A study towards the development of low damage moment-resisting connections using blind bolts, CFCHS columns, and a replaceable energy dissipating device." The New Zealand Society for Earthquake Engineering, Rotorua, New Zealand, pp. 243-252.

Pryor, S.E., and Anderson, G.T. (2011). "Moment frame links wall." *U.S. Patent No. US8001734B2*. Washington, DC: U.S. Patent and Trademark Office.

Rahai, A.R., Alinia, M.M., and Salehi, S.M.F. (2009). "Cyclic performance of buckling restrained composite braces composed of selected materials." International Journal of Civil Engineering, Vol. 7, No. 1, pp. 1-8.

Ricles, J.M., Sause, R., Peng, S.W., and Lu, L.W. (2002). "Experimental evaluation of earthquake resistant posttensioned steel connections." Journal of Structural Engineering, Vol 128, No. 7, pp. 850–859.

Sarti, F., Smith, T., Palermo, A., and Pampanin, S. (2013). "Experimental and analytical study of replaceable Buckling-Restrained Fuse-Type (BRF) mild steel dissipaters." The New Zealand Society for Earthquake Engineering, Wellington, New Zealand, pp 1-8.

Simpson Strong-Tie. (2019). "Strong Frame Special Moment Frame, Yield-Link Structural Fuse," Retrieved on March 7, 2019 from <https://www.strongtie.com/products/lateral-systems/strong-frame-moment-frames/special-moment/yield-link-structural-fuse>.

Surendran, N., and Varma, A. (2017). "Buckling Restrained Braces (BRB) - A Review." International Research Journal of Engineering and Technology, Vol. 4, No. 3, pp. 2320-2324.

Takeuchi, T., Hajjar, J., Matsui, R., Nishimoto, K., and Aiken, I. (2012). "Effect of local buckling core plate restraint in buckling restrained braces." Engineering Structures, Vol. 44, pp. 304–311.

Takeuchi, T., Maeda, Y., Suzuki, K., Okada, K., Yamada, S., and Wada, A. (2009). "Column-and-beam join structure." *U.S. Patent No. US7497054B2*. Washington, DC: U.S. Patent and Trademark Office.

Watanabe, A., Hitomoi, Y., Saeki, E., Wada, A., Fujimoto, M. (1988). "Properties of braced encased in buckling-restraining concrete and steel tube." The Proceedings of Ninth World Conference on Earthquake Engineering, Japan Association for Earthquake Disaster Prevention, Tokyo-Kyoto, Japan, Vol. 4, pp. 719-24.

Wiebe, L., Christopoulos, C., (2015). "Performance-based seismic design of controlled rocking steel braced frames. 1: Methodological framework and design of base rocking joint." Journal of Structural Engineering, Vol. 141, No. 9, pp. 1-11.

Wu, B., and Mei, Y. (2015). "Buckling mechanism of steel core of buckling-restrained braces." Journal of Constructional Steel Research, Vol. 107, pp. 61–69.

Moghaddasi, B., and Zhang, Y. (2013). "Seismic analysis of diagrid structural frames with shear-link fuse devices." Earthquake Engineering and Engineering Vibration, Vol. 12, No. 3, pp. 463–472.

Chapter 3: Proposed Repairable Moment-Resisting Joints for Steel Buildings

3.1 Introduction

In the present chapter, new repairable steel moment-resisting joints are proposed and discussed. Two alternatives incorporate buckling restrained fuses (BRFs), and three alternatives incorporate buckling restrained reinforcement (BRR). The main goals of using these buckling restrained devices are to repair the joints by replacing BRFs or BRR, and to enhance the seismic performance of steel beam-column connections in terms of ductility. The yielding and failure are localized into these devices. A mechanical shear pin is included in the repairable detailing to allow free rotations of the beam resulting in maximum nonlinear strains in the fuses. The new join details are discussed herein.

3.2 Repairable Joints with Buckling Restrained Fuses

This section presents the beam-column joint detailing that incorporates BRF, which is a miniature version of buckling restrained braces (BRB) discussed in the previous chapter. The design method for BRF is the same as those currently available for BRB.

Two joint detailing alternatives are proposed with one incorporating BRFs and a shear pin at the middle of the BRF (BRF-M), and the other using BRFs and a shear pin at the end of the beam (BRF-B). These naming conventions specifically refer to the beam-column

connections in which the shear pin (mechanical hinge) is located directly below the

centroid of BRF and at the end of the beam, respectively.

3.2.1 Joints with BRFs and Hinge at Middle of Fuse (BRF-M)

Figure 3.1 shows the beam-column configuration for the BRF-M alternative. This joint

detailing consists of BRFs (composed of a dog-bone steel plate, anchoring end plates,

encasing box/tube, and a filler material such as grout), a shear pin (mechanical hinge),

shear plates, and a steel corbel at the face of column to accommodate BRFs. This

alternative is designed with a hinge directly above/below the centroid of BRFs.
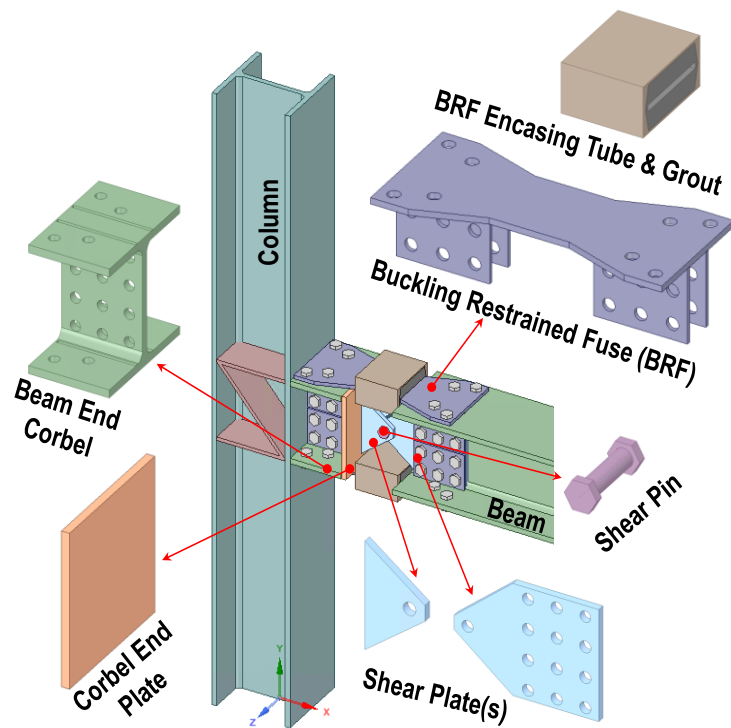
Figure 3.1 – BRF repairable joint with shear pin at middle of fuse (BRF-M)

When a steel frame built with the proposed joints is laterally displaced, one of the BRFs

is axially tensioned and another one is in compression forming a T and C couple to resist

moments. BRFs have a doge-bone core to be the weak link of the connection and to

localize the yielding and damage. It is obvious that other members should be designed to

remain linear elastic. The BRF core is restrained against buckling to resist large compressive forces and to avoid low-cycle fatigue. Due to the cyclic nature of earthquakes, the fuses should be restrained against buckling at both the top and bottom of the beam. BRFs are connected to the beams and corbels using slip-critical bolts. Therefore, BRFs can be replaced after an event as a quick and cost-effective method of repair.

Not explicitly shown in Fig. 3.1 is the debonding agent used in BRFs to decouple the steel core and the filler material. This debonding layer is included so that the entire axial forces that are developed are resisted solely by the steel core. Due to the rigidity of the encasing tube/box and the filler grout, support against buckling of the steel core is provided. The tube/box for the encasing mechanism can be made of two small steel C-shaped profiles that are welded together, which are then filled with a grout.

The shear pin shown in Fig. 3.1 is a hand-tight bolt that passes through the holes of the shear plates. The pin allows the beam to easily rotate, which then allows the fuse to reach its ultimate strains resulting in a large displacement capacity for steel frames using this connection. The shear pin and the shear plates are designed to transfer the plastic shear forces while they are in the elastic range.

Regarding the shear plates welded to the beam web, the holes shown in the plates are to account for the number of slip-critical bolts that pass through the BRF anchoring plates. The shear plates should be designed with sufficient geometry (e.g. edge distance and hole spacing) to fully resist the shear plastic forces.

The corbel shown in Fig. 3.1 is welded to the column and is to provide a space for BRFs to be fully anchored. The corbel is also designed to resist the plastic forces while

remaining elastic. An end plate is welded to the corbel, which will serve as base plate for the shear plates discussed above.

It should be noted that all steel columns and beams should also be designed as capacity protected members. Therefore, repairable frames built with the proposed joint detailing should have larger beams and columns compared to conventional steel moment-resisting frames to exhibit the same lateral strength. Alternatively, if the size of the beams and columns is kept the same as that of conventional steel moment-resisting frames, the repairable frames will show a lower lateral strength. The latter design is more cost-effective and may be more favorable.

3.2.2 Joints with BRFs and Hinge at Beam End (BRF-B)

Figure 3.2 shows another joint detailing alternative incorporating BRFs, but the shear pin is at the end of the beam. Therefore, this design alternative only requires shear plates that are welded to the corbel end plate, and not the beam web (e.g. Fig. 3.1). All of the other components and their functionality remain the same as those discussed in the previous section for BRF-M.
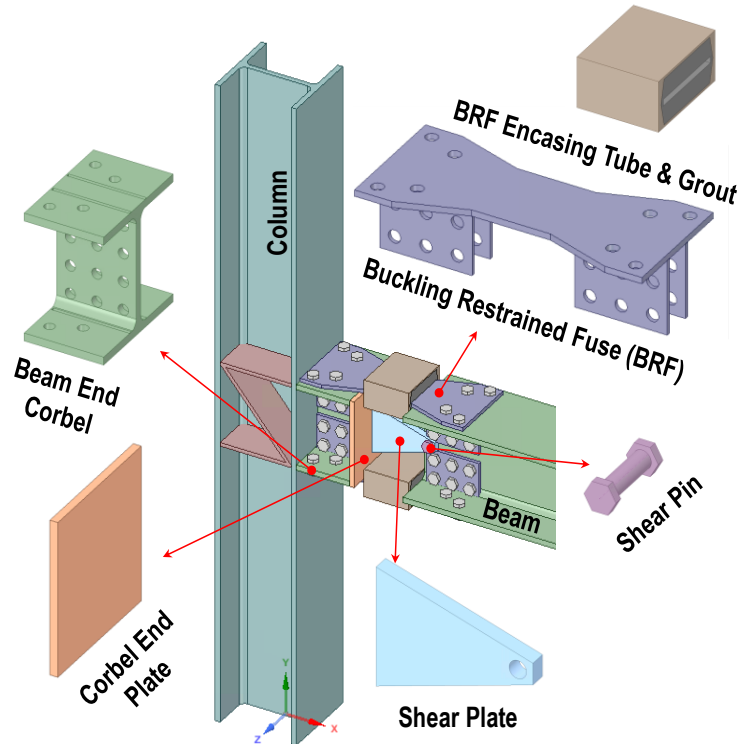
Figure 3.2 – BRF repairable joint with shear pin at beam end (BRF-B)

3.2.3 Joints with All-Steel BRF

As discussed in Chapter 2, it is feasible to use a buckling restrained brace (BRB) that is entirely composed of steel components. Figure 3.3 shows one sample of all-steel BRB proposed by Hoveidae et al. (2012). The core of all-steel BRB is the same as typical BRBs; however, the core is restrained against buckling using steel stiffeners. Hoveidae et al. (2012) reported that the ratio of the Euler buckling load to the yield load of the core plate should not be taken less than 1.5 to prevent overall buckling. The core of BRFs in the proposed repairable steel joint may be restrained against buckling using the all-steel detailing.
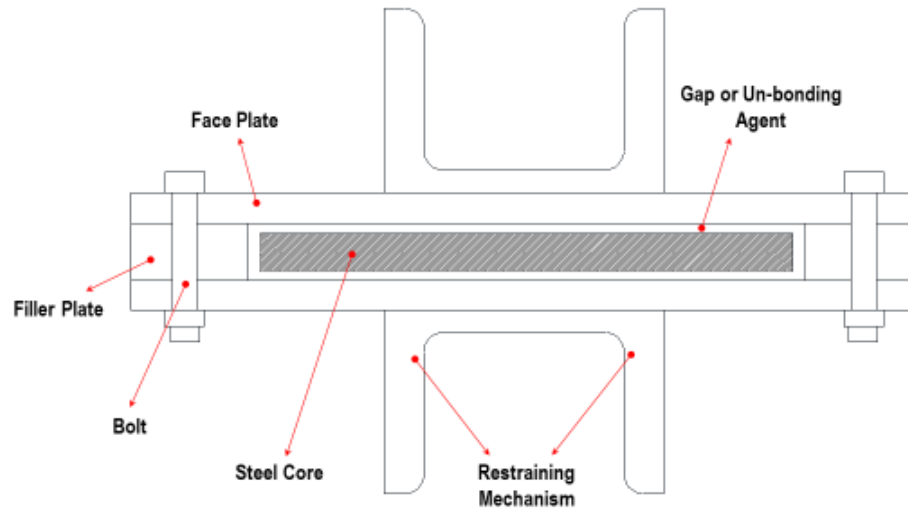
Figure 3.3 – Cross section of all-steel BRB proposed by Hoveidae et al. (2012)

3.3 Repairable Joint with Buckling Restrained Reinforcement

This section discusses the details of the proposed repairable beam-column connections that incorporate buckling-restrained reinforcement (BRR). Three models are proposed in which the only difference is the location of the shear pin. Joints incorporating BRR and a shear pin at the middle of BRR (BRR-M), joints incorporating BRR and a shear pin at the column face (BRR-M), and joints incorporating BRR and a shear pin at the beam end (BRR-B) are proposed. A brief discussion of each alternative, its components, and the function of each component is presented herein.

3.3.1 Joints with BRR and Hinge at Middle of Bar (BRR-M)

Figure 3.4 shows the beam-column configuration for the BRR-M alternative. This joint consists of BRR components (composed of a core reinforcing bar, encasing steel tube, and a filler material such as grout), anchoring angles for BRR, a shear pin, and shear connecting plates. This alternative is designed to have a mechanical hinge directly below the centroid of the reinforcing bars. As the beam rotates, the top or bottom BRR axially

resists either compressive or tensile forces developing internal moments through a T and C coupling mechanism.
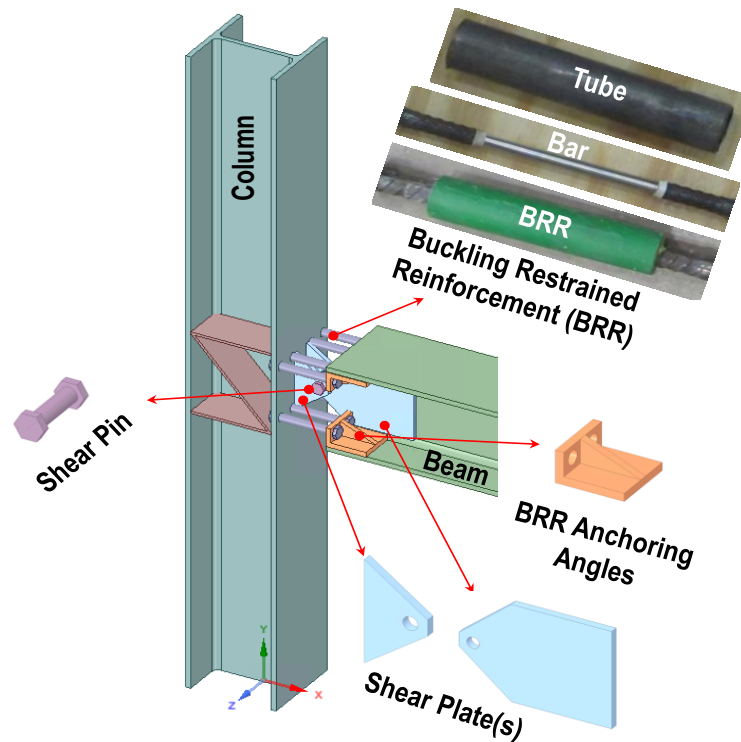
Figure 3.4 – BRR repairable joint with shear pin at middle of bar (BRR-M)

Figure 3.4 also shows the BRR components. Similar to BRF, BRR is restrained against buckling using the grout that is confined by the encasing steel tube. This is to avoid low-cycle fatigue of the bar and to allow the bar to reach its ultimate strain. All nonlinearity of the beam-column assembly is concentrated to BRR, and upon yielding or failure after an event, the bolted BRR components can be removed and easily replaced with new ones. This detailing offers a quick and cost-effective repair method for moment-resisting steel structures. Furthermore, since BRR are inside the beam, both top and bottom BRR can be accessed from the lower floor for inspection and replacement.

Expect BRR, all other components for this alternative have the same functionality as those discussed for joints with BRF and they should be designed to remain linear elastic. Therefore, there would be generally two options to design steel frames with BRR. One needs larger beams and columns compared to conventional steel moment-resisting frames to exhibit the same lateral strength. Another can have beams and columns with the same sizes compared to conventional frames but with a smaller lateral strength.

3.3.2 Joints with BRR and Hinge at Column Face (BRR-C)

Figure 3.5 shows the repairable beam-column configuration incorporating BRR with the shear pin at the column face (BRR-C). This system is similar to the BRR-M alternative discussed in the previous section, but the location of the hinge has shifted closer to the column. This was done to investigate the best location of the pin in achieving a larger strength or ductility. The only notable difference between the two alternatives is the geometry of the shear plates, which still must be able to resist the shear plastic forces while remaining linear elastic.
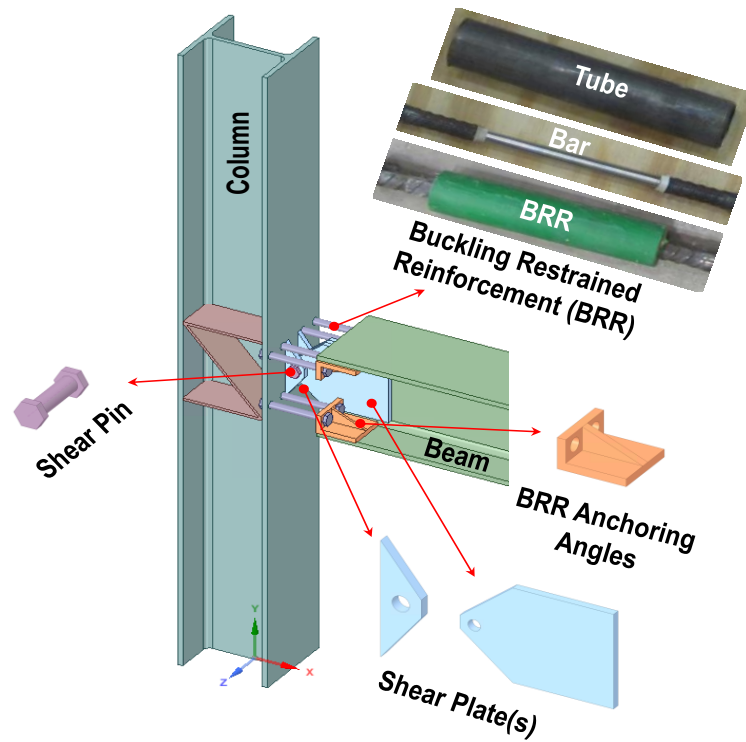
Figure 3.5 – BRR repairable joint with shear pin at column face (BRR-C)

3.3.3 Joints with BRR and Hinge at Beam End (BRR-B)

Figure 3.6 shows the repairable BRR-B beam-column configuration in which the shear pin is at the beam end. This system is similar to the previous BRR models but with a different hinge location. All other components and their functionality remain the same.
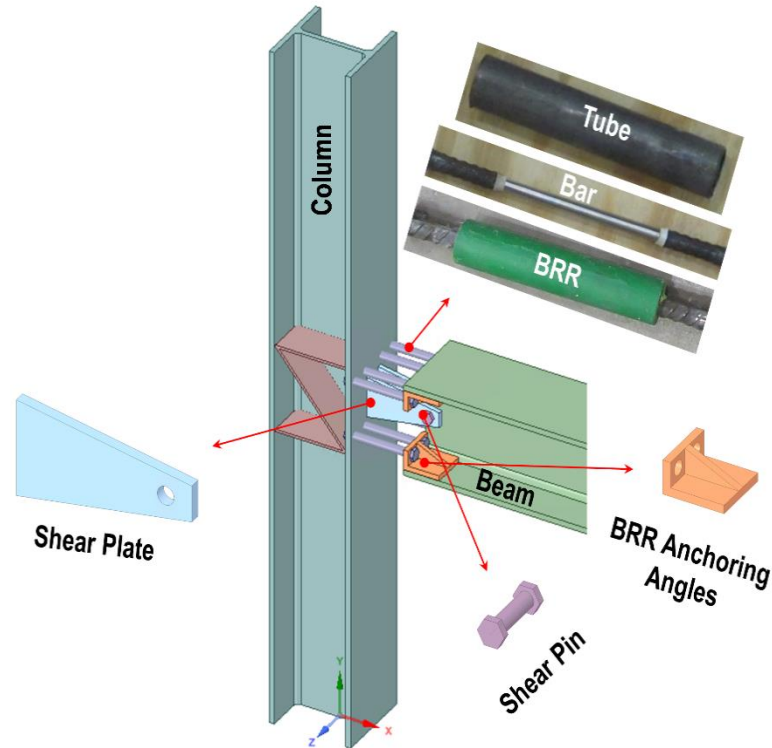
Figure 3.6 – BRR repairable joint with shear pin at beam end (BRR-B)

3.3.4 Advanced Materials and Devices in/as BRR

Shape memory allow (SMA) was introduced in Chapter 2. Superelastic SMA exhibits a flag-shape stress-strain behavior with insignificant residual strains up to 8% strain demands. It is feasible to use SMA bars as the core of BRR. In this case, the moment-resisting frame built with SMA-BRR will show insignificant permanent lateral deformations after severe earthquakes, which will result in a minimal repair.

Several BRR might be needed to develop large moments comparable to those seen in conventional steel moment-resisting joints. High-strength steel bars can be used as the BRR core to reduce the number or area of the reinforcement. ASTM A615 or A706 Grade 60 reinforcing steel bars with a specified yield and ultimate tensile strength of 60 ksi (414 MPa) and 95 ksi (655 MPa) are currently used in concrete structures. Alternatively, the BRR core can be made of ASTM A1035 Grade 100 bars with a specified yield and tensile

strength of 100 ksi (690 MPa) and 150 ksi (1034 MPa), respectively. Furthermore, ASTM A1035 bars have five times better corrosion resistance compared with conventional reinforcing bars (Harris Supply Solutions, 2019).

Several types of dampers have been proposed to reduce seismic demands of buildings and bridges. Different damper types and their seismic performance were reviewed by Heysami (2015). This study identified the main advantages of using dampers in seismic applications as the high energy dissipation capacity and the ease of installation and replacement. Samples of friction dampers, Penguin Vibration Damper (PVD), and metallic dampers are shown in Fig. 3.7 to 3.9. The performance of SMA dampers was investigated for cable-stayed bridges by Sharabash et al. (2009) as shown in Fig. 3.10. The results from this study demonstrated the effectiveness of the dampers in reducing the shear and bending moment demands on bridges.

Of many types, rod-form dampers (e.g. viscous dampers) might be used instead of BRR to develop internal moments and to improve the joint overall performance similar to the damper shown in Fig. 3.11 (Taylor Devices Inc., 2019). Several other viscous dampers are widely used in seismic applications including those made available by ITT Enidine Inc. (2019) shown in Fig. 3.12 and Victor Seismic (2019) shown in Fig. 3.13.

Figure 3.7 – Rotational friction damper (Heysami, 2015)

Figure 3.8 – PVD damper (Heysami, 2015)

Figure 3.9 – Metallic dampers (Heysami, 2015)
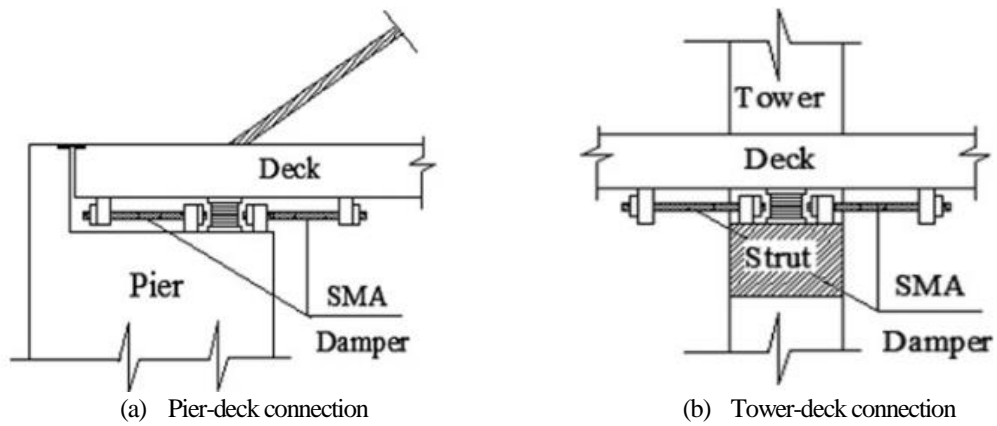
(a) Pier-deck connection   (b) Tower-deck connection
Figure 3.10 – Rotational friction damper (Sharabash et al., 2009)

Figure 3.11 – Seismic damper produced by Taylor Devices Inc. (2019)

Figure 3.12 – Viscous damper produced by ITT Enidine (2019)

Figure 3.13 – Viscous damper produced by Victor Seismic (2019)

3.4 References

Bharti, S., Dumne, S., and Shrimali, M. (2010). "Seismic response analysis of adjacent buildings connected with MR dampers." Engineering Structures, Vol. 32, No. 8, pp. 2122–2133.

Harris Supply Solutions. (2019). "A1035 Rebar," Retrieved on March 19, 2019 from <www.harrissupplysolutions.com/a1035-rebar-astm-a1035-grade-reinforcing-bar.html>.

Heysami, A., (2015). "Types of dampers and their seismic performance during an earthquake," Current World Environment, Vol. 10, No. 1, pp. 1002-1015

Hoveidae, N., and Rafezy, B. (2012). "Overall buckling behavior of all-steel buckling restrained braces." Journal of Constructional Steel Research, Vol. 79, pp. 151–158.

ITT Enidine Inc., (2019), "Viscous dampers," Retrieved on April 2, 2019 from <http://www.itt-infrastructure.com/en-US/Products/Viscous-Dampers/>.

Inoue, K., Suita, K., Takeuchi, I., Chuslip, P., Nakashima, M., and Zhou, F. (2006). "Seismic-resistant weld-free steel frame buildings with mechanical joints and hysteretic dampers." Journal of Structural Engineering, Vol 132, No. 6, pp. 864-872.

Sharabash, A., Andrawes, B., "Application of shape memory alloy dampers in the seismic control of cable-stayed bridges," Engineering Structures, Vol. 31, No. 2, pp. 607-616.

Taylor Devices Inc. (2019) "Seismic dampers," Retrieved on April 2, 2019 from <http://seismicdampers.taylormachinedsprings.com/applications/?anchor=seismic-dampers>.

Victor Seismic. (2019) "Fluid viscous dampers," Retrieved on April 2, 2019 from <https://www.victorseismic.co.nz/seismic-dampers>.

Chapter 4: Analytical Studies: Joint Performance

The proposed details for repairable steel moment-resisting frames were discussed in Chapter 3. The behavior of the proposed joints needs to be established through experimental and analytical studies. This chapter is focused on the analytical studies.

Finite element analysis (FEA) is a robust numerical tool used to investigate the behavior of structural components and systems under difference loading regimes. FEA is advantageous in that it gives a specific breakdown of quantities of interest, such as stress or strain concentration, over the body of each element.

In this chapter, first, a FE modeling method and its validation are presented for a reference buckling restrained brace (BRB) tested under uniaxial compression. Subsequently, FE modeling method is discussed for a steel moment-resisting (MR) beam-column specimen that was tested under a slow cyclic loading. The experimental and analytical results are compared. Finally, the reference specimen was modified using the proposed repairable detailing and then FEA were performed using the validated models incorporating either buckling restrained fuses (BRFs) or buckling restrained reinforcement (BRR).

4.1 Buckling Restrained Brace (BRR) Component Modeling

Nonlinear FEA was conducted on a buckling restrained brace component, which was tested by Gheidi et al. (2011). ANSYS 18.2 (2017) with a static structural analysis system was used for the analytical study. As discussed in Chapter 2, Gheidi et al. (2011) performed uniaxial tests on BRBs with different filler materials, and tested BRBs as part of a braced frame. In this chapter, the discussion is focused on the uniaxial BRB test (SP3), which had normal-weight concrete as the BRR filler. The objective was to verify the proposed analytical modeling method for BRBs at the component level.

SP3 had a rectangular cross-section with a width of 3.15 in. (80 mm) and a thickness of 0.315 in. (8 mm). The encasing tube was a hollow steel square tube with the dimensions of 4.73 in. by 4.73 in. by 0.118 in. (120 mm by 120 mm by 3 mm). Figure 4.1 shows a schematic and photograph of the uniaxial testing apparatus with the test specimen in place. The length of the yielding steel core was 23.6 in. (60 cm).

To simplify the modeling procedure and to reduce computational time, only the encased region of SP3 was modeled and analyzed. It should be noted that all geometric modeling was done using the ANSYS built-in "SpaceClaim" tool. The BRB geometry was based on that provided by Gheidi et al. (2011), and all bodies were modeled as solid bodies. The general modeling and analysis procedure are discussed herein.
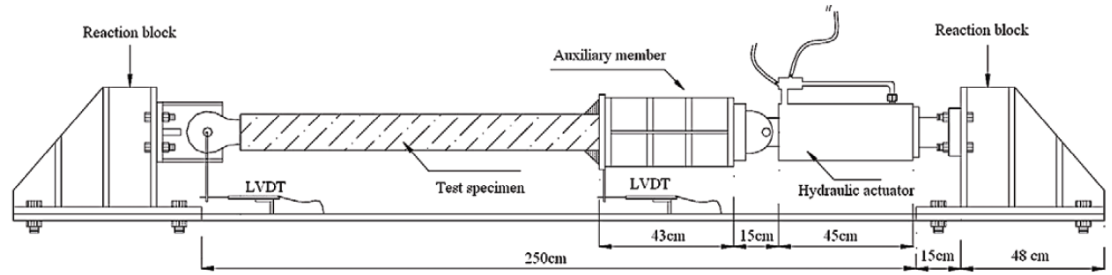
(a) Schematic of BRB test

(b) Photograph of BRB test

Figure 4.1 – Uniaxial testing configuration by Gheidi et al. (2011)

4.1.1 BRB Test Specimen Material Properties

Table 4.1 presents the measured BRB material properties according to Gheidi et al. (2011). These properties were used in the FEA of SP3. Nonlinear material models were used for all components. A multilinear kinematic hardening plasticity model was used for the BRB core steel and steel tube. Figure 4.2 shows the analytical stress-strain relationships for the two steel profiles. Since only the yield and ultimate values were reported in the study, a bilinear stress-strain relationship was selected for the analysis. A nonlinear concrete material model was used for the tube filler material with the modulus of elasticity of concrete as a user-input parameter.

Table 4.1 – Measured Material Properties for BRB Tested by Gheidi et al. (2011)

Component	Material	Measured Material Properties		ANSYS Bilinear Properties
Core Steel	Structural Steel	Yield Stress, ksi (MPa)	43.2 (297.5)	43.3 (298.2)
		Ultimate Stress, ksi (MPa)	65.2 (449.8)	78.9 (544.3)
		Yield Strain	0.0022	0.0022
		Ultimate Strain	0.21	0.180
Steel Tube	Structural Steel	Yield Stress, ksi (MPa)	53.7 (370.0)	53.8 (370.9)
		Ultimate Stress, ksi (MPa)	58.5 (403.4)	77.8 (536.5)
		Yield Strain	0.0025	0.0025
		Ultimate Strain	0.33	0.29
Tube Filler	Concrete	28-day Strength, ksi (MPa)	4.4 (30.0)	N/A
		Modulus of Elasticity, ksi (MPa)	3733.7 (25743.0)	N/A

Note: All values are engineering properties. True material properties were used in ANSYS.
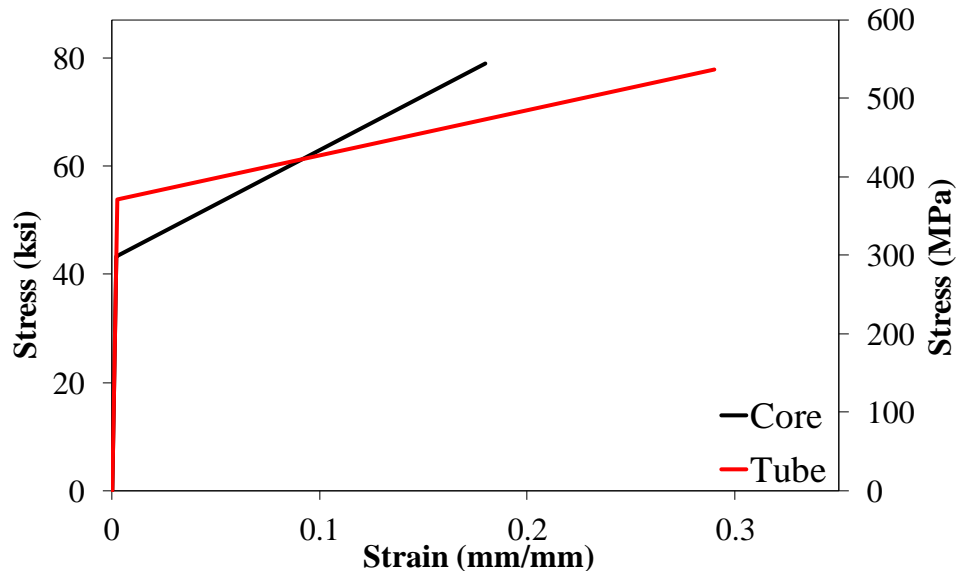
Figure 4.2 – Analytical stress-strain relationships for BRB steel components

4.1.2 BRB Analytical Model Connections and Contact Regions

Two contact regions were defined: (1) the contact between the encasing tube and the grout (Fig. 4.3), and (2) the contact between the grout and the steel core (Fig. 4.4). The contact region between the encasing tube and grout was assumed to be "bonded", which

constrains all translations in any direction. The region between the steel core and the grout

was modeled using a "frictional contact", with a friction coefficient of 0.3. Since the

rubber sheets that were used in the test as the debonding material were not explicitly

modeled, a frictional contact simulates the same behavior in that it de-couples the steel core

and grout to allow the core to translate in the horizontal direction, while also simulating a

gap in the contact region.
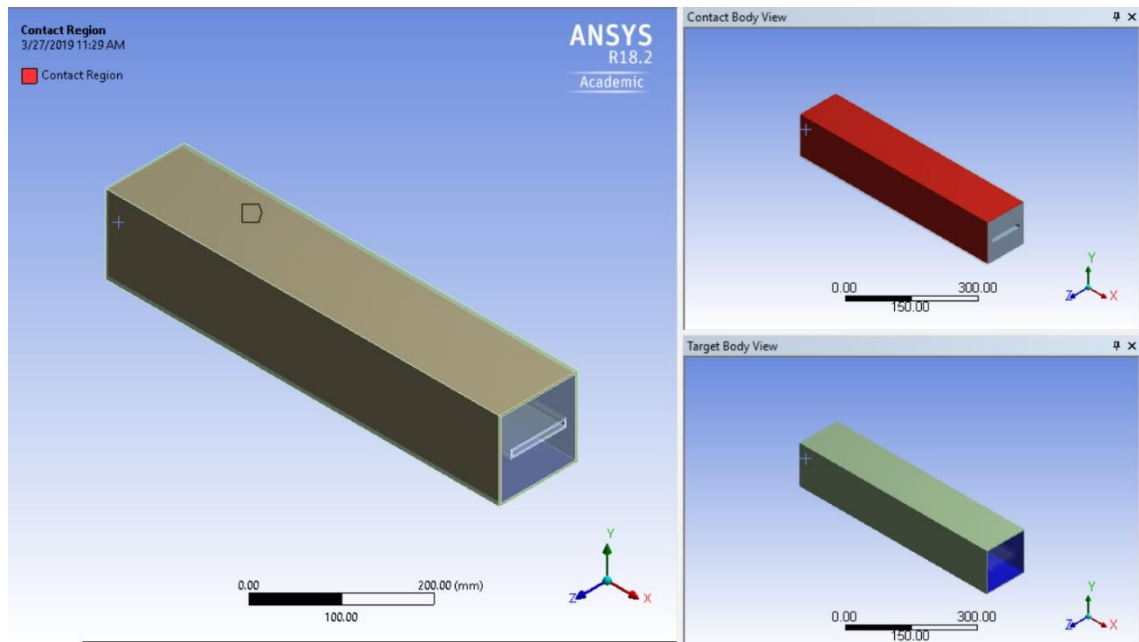
Figure 4.3 – Bonded contact between encasing tube and grout in BRB analytical model
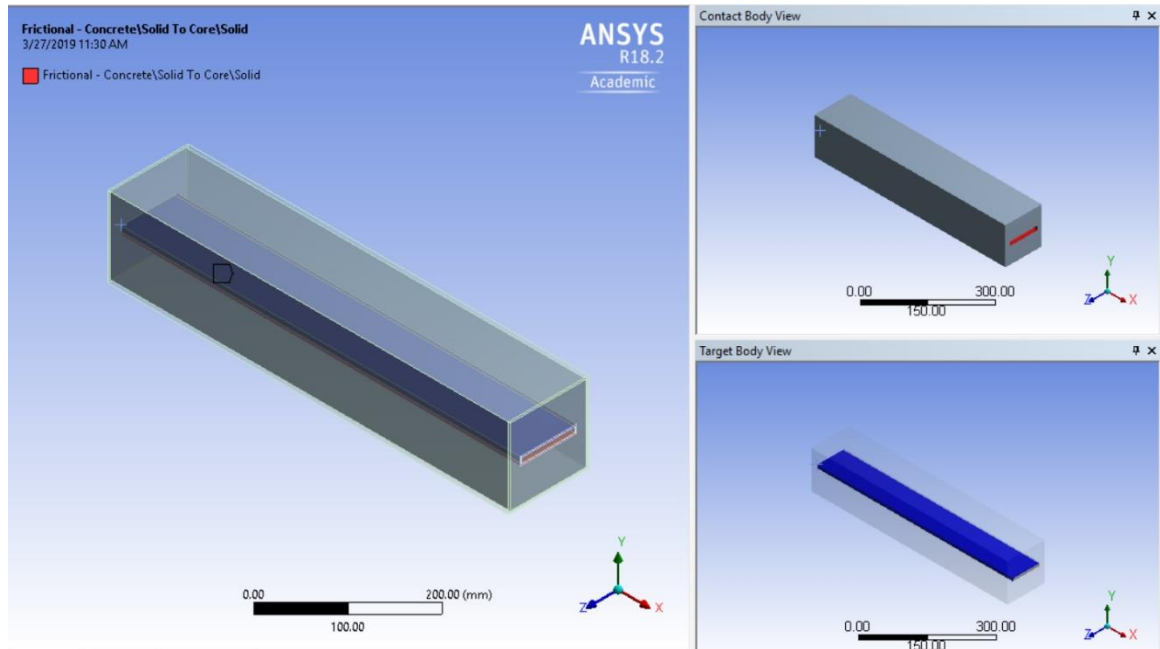
Figure 4.4 – Frictional contact between grout and steel core in BRB analytical model

4.1.3 BRB Analytical Model Meshing

ANSYS can automatically generate a mesh based on user-specified preferences of coarse, medium, and fine relevance centers and span angle centers. For the BRB model, an automatic mesh of a medium size was selected, consisting of 20420 nodes and 3705 elements (Fig. 4.5). It is desirable to have a mesh with a uniform pattern to avoid any irregularities that may develop in the structure while maintaining the efficiency of the model in terms of computational time and effort.
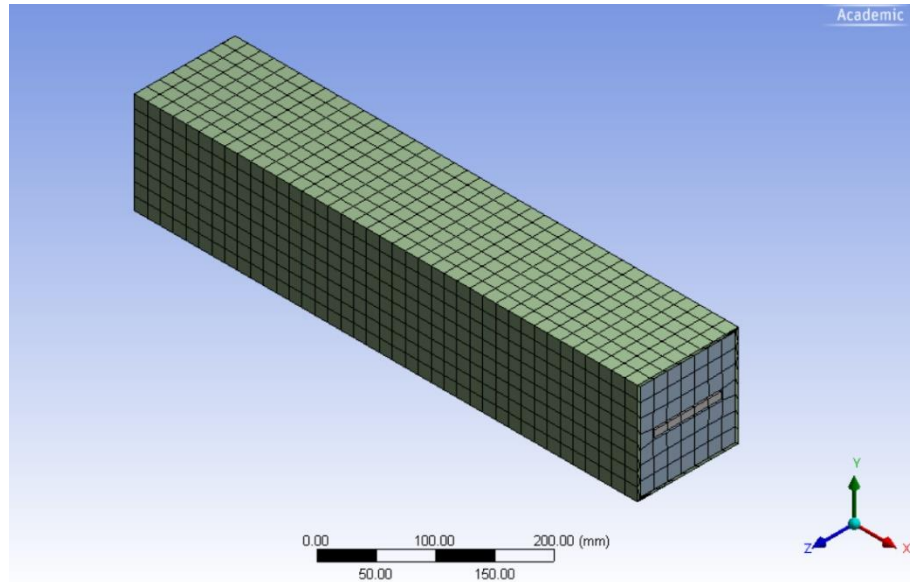
Figure 4.5 – Mesh detailing for BRB analytical model

4.1.4 BRB Analytical Model Boundary Conditions and Applied Displacement

As previously mentioned, to reduce computational time and effort, the specimen was only modeled and analyzed over the length of its encased core. In terms of boundary conditions, to simulate the uniaxial test, the face of the core plate on one end was fixed, which prevents translations or rotations in any direction. A displacement corresponding to the test peak displacement (approximately 1.38 in. or 35 mm) was applied at the other face of the steel core. The displacement was applied in the negative x-direction to simulate compressive forces.

4.1.5 BRB Analysis and Results

Figure 4.6 shows the calculated and measured force-deformation relationships for SP3. A reasonable accuracy was achieved. Figure 4.7 shows the equivalent stress and equivalent total strain contours for the BRB model. It was seen that all nonlinearity was concentrated to the steel core, which is desired and observed in the test. Note the grout and encasing tube were not shown for clarity.

Overall, it can be concluded that the proposed FE model is sufficiently accurate in reproducing the BRB global and local behavior. This analytical model is used later in this study to simulate the behavior of replaceable buckling restrained fuses (BRFs).
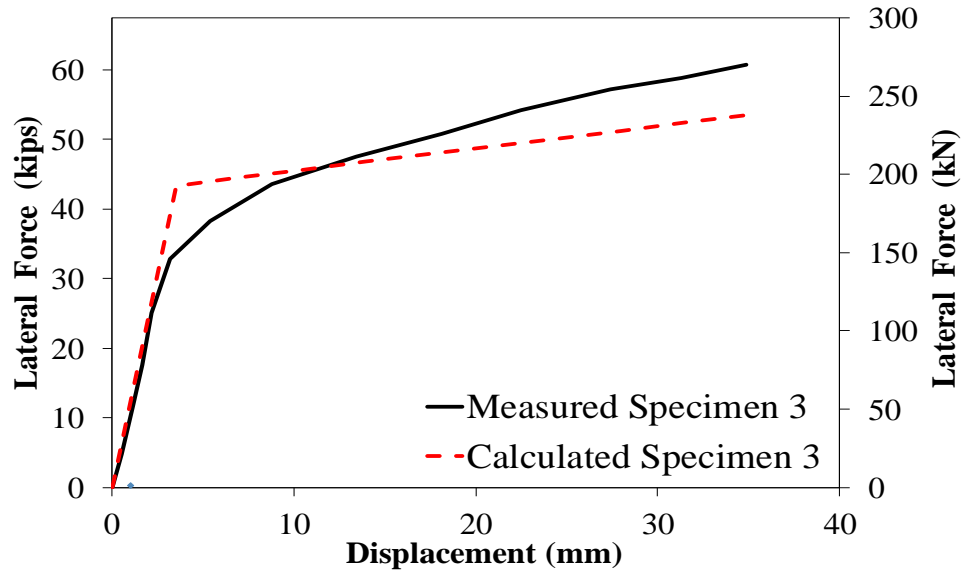
Figure 4.6 – Calculated and measured and force-deformation behavior for BRB tested by Gheidi, et al. (2011)
[Test data reprinted with the author's permission]
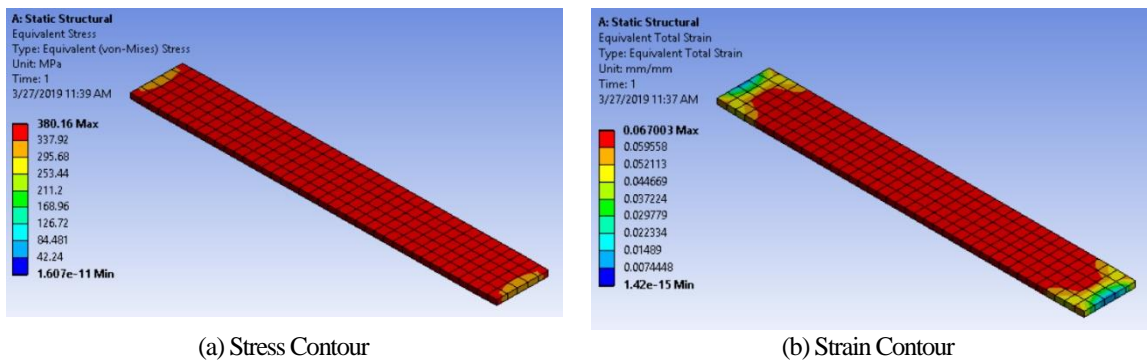
(a) Stress Contour   (b) Strain Contour
Figure 4.7 – Calculated Stress and Strain Distribution for BRB tested by Gheidi, et al. (2011)

4.2 Steel Moment-Resisting Beam-Column Joint Modeling

4.2.1 Beam-Column Test Specimen

Upon validation of the BRB component FE modeling procedure, it is desirable to

validate the overall structural behavior of a moment-resisting beam-column assembly. The

specimen considered was a cover-plate moment-resisting beam-column joint tested by Kim

et al. (2002). Figure 4.8 shows the general test setup, and Fig. 4.9 shows the joint details

for RC01, which consisted of a W14x176 column, a W30x99 beam, cover plates on the top

and bottom flanges of the beam, and column stiffeners. Displacement was applied at the

free end of the beam using an actuator, and the column was supported at the top and

bottom.
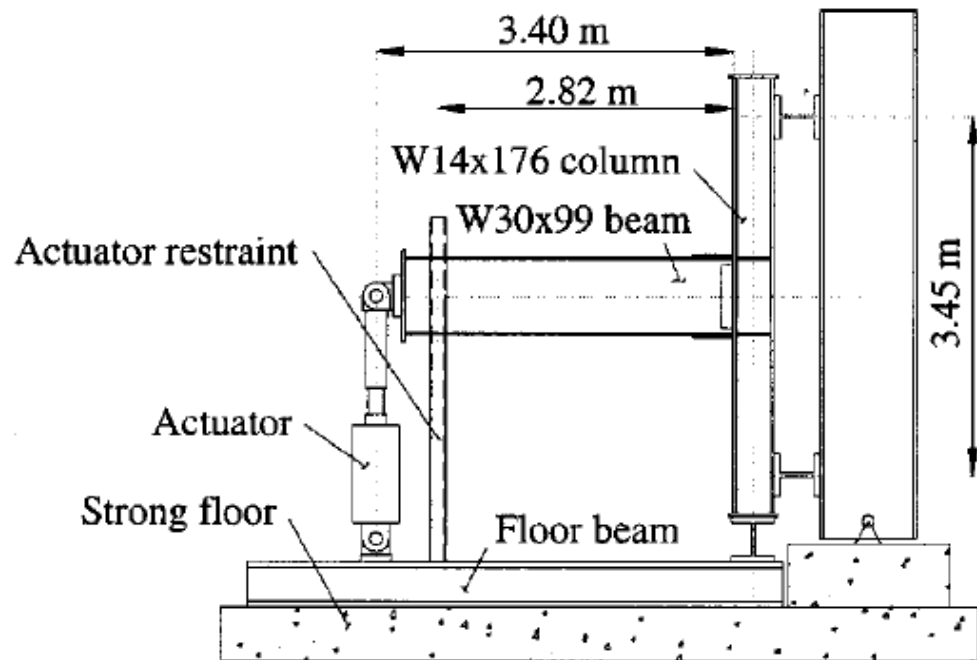
Figure 4.8 – Test setup for beam-column specimen RC01 tested by Kim et al. (2002)
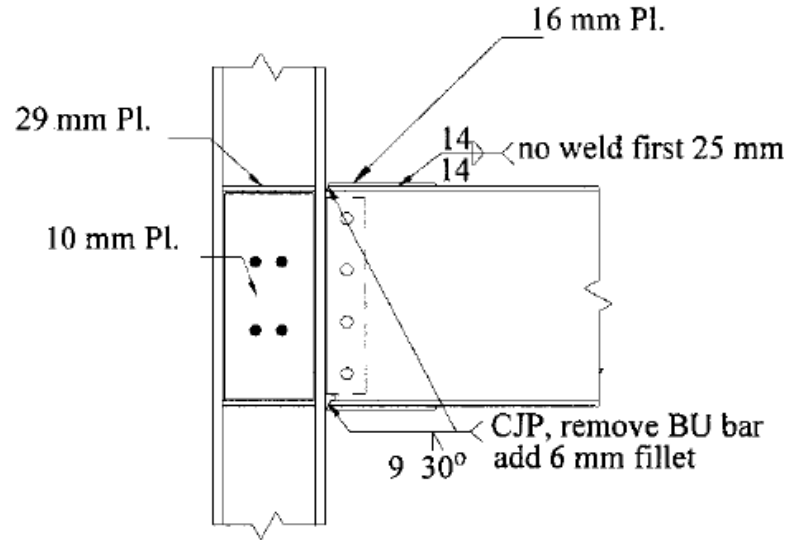
Figure 4.9 – Detailing of beam-column specimen RC01 (Kim et al., 2002)

4.2.2 Beam-Column Test Specimen Material Properties

Table 4-2 presents the measured engineering material properties used in RC01. Figure

4.10 shows the measured stress-strain diagram for the steel used in RC01 obtained from a

coupon test. In FEA, true material properties are needed, which are also shown in the

table. A multilinear kinematic hardening material model was used for all steel components.

Table 4.2 – Measured Material Properties for RC01 Tested by Kim et al. (2002)

Component	Material	Measured Material Properties		ANSYS Bilinear Properties
Beam and Column	Structural Steel	Yield Stress, ksi (MPa)	53.5 (368.9)	53.6 (369.6)
		Ultimate Stress	71.6 (493.7)	78.1 (538.5)
		Yield Strain	0.0018	0.0018
		Ultimate Strain	0.09	0.0086
Plates	Structural Steel	Yield Stress	53.0 (365.4)	53.1 (366.1)
		Ultimate Stress	72.0 (496.4)	78.5 (541.2)
		Yield Strain	0.0018	0.0018
		Ultimate Strain	0.09	0.086

Note: True material properties used in the analysis instead of engineering values.
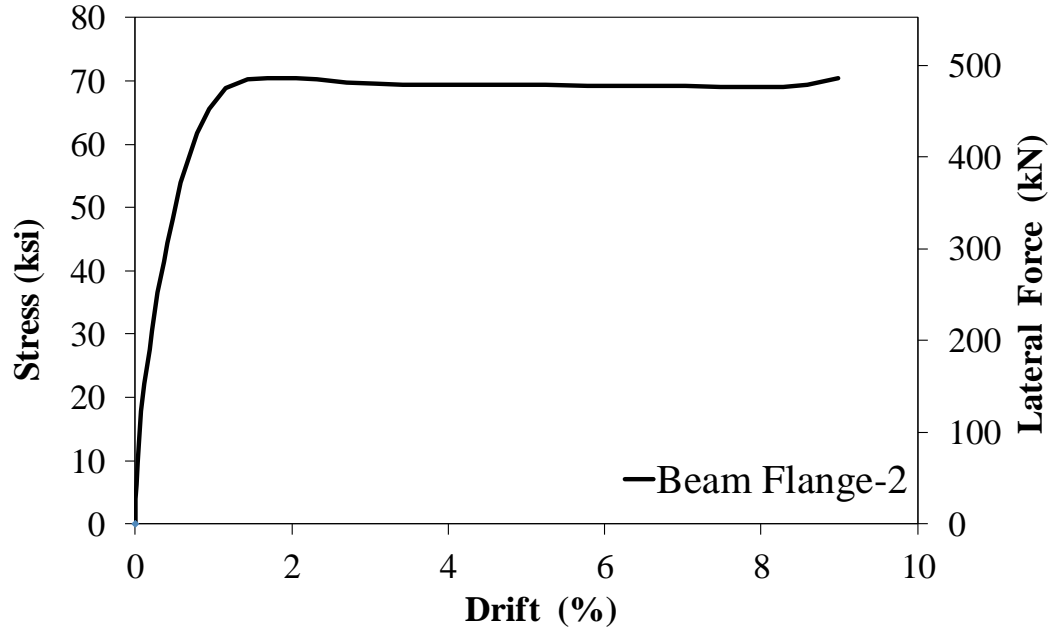
Figure 4.10 – Measured stress-strain relationship for beam flange of RC01 (Kim et al., 2002)

4.2.3 RC01 Beam-Column Analytical Model

FEA was carried out to simulate the behavior of RC01 using ANSYS version 18.2

(2017) static structural system. The specimen geometry was generated using the ANSYS

built-in SpaceClaim tool (Fig. 4.11).
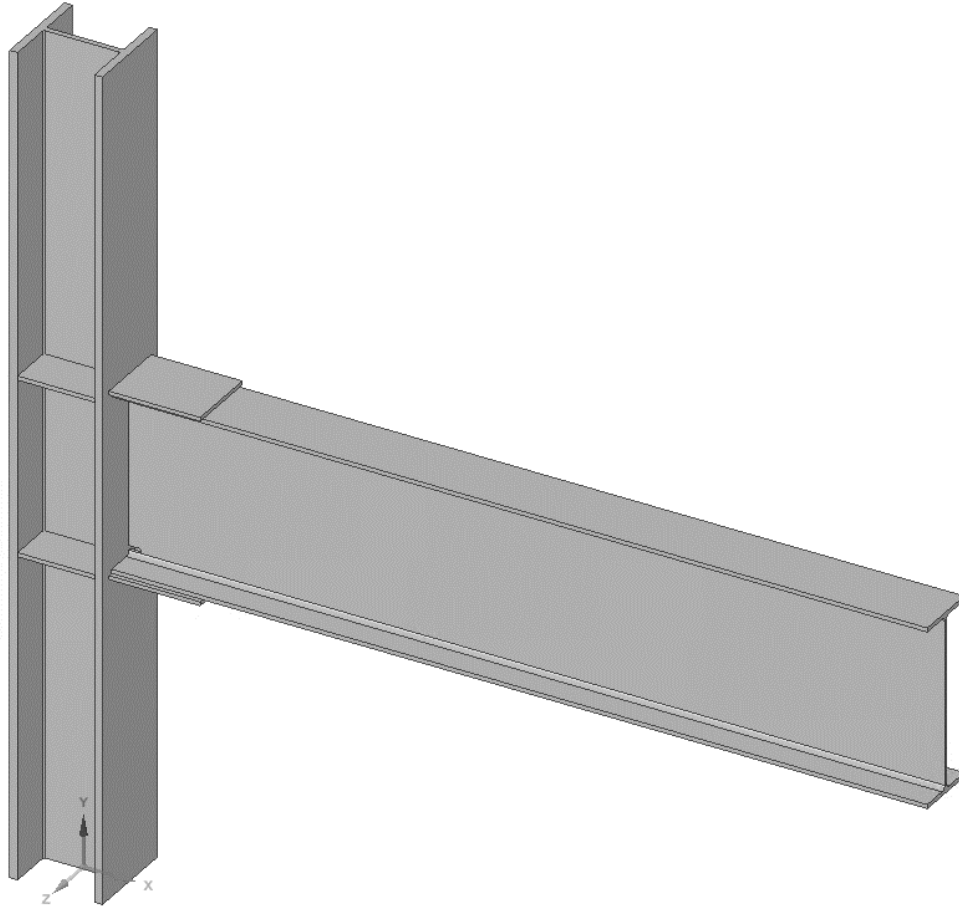
Figure 4.11 – Beam-column Specimen RC01 ANSYS model

4.2.4 Beam-Column Analytical Model Connections and Contact Regions

Since all components in the beam-column assembly were welded, all contact regions were assumed to be bonded. All connecting regions were inspected to ensure that all of the bodies/faces accurately represented that of the actual connection.

4.2.5 Beam-Column Analytical Model Meshing

A user-specified fine mesh was used in the analysis (Fig. 4.12), which consisted of 17465 nodes and 36522 elements. The analysis was stopped once the maximum strain in the beam was reached, therefore a face mesh was applied under the beam flange to refine the mesh and to produce more accurate results.
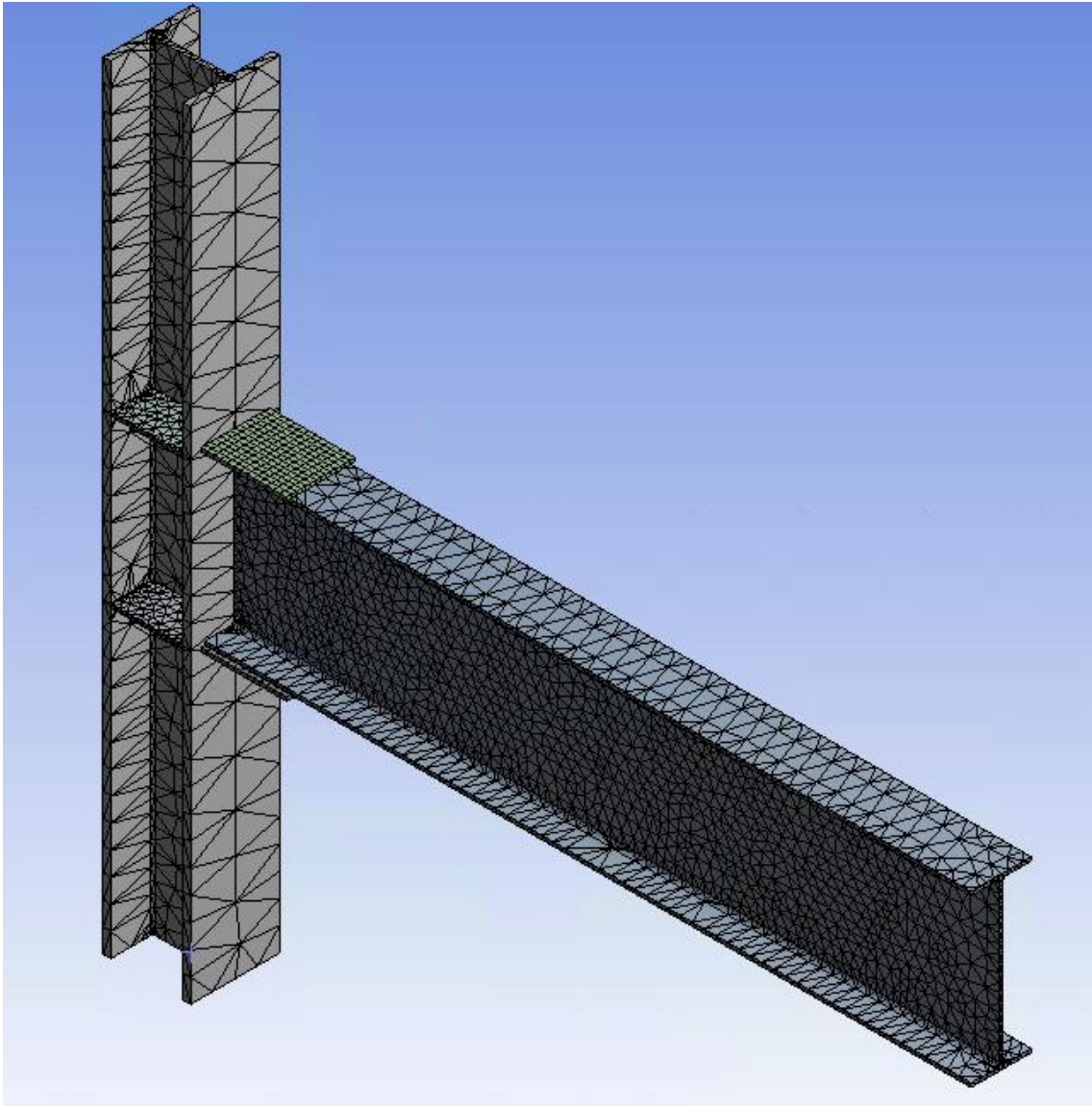
Figure 4.12 – Mesh detailing for beam-column specimen RC01

4.2.6 Beam-Column Analytical Model Boundary Conditions and Applied Displacements

To match the test boundary conditions, restraints at the top and bottom of the column were included to prevent translations in any direction. The bottom support was also restrained against rotation in all directions, while the top support was restrained from rotation in the x and y directions. The beam was a cantilever, so the beam end remained

free from any restraints. Displacements were applied at the free end of the beam until failure was observed.

4.2.7 Beam-Column Analysis and Results

Total deformation of the beam end to calculate drift ratio, reactions at the top and bottom of the column, and the strain distribution in the beam to determine the failure point were processed in the FEA. The failure point is defined where the steel reaches its ultimate strain.

Figure 4.13 shows the calculated and measured force-displacement relationships for RC01. A reasonable accuracy was observed in terms of initial stiffness and the strength. However, the drift capacity was significantly overestimated by a factor of 2.1. Also included in this figure is the design code calculated strength based on the beam plastic moment (AISC Steel Construction Manual, 2011). The moment was then divided by the beam length to determine the joint strength. The code-calculated strength without any reduction factor was 15% lower than the measured strength.
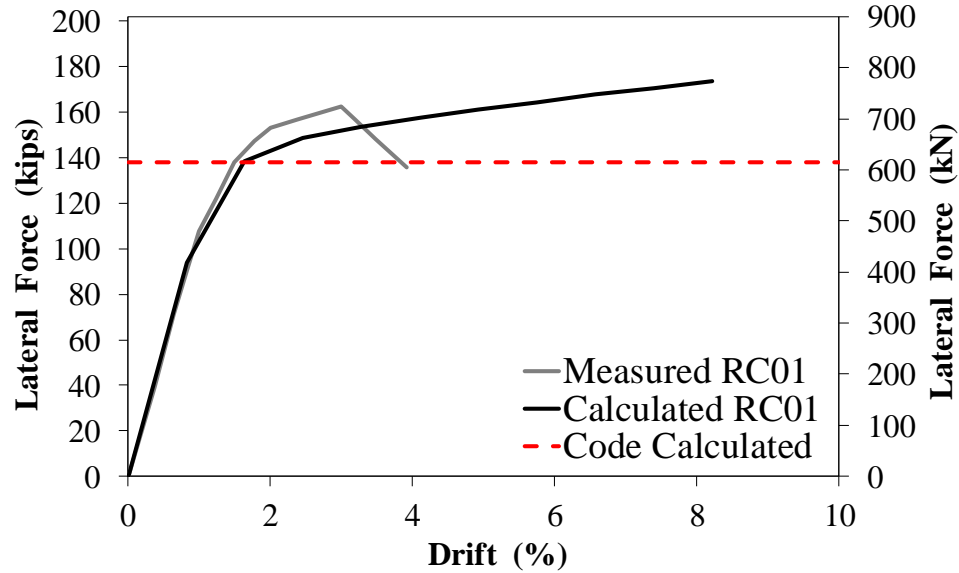
Figure 4.13 – ANSYS Calculated and measured force-drift relationships for beam-column specimen RC01

Figure 4.14 shows the calculated stress and strain contours for RC01. The maximum stresses and strains were observed at the end of cover plates, which also correlate to the results obtained from the experiment.

(a) Stress Contour   (b) Strain Contour
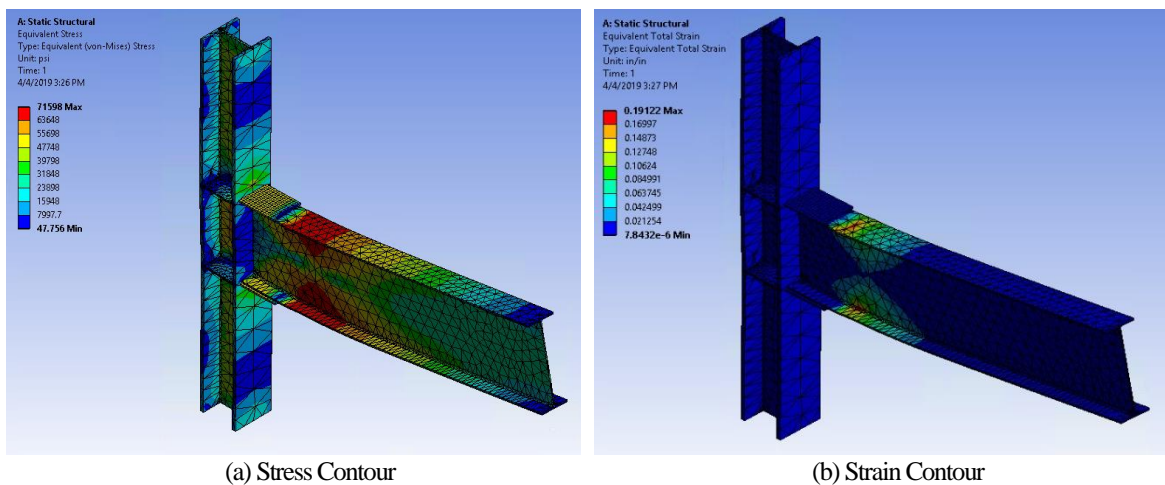
Figure 4.14 – ANSYS calculated stress-strain distribution for beam-column specimen RC01

4.2.8 Alternative Modeling Method for Beam-Column Specimen RC01

ANSYS is a general and robust FEA software. However, the computational time for large structures or systems is excessive. OpenSees (2013), the Open System for Earthquake Engineering Simulation, is an alternative FE software that is programmed to quickly solve large size problems. This software is also used to simulate the behavior of RC01.

A three-dimensional (3D) fiber-section model (Fig. 4.15) consisting of five nodes and four elements was generated to represent RC01. All elements were modeled using the "nonlinearBeamColumn" element. The nodal coordinates correspond to the centerline of the structural elements. The nodes at the top and bottom of the column were restrained from translations, similar to the ANSYS model. Opensees has a library of material models for steel and concrete. To identify the best material model for steel, three different models were used: Steel02 (Fig. 4.16), Hysteretic (Fig. 4.17) and Multilinear (Fig. 4.18). The measured material properties (Table 4.2) were used as the input for these models.
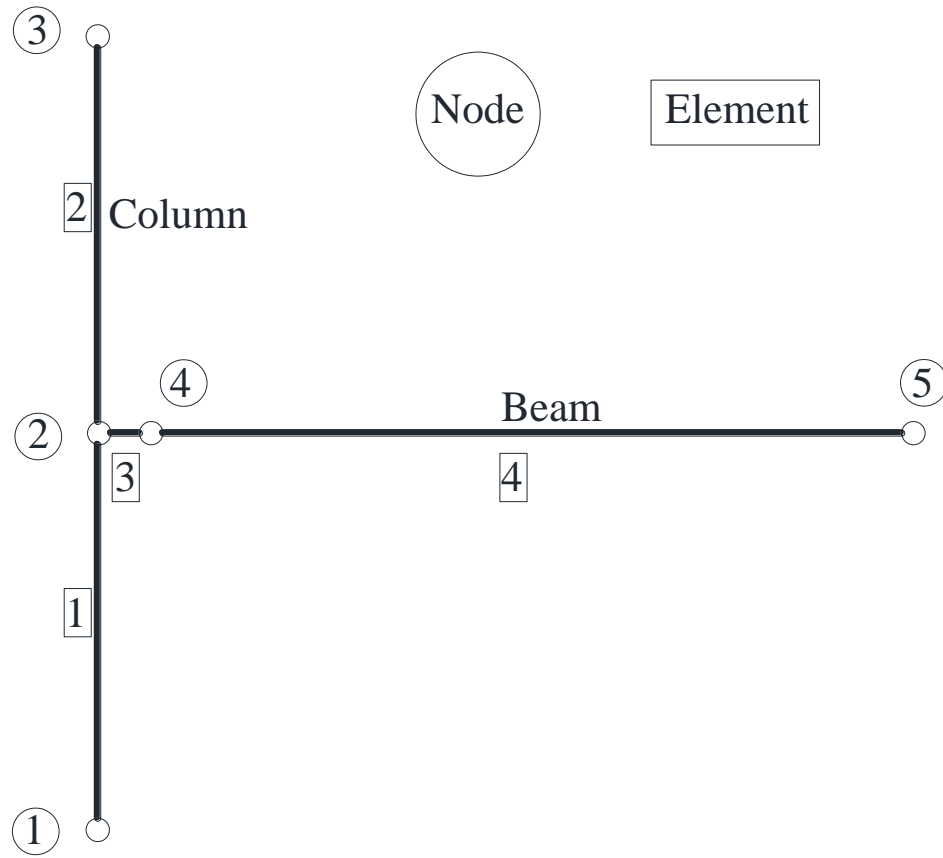
Figure 4.15 – OpenSees model for beam-column specimen RC01
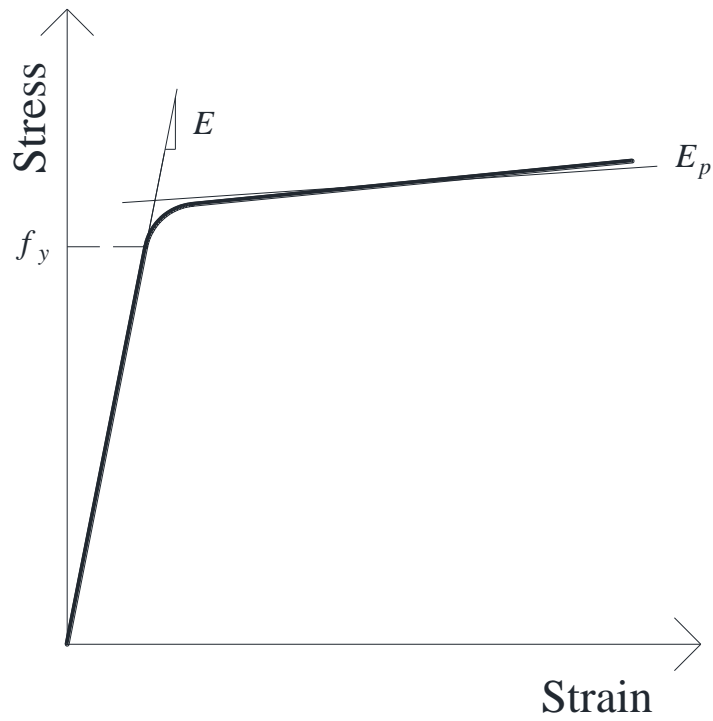
Figure 4.16 – OpenSees Steel02 material model
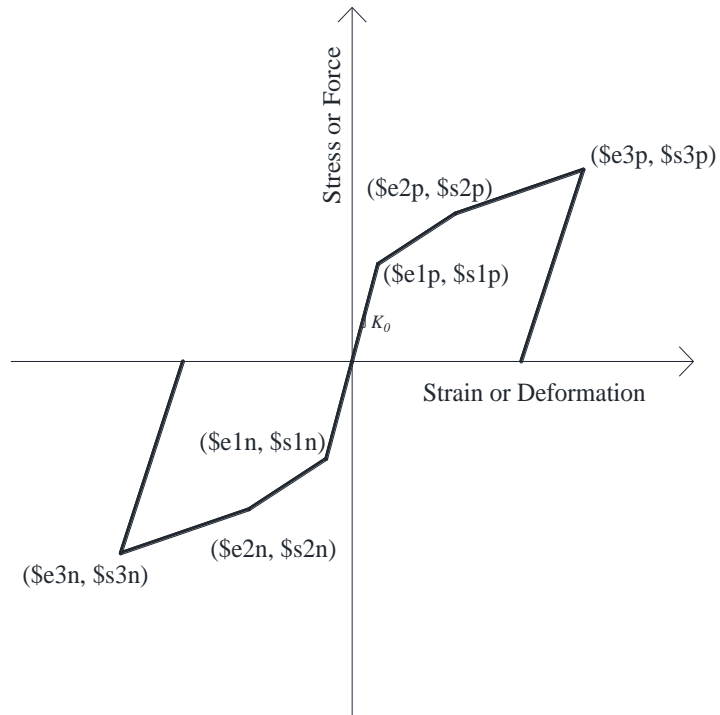
Figure 4.17 – OpenSees Hysteretic material model
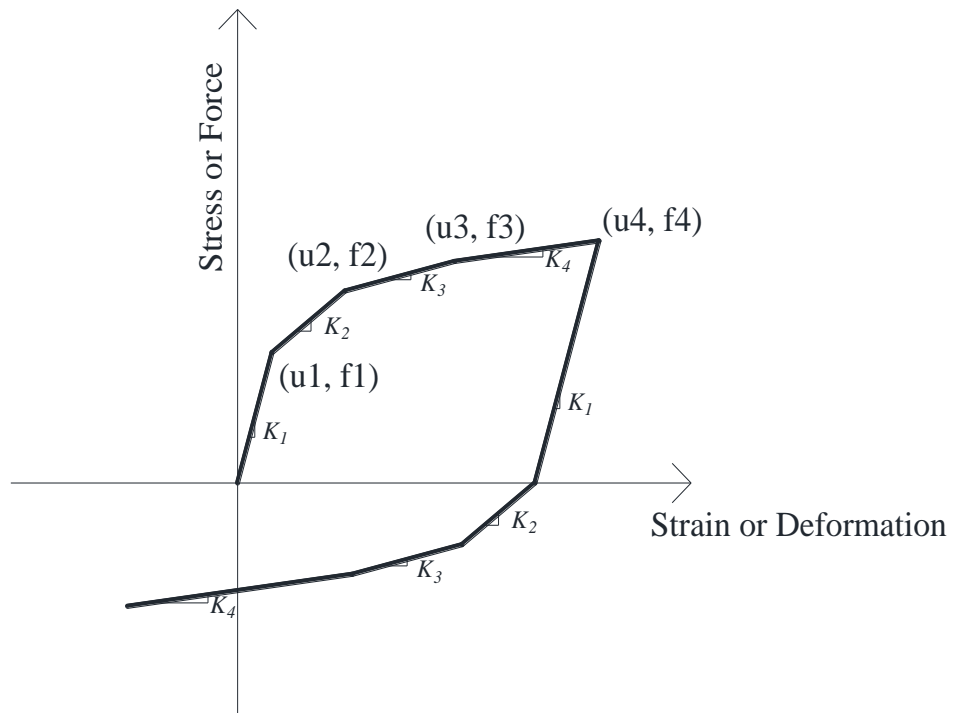
Figure 4.18 – OpenSees Multilinear material model

Figure 4.19 shows the OpenSees calculated and measured force-deformation relationships for RC01. The calculated data obtained from the ANSYS analysis is also included for completeness. It can be inferred that all three material models used in OpenSees resulted in the same behavior. However, the use of "Hysteretic" or "Multilinear" model is recommended since they can show an abrupt drop in the strength when the steel fiber reaches its strain capacity. This will help to determine the displacement capacities especially when a large structure is analyzed. Furthermore, the OpenSees responses are in good agreement with the ANSYS response. As was discussed, both models could reproduce the test data with a reasonable accuracy. However, both analytical tools overestimated the drift capacity of RC01 by a factor of two. A reduced ultimate strain may be used to calibrate both ANSYS and OpenSees models to capture the ultimate displacement. For example, using 4% strain capacity for steel (instead of 9% from the coupon test) will result in a perfect match with the test displacement capacity. Overall, the proposed modeling procedure using OpenSees is viable, and may be used in the analysis of large size structures.
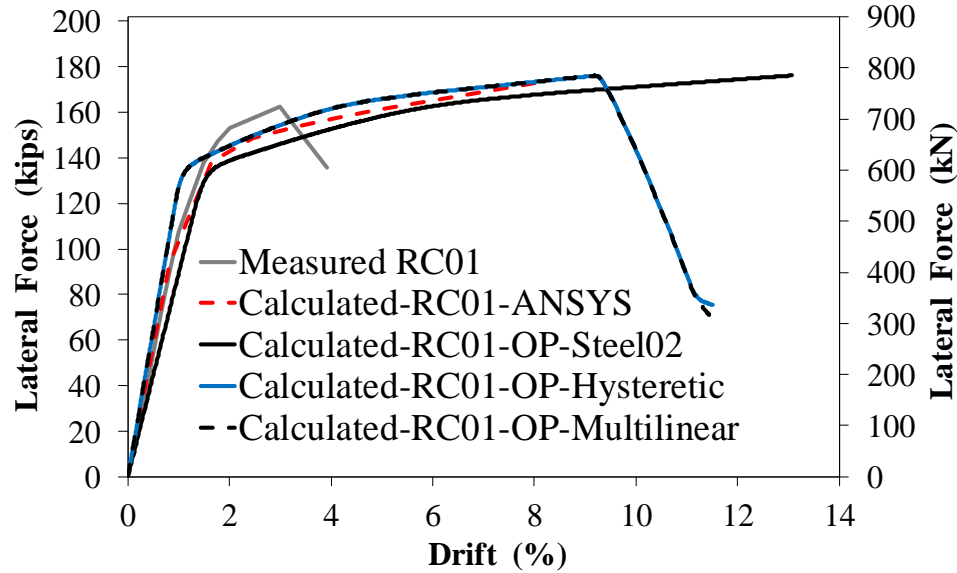
Figure 4.19 – OpenSees Calculated and measured force-drift relationships for beam-column specimen RC01

4.3 Buckling Restrained Fuse Repairable Joint Modeling

The modeling method and the verification for a conventional moment-resisting beam-column joint tested by Kim et al. (2002) were discussed in the previous section. The detailing of the reference beam-column specimen was modified using the proposed repairable details (Ch. 3) and then FEA were performed to investigate the structural performance of the repairable joints. This section discusses the modeling methods and results for two repairable joints: one incorporating buckling restrained fuses (BRFs) and a shear pin at the middle of the BRF (BRF-M), and another joint incorporating BRFs and a shear pin at the end of the beam (BRF-B). The modeling methods previously discussed for BRB and the beam-column specimen were used as the baseline of the analysis for the repairable joints. Note BRF is a miniature version of BRB and thus the BRB modeling methods can be used for BRF.

4.3.1 Joints with BRFs and Hinge at Middle of Fuse (BRF-M)

Figure 4.20 shows the BRF-M analytical model developed in ANSYS. The BRFs on the top and bottom of the beam flanges were designed to resist the tensile and compressive axial forces, while buckling is restrained due to the encasing mechanism. All elements are designed to remain linear elastic, while all nonlinearity is to be concentrated in the core of the BRF. The BRF component could then be replaced upon failure of the core after a severe event.

To keep the beams and columns linear elastic, either the BRF should be downsized or the beams and columns should be oversized. The former will result in a lower lateral strength compared to conventional moment-resisting frames and the latter can result in a same later strength when compared to conventional frames. In this chapter, the latter is selected to match the joint strength.

RC01 was constructed using a W30x99 beam and a W14-176 column. The repairable version of that was made of HP18x204 for both the beam and column. The moment capacity of this steel profile is 28% higher than that for W30x99, and it provides sufficient flange width to accommodate BRFs. BRFs were designed according to a simple method proposed at the end of this chapter.
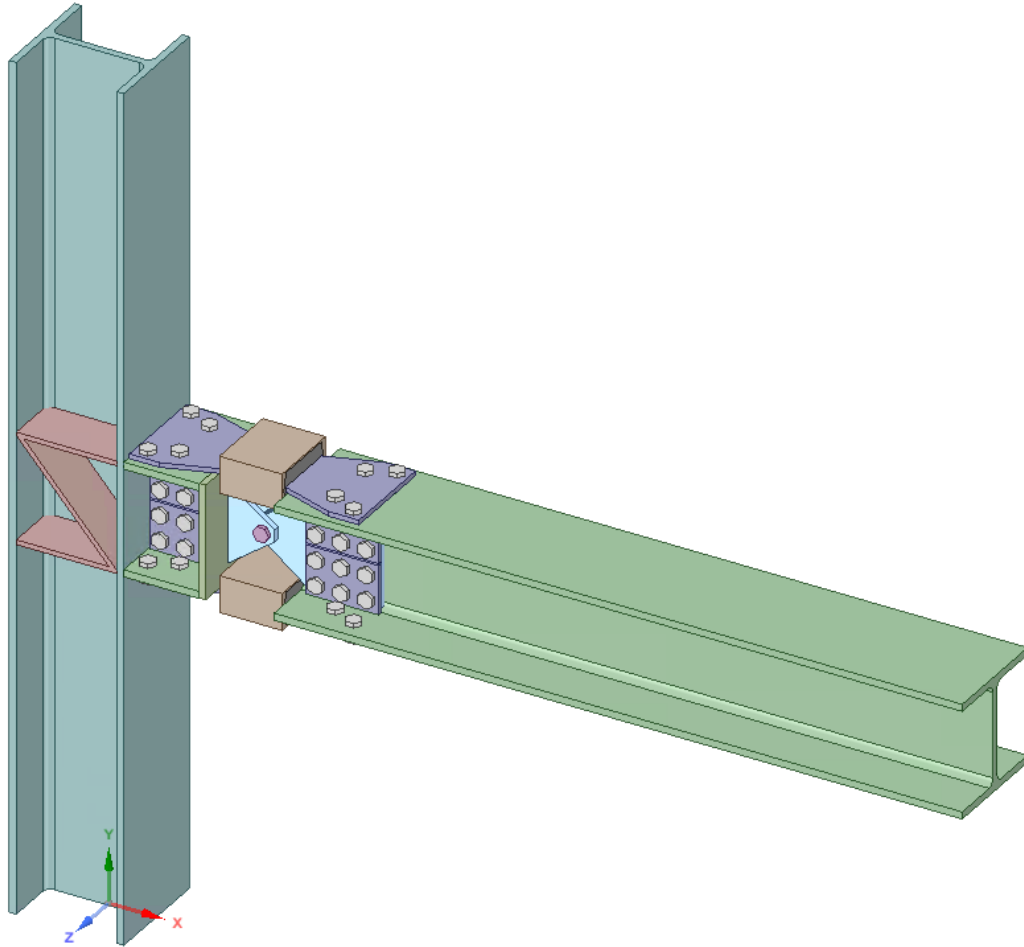
Figure 4.20 – BRF-M ANSYS model

4.3.1.1 BRF-M Material Properties

Table 4.3 presents the specified engineering material properties used in the FEA. The steel component material properties were according to the AISC Steel Construction Manual (2011). Grade 55 steel was used for the beam, column, and column stiffeners. The core of the BRF, and the shear plates are of a Grade 80 steel. The encasing BRF tube is A36 steel, and the grout was of a nonlinear concrete material model. A325 bolts were used. A bilinear stress-strain relationship was used for all steel components as shown in Fig. 4.21.

Table 4.3 – Specified Material Properties for Repairable Joints Using BRFs

Component	Material	Measured Material Properties		ANSYS Bilinear Properties
HP Beam, HP Column, Stiffeners	Grade 55 Structural Steel	Yield Stress, ksi (MPa)	55.0 (379.2)	55.1 (379.9)
		Ultimate Stress, ksi (MPa)	70.0 (482.6)	80.5 (555.0)
		Yield Strain	0.0019	0.0019
		Ultimate Strain	0.15	0.14
BRF Core and Shear Plates	Grade 80 Structural Steel	Yield Stress, ksi (MPa)	86.0 (593.0)	86.3 (595.0)
		Ultimate Stress, ksi (MPa)	105.0 (724.0)	122.9 (847.4)
		Yield Strain	0.0030	0.0030
		Ultimate Strain	0.17	0.16
BF Encasing Tube	A36 Structural Steel	Yield Stress, ksi (MPa)	36.0 (248.2)	36.1 (248.9)
		Ultimate Stress, ksi (MPa)	58.0 (399.9)	58.1 (400.6)
		Yield Strain	0.0012	0.0012
		Ultimate Strain	0.19	0.17
Grout as Tube Filler	Concrete	28 Day Compressive Strength, ksi (MPa)	4.0 (27.6)	N/A
		Modulus of Elasticity, ksi (MPa)	3605.0 (24855.6)	N/A
A325 Bolts	Structural Steel	Yield Stress, ksi (MPa)	81.0 (558.5)	81.3 (560.5)
		Ultimate Stress, ksi (MPa)	120.0 (827.4)	120.4 (830.1)
		Yield Strain	0.003	0.003
		Ultimate Strain	0.14	0.13

Note: True material properties were used in FEA instead of engineering values.
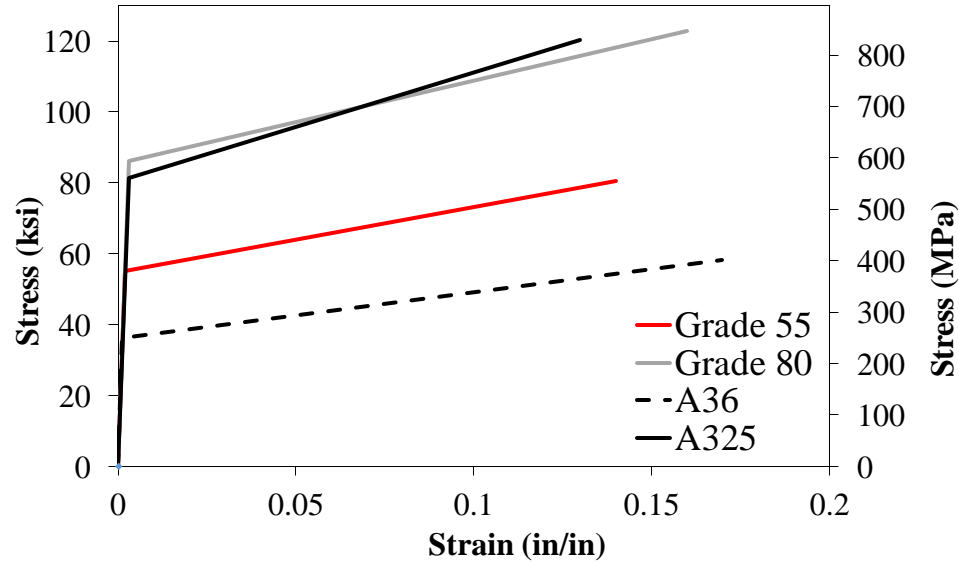
Figure 4.21 – Structural steel material properties used in repairable joints

4.3.1.2 BRF-M Connections and Contact Regions

As previously mentioned, ANSYS automatically generates bonded contacts between any structural faces. However, a frictional contact was used between the shear pin and the shear connecting plates with a coefficient of 0.2, and between the BRF steel core and the grout with a coefficient of 0.3 (see Sec. 4.1). It should be noted that contacts between stiffener bolts/holes and core bolts/holes were also assigned to be bonded due to convergence issues. Furthermore, this assumption will result in a stiffer force-displacement response for the repairable joints with lower displacement capacity, which is conservative.

4.3.1.3 BRF-M Meshing

A user-specified medium mesh was used in the analysis, which consisted of 50381 nodes and 21644 elements (Fig. 4.22). A "MultiZone" meshing technique with a "hexa" mesh type was used for the grout and shear connecting plates. The automatically generated mesh was not sufficient in that these components had only one element through the thickness, therefore a refined mesh had to be applied to aid in convergence issues.
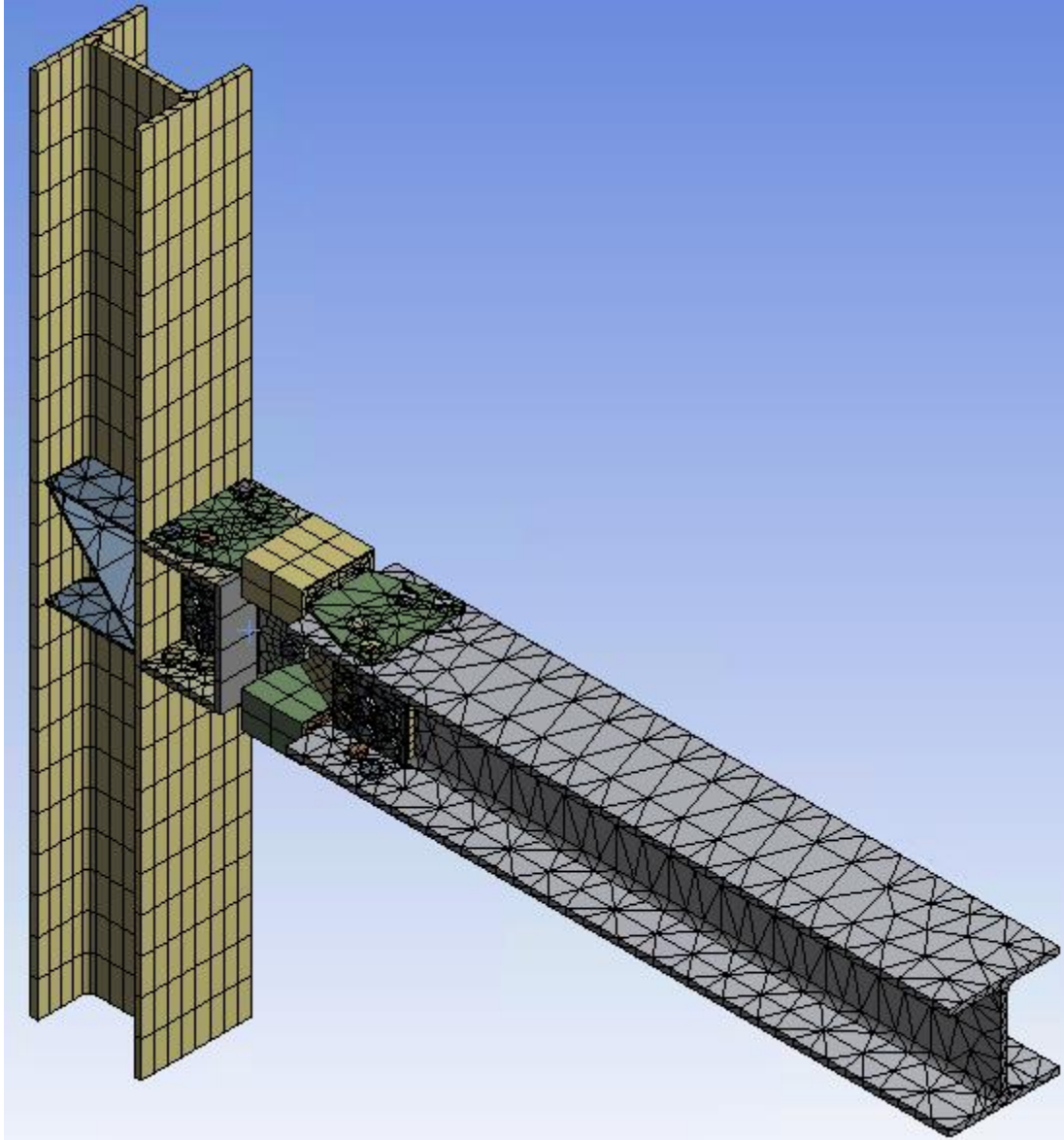
Figure 4.22 – Mesh detailing for BRF-M

4.3.1.4 BRF-M Boundary Conditions and Applied Displacements

The boundary conditions and the loading regime were the same as those discussed for

RC01 (Sec. 4.2).

4.3.1.5 BRF-M Analysis and Results

Figure 4.23 shows the calculated force-drift relationship for the BRF-M alternative.

The measured and calculated responses of RC01were added for completeness. The

proposed repairable detailing showed a lower initial stiffness (approximately 34%) and achieved the same lateral strength compared to the conventional joint. However, the proposed detailing exhibited significantly higher drift capacity (more than twice). It can be concluded that the proposed repairable detailing can improve the seismic performance while providing reparability after a severe earthquake.
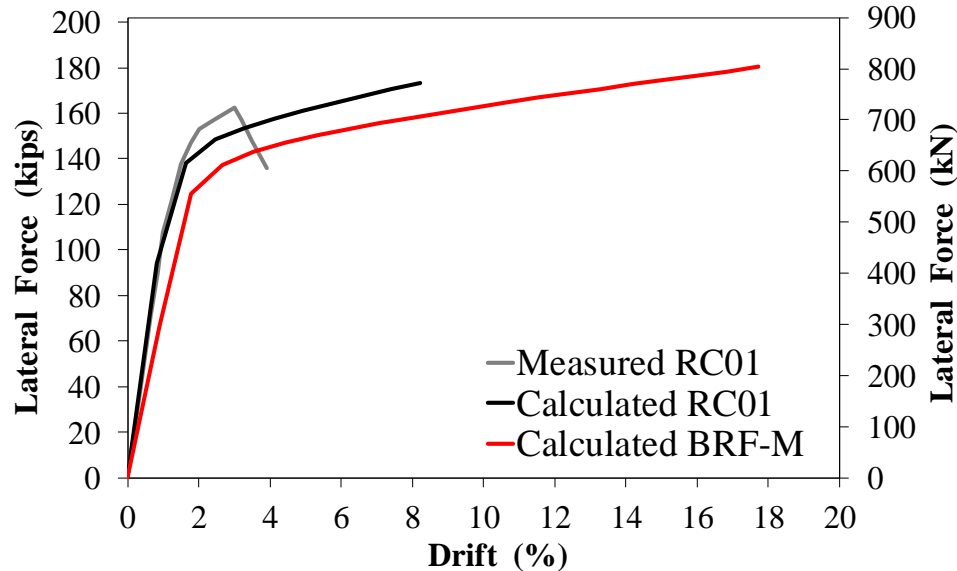
Figure 4.23 – ANSYS Calculated force-displacement relationships for BRF-M

Figure 4.24 shows the stress and strain distribution for BRF-M. It can be seen that the yielding and damaged was concentrated in the core of BRF while some minor yielding occurred in other elements. Therefore, the design objective was met.

(a) Stress Contour   (b) Strain Contour
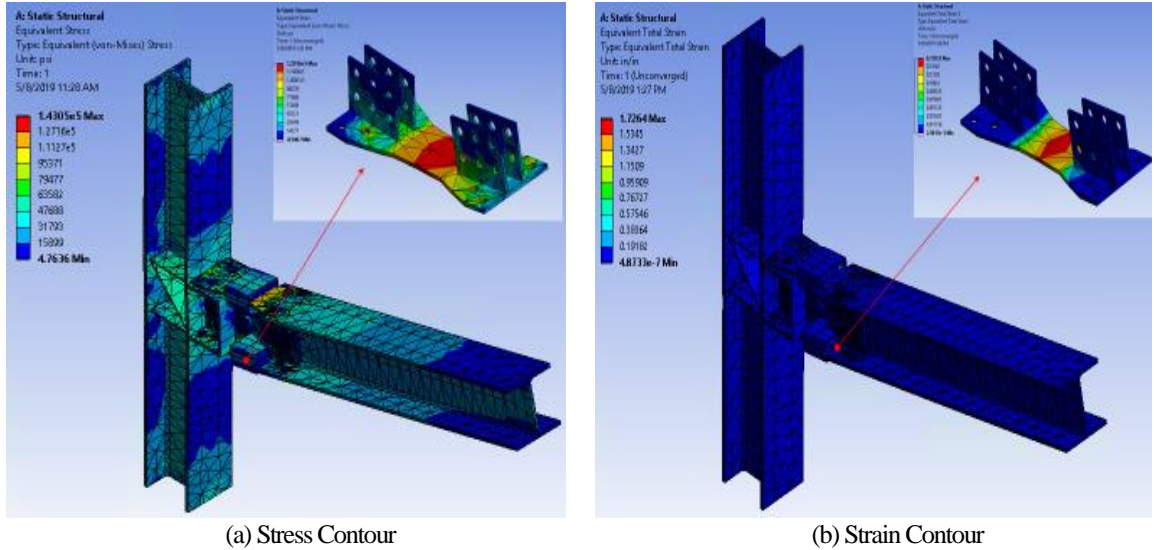
Figure 4.24 – ANSYS calculated stress-strain distribution for BRF-M

4.3.2 Joints with BRFs and Hinge at Beam End (BRF-B)

Figure 4.25 shows the proposed BRF-B model developed in ANSYS. Similar to BRF-M, compressive and tensile axial forces are resisted by the BRF component, and buckling is prevented by the encasing mechanism. All elements are designed to remain elastic, while all nonlinearity is designed to occur within the yielding steel core of the BRF. The BRF is then able to be replaced upon failure of the core. The sizes of the beam and column remained the same as the BRF-M alternative discussed in the previous section.
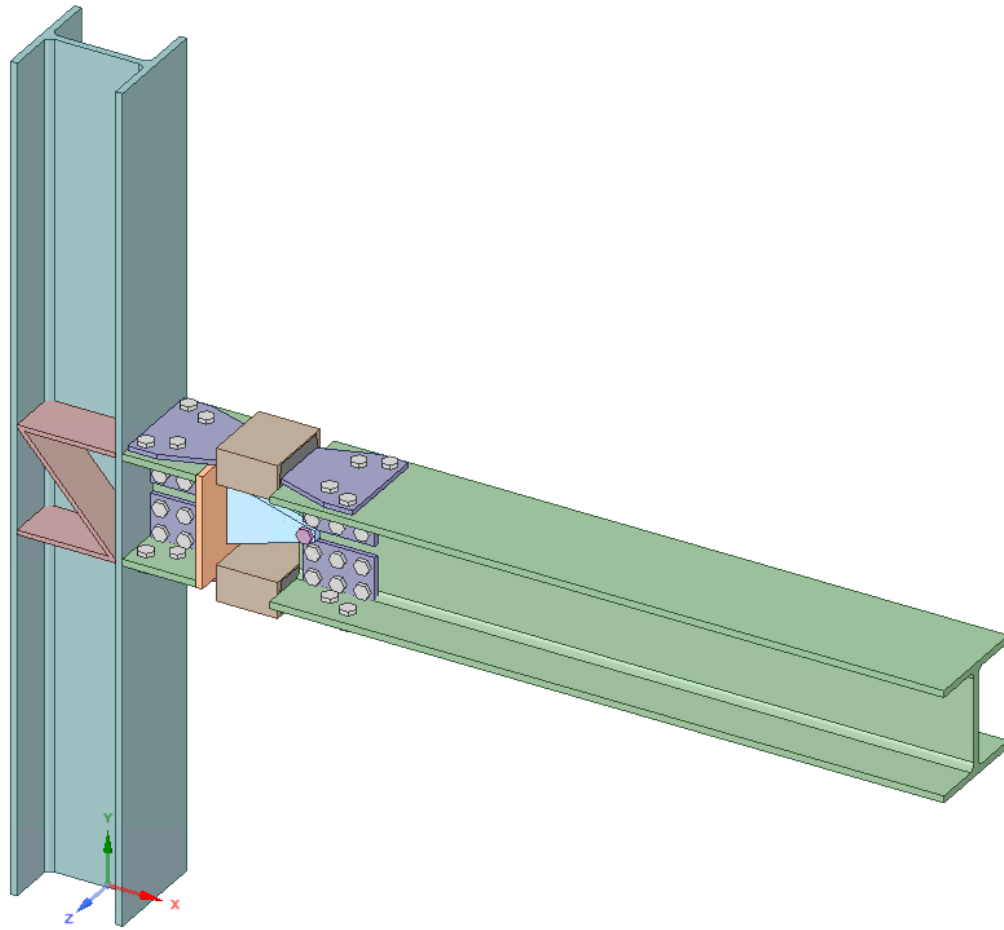
Figure 4.25 – BRF-B ANSYS model

4.3.2.1 BRF-B Material Properties

The material properties used for this model were the same as those used in BRF-M

listed in Table 4-3, with the steel bilinear stress-strain relationship shown in Fig. 4.21.

4.3.2.2 BRF-B Connections and Contact Regions

The same contact regions were defined for this alternative as those that were previously

discussed in section 4.3.1.2.

4.3.2.3 BRF-B Meshing

A user-specified medium mesh was used in the analysis, which consisted of 63252 nodes and 25845 elements (Fig. 4.26). Similar to BRF-M, a "MultiZone" meshing technique with a "hexa" mesh type was applied to the grout and shear connecting plates, and a refined mesh had to be applied to aid in convergence issues.
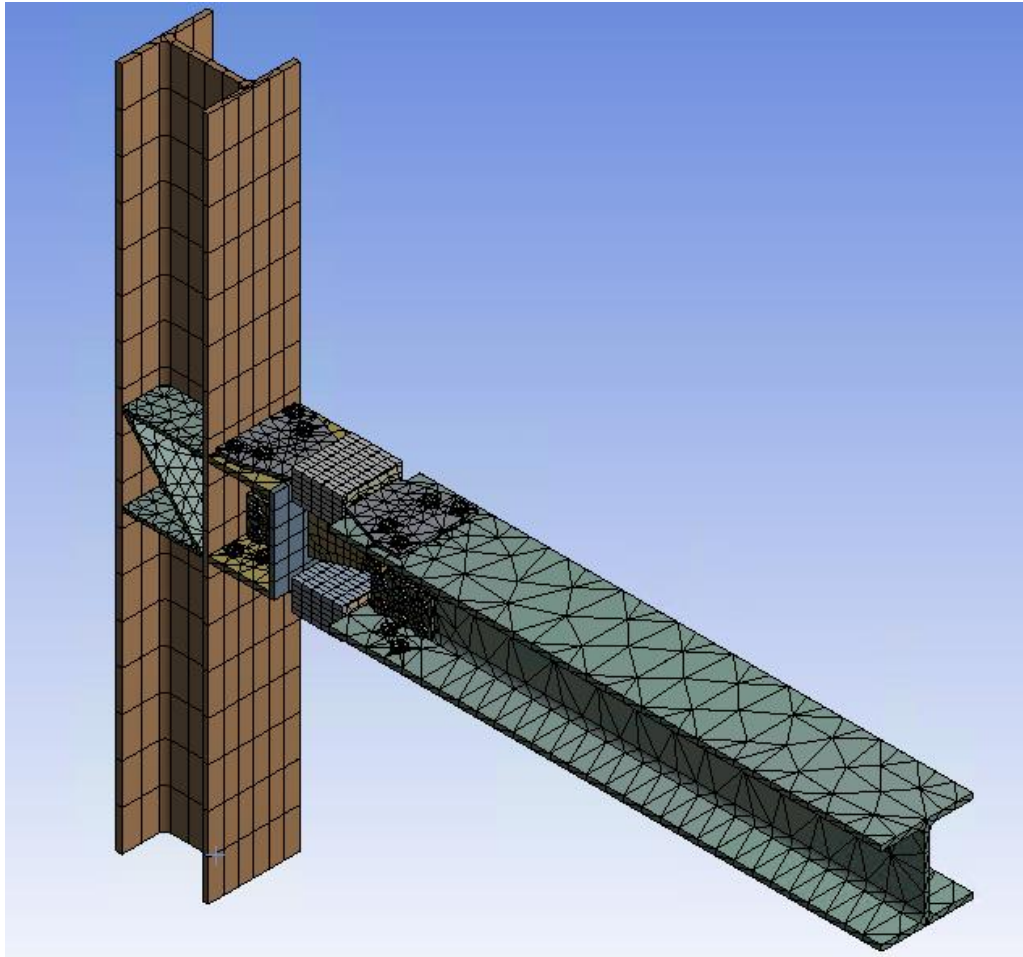
Figure 4.26 – Mesh detailing of BRF-B

4.3.2.4 BRF-B Boundary Conditions and Applied Displacements

The boundary conditions and loading regime were the same as those discussed for RC01 (Sec. 4.2).

4.3.2.5 BRF-B Analysis and Results

Figure 4.27 shows the calculated force-drift relationship for the BRF-B alternative. The measured and calculated RC01 responses were added for completeness. The proposed repairable detailing showed a lower initial stiffness (44%) and achieved the same lateral strength compared to the conventional joint. However, the proposed detailing exhibited significantly higher drift capacity (more than twice). It can be concluded that the proposed repairable detailing can improve the seismic performance while provide reparability after a severe earthquake.
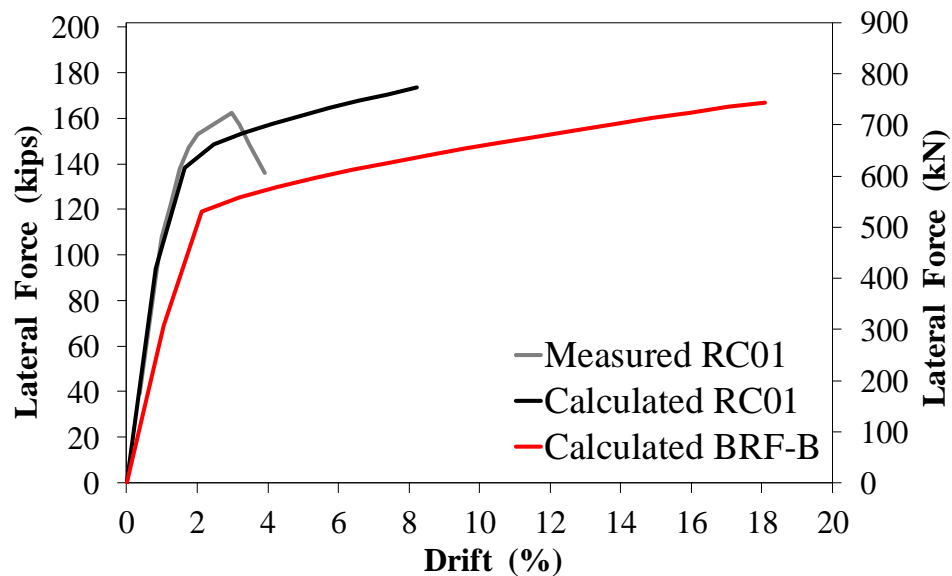
Figure 4.27 – ANSYS Calculated force-displacement relationships for BRF-B

Figure 4.28 shows the stress and strain distribution for BRF-B. It can be seen that the yielding and damaged was concentrated in the core of BRF while some minor yielding occurred in other elements. Therefore, the design objective was met.

(a) Stress concentration   (b) Strain concentration
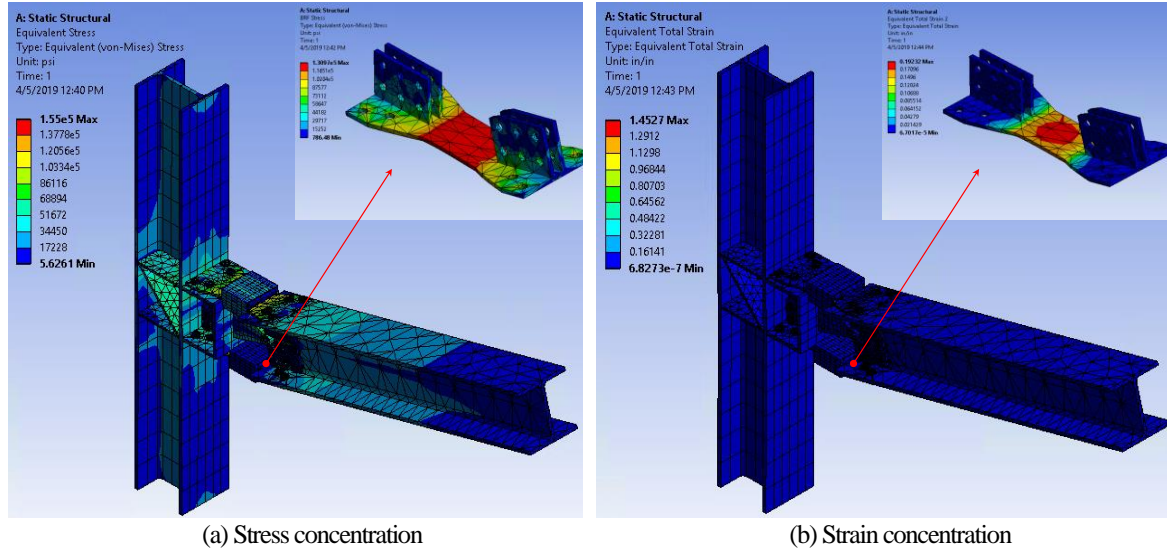
Figure 4.28 – ANSYS solution results for BRF-B

4.4 Buckling Restrained Reinforcement Repairable Joint Modeling

Buckling restrained reinforcement (BRR) can also be used in repairable joints. OpenSees was used to investigate the seismic performance of repairable detailing using BRR. Chapter 3 includes three alternatives: joints incorporating BRR and a shear pin at the middle of BRR (BRR-M), joints incorporating BRR and a shear pin at the beam end (BRR-B), and joints incorporating BRR and a shear pin at the column face (BRR-C).

As discussed previously, OpenSees will provide a quick solution for large size problems. In an attempt to use this software for multi-story repairable steel buildings, a component-level verification is needed. Since there is no test data on the proposed repairable joints, the response of an OpenSees model of BRF-M is compared with that of ANSYS.

4.4.1 BRF-M Model Using OpenSees

Figure 4.29 shows a 3D OpenSees model of BRF-M using 16 nodes and 16 elements (a significant reduction in the problem size compared with the ANSYS model). The steel

core of BRFs was modeled using a nonlinear truss element. To form the joint, BRF

elements were horizontally connected to linear elastic elements. Then, vertical linear

elastic elements were used to form the beam depth and to connect the BRF elements to the

beam elements. To model the shear pin, the rotation at the connecting ends of the beam

elements was released using the "equalDOF" function of OpenSees. A

"nonlinearBeamColumn" element using "Steel02" material model was used for the beam

and column elements. "Hysteretic" material model (Fig. 4.17) was used for the steel core

of BRFs. An "elasticBeamColumn" element was used for other members. The boundary

conditions and the loading protocol were the same as those in the ANSYS model. P-Δ

effects were also included for the column. A gravity load representing the self-weight of

the beam was also included.
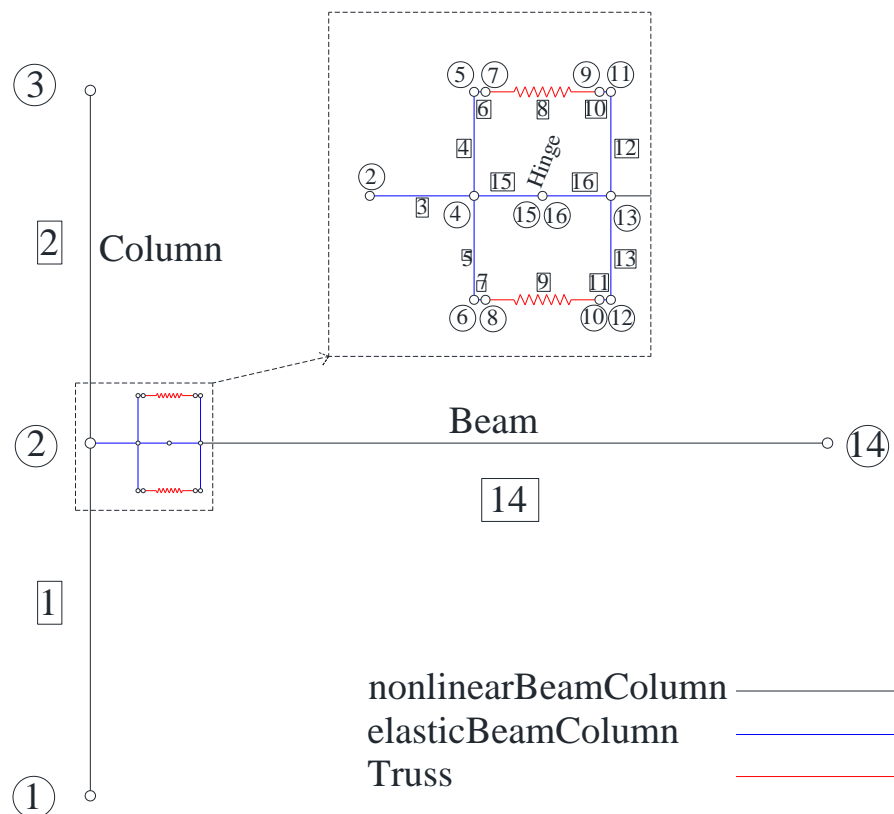
Figure 4.29 –OpenSees model of BRF-M

Figure 4.30 shows the OpenSees calculated force-deformation relationship for BRF-M. Approximately the same drift capacity as the ANSYS model was observed. However, the joint strength was 29% lower in OpenSees model compared with the ANSYS model. Since the most important seismic design parameter is the displacement capacity of a structure, the proposed simple OpenSees modeling method may be adopted but noting that the lateral strength of the structure is underestimated using the simplified model (Fig. 4.28). It should be obvious that an ANSYS model of a multi-story conventional or repairable building requires extremely large computational capabilities and will be time consuming. For BRF-M, the ANSYS model had 21644 elements while the OpenSees model was built with only 16 elements.
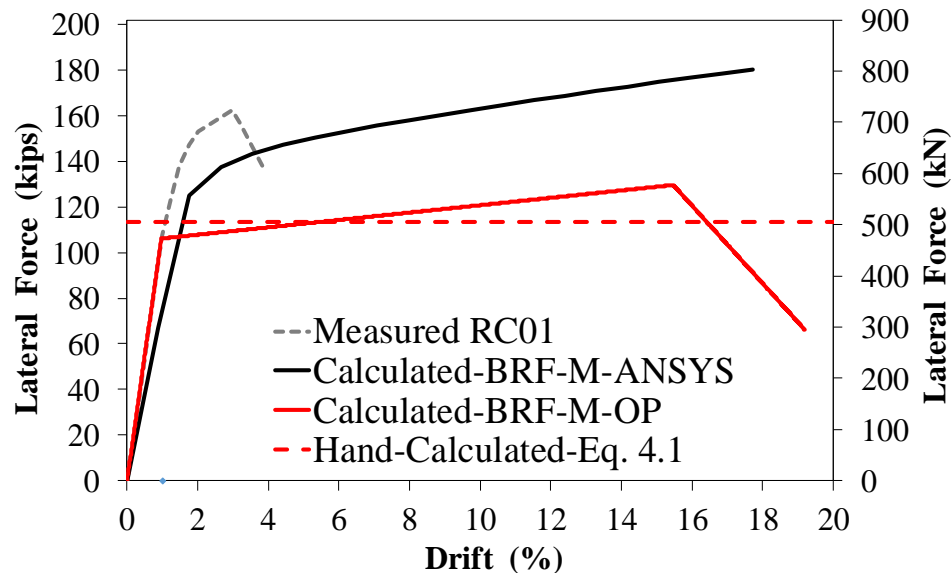
Figure 4.30 – BRF-M force-displacement relationships using OpenSees and ANSYS

The OpenSees model discussed above for BRF-M is used in the next sections to explore the performance of repairable joints using BRR. The only differences between the

two models are (1) the core area of the yielding device, and (2) the depth of the yielding

device since BRFs are placed outside of the beams while BRR are placed inside the beams.

4.4.2 Repairable Joints with BRR

The BRR-M alternative had the same configuration as the BRF-M alternative as

discussed in the previous section. Similarly, new models were developed for BRR-B and

BRR-C and then pushover analyses were carried out. The only difference was the location

of the shear pin. Figure 4.31 shows the calculated force-displacement relationships for all

BRR models. The model is sensitive to the location of the shear pin. When the pin was

close to the column face, the highest displacement capacity and the lowest strength were

observed. The lowest displacement capacity and the highest strength was for the case

where the shear pin was at the beam end. The joint with shear pin at the middle of BRR

showed a response between the other two cases. All three alternatives showed significantly

higher displacement capacity compared to the conventional moment-resisting joint. For

seismic applications, the BRR-M detailing is recommended due to the cyclic nature of

earthquakes. Note that the strength of BRR models can be easily increased by using high-

strength bars or more reinforcement.
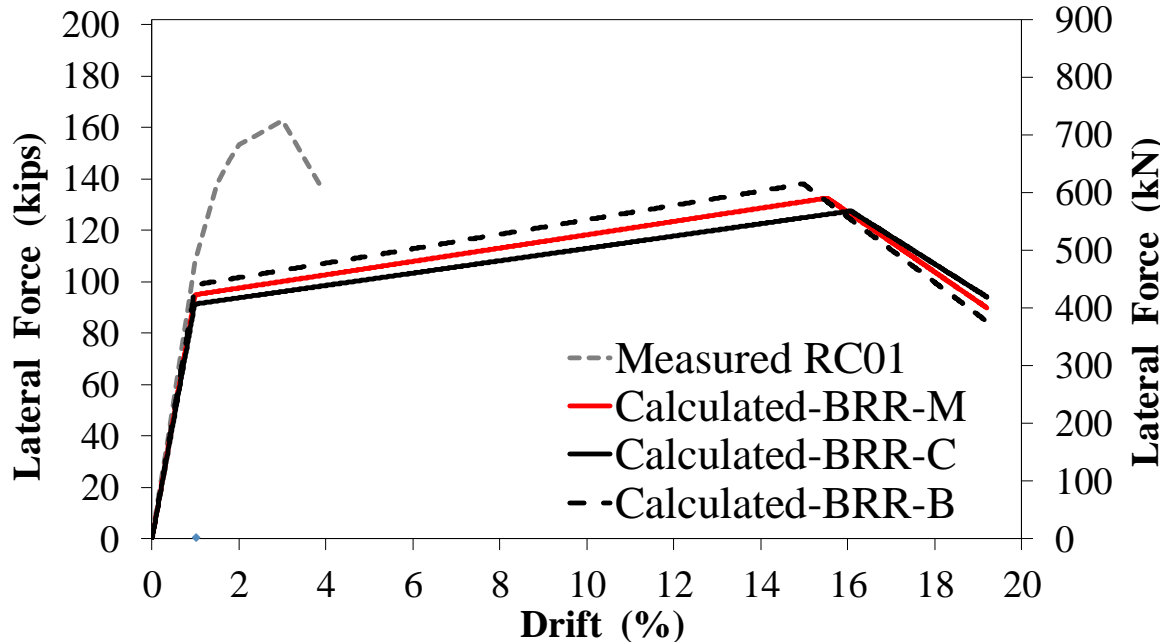
Figure 4.31 – Force-displacement relationships of Repairable Joints using BRR

4.5 Proposed Simple Design Method for Repairable Joints

A simple design method was developed to size the yielding device (core of BRF or

BRR). For a reparable joint, the maximum tensile and compressive forces will be

developed at the center of the top and bottom BRF/BRR. Since the yielding devices are

restrained against buckling and the beam is symmetric over its x-axis, the tensile and

compressive forces can be assumed to equal. Therefore, the following equation can be

developed:

$$M_p = T \times d_{core} \qquad \qquad \text{(Eq. 4.1)}$$

$$T = C = A_{core} \times f_{u-core} \qquad \qquad \text{(Eq. 4.2)}$$

where d_{core} is the moment arm from the center-to-center of BRF/BRR, A_{core} is to the area of

the BRF/BRR core, and f_{u-core} is the ultimate tensile strength of the BRF/BRR core.

When a building is designed using conventional steel profiles, the plastic moment of

each beam is known. Equations 1 and 2 may be used to size the BRF/BRR core steel and

to select the core material types. When these parameters are known for the core, the design of other components of BRF follows what has been developed in the literature for buckling restrained braces (BRBs). The method developed by Boudaqa et al. (2017) can be used to design the BRR other components.

This method was used to size BRF and BRR presented in this chapter. Figure 4.29 shows the strength of the repairable BRF-M joint calculated using the two FE software and the proposed design method. It can be seen that the proposed design method is simple and conservative and may be used for initial design of repairable moment-resisting frames.

4.6 Summary of Analytical Results for Beam-Column Joints

Table 4.4 shows a summary of all analyses on the beam-column joints. The measured value refers to the maximum bending moment of the RC01 specimen tested by Kim et al. (2000). The calculated strength of RC01 using either ANSYS or OpenSees was within 10% of the measured strength. The general trend for repairable joints was that the ANSYS models showed a higher strength compared with OpenSees models. Both software showed approximately the same stiffness and displacement capacity. The simple design method was found to be viable and conservative.

In summary, the proposed detailing can improve the seismic performance of steel moment-resisting frames with an additional benefit of repairability. The damage is limited to BRF or BRR, which can be replaced after an earthquake. This will eliminate the structure total replacement.

Table 4.4 – Maximum force and bending moment comparison

Method	Notes	Force, kips	Moment, kip-ft	Ratio to Measured
Measured	W30x99 beam, W14x176 column, $f_y = 53.5$, $f_u = 71.6$	162.6	1813.8	1
Code Calculated	$M_p = f_y . Zx$ W30x99 beam	138.0	1539.4	0.85
ANSYS RC01	W30x99 beam, W14x176 column, $f_y = 53.5$, $f_u = 71.6$	178.64	1992.7	1.10
OpenSees RC01	Steel02, W Section, $f_y = 53.5$, $f_u = 71.6$, NonlinearBeamColumn	176.2	1965.5	1.08
ANSYS BRF-M	Grade 50 ($f_y = 53.5$, $f_u = 71.6$) col, beam, corbel, stiffeners, with Grade 80 ($f_y = 86$, $f_u = 105$) BRB corbel end plate Core = 7.5 sq.in.	174.7	1948.8	1.07
OpenSees BRF-M	HP18x204 and Steel02 for beam & column, hysteretic for truss, elastic elements for others, equalDOF at middle node, Core Area=7.5 sq.in. ($f_y = 86$, $f_u = 105$)	131.8	1470.2	0.82
ANSYS BRF-B	Grade 50 ($f_y = 53.5$, $f_u = 71.6$) col, beam, corbel, stiffeners, with Grade 80 ($f_y = 86$, $f_u = 105$) BRB corbel end plate Core = 7.5 sq.in.	176.5	1968.8	1.09
OpenSees BRR-M	HP18x204 and Steel02 for beam&column, hysteretic for truss, elastic elements for others, equalDOF at middle, #18 bars ($f_y = 68$, $f_u = 95$)	132.50	1551.8	0.81
OpenSees BRR-B	HP18x204 and Steel02 for beam&column, hysteretic for truss, elastic elements for others, equalDOF at beam, #18 bars ($f_y = 68$, $f_u = 95$)	138.00	1857.2	0.84
OpenSees BRR-C	HP18x204 and Steel02 for beam&column, hysteretic for truss, elastic elements for others, equalDOF at column face, #18 bars ($f_y = 68$, $f_u = 95$)	127.50	1368.6	0.78
Hand Calculated (Eq. 4.1)	BRF-M Our Method HP18x204 beam	113.4	1250.2	0.80

Note: 1 in. = 25.4 mm; 1 kip = 4.45 kN, 1 ksi = 6.90 MPa,

4.7 References

AISC. (2011). "Steel Construction manual." 14th Edition., American Institute of Steel

Construction, Chicago, IL.

ANSYS (2017). "Analysis Systems-Workbench," Release 18.2, Canonsburg, PA.

Boudaqa, A., Tazarv, M., and Tuhin, I. (2017). "Ductility without confinement a new design and construction approach for RC bridge columns." International Journal of Bridge Engineering, pp. 53–77.

Gheidi, A., Mirtaheri, M., Zandi, A.P., Alanjari, P., and Samani, H. (2009). "Experimental optimization studies on steel core lengths in buckling restrained braces." Journal of Constructional Steel Resarch, Vol. 67, No.8, pp. 1244–1253.

Kim, T., Whittaker, A., Gilani, V., Bertero, V., and Takhirov, S. (2000). "Experimental evaluation of plate-reinforced steel moment-resisting connections." Journal of Structural Engineering, Vol. 128, No. 4, pp. 483-491

OpenSees. (2013). "Open System for Earthquake Engineering Simulations," Version 2.4.1, Berkeley, CA. Available online: http://opensees.berkeley.edu.

Chapter 5: Summary and Conclusions

5.1 Summary

Steel buildings usually have a lower mass compared to reinforced concrete (RC)

buildings and can exhibit significant ductility under large earthquakes. However, steel

structures that undergo significant nonlinear deformations during a major event such as an

earthquake often experience yielding or failure of structural components and may require a

total replacement. A new design approach is to implement connections that localize the

yielding and failure to fuses. A more sophisticated approach is to be able to replace these

fuses after the event.

The main objective of this study was to develop repairable moment-resisting (MR)

joints for steel structures that localizes the yielding and damage to replaceable fuses within

the joint, while the other structural members remain linear elastic. Two details were

proposed using either buckling restrained fuses (BRFs) or buckling restrained

reinforcement (BRR). Nonlinear finite element analyses (FEA) were performed using two

software packages to investigate the seismic performance of the proposed joints.

5.2 Conclusions

The following key conclusion can be drawn based on the analytical work conducted:

- The proposed modeling procedures for the conventional steel MR beam-column

  connection and a buckling restrained brace (BRB) were found viable. The

verified modeling methods were then used to model the proposed joint connections.

- The FEA of the repairable joints incorporating BRFs showed an increase in displacement capacity by a factor 2 when compared with a conventional steel MR beam-column connection. The same lateral strength could also be observed. However, the initial stiffness of the BRF repairable joint was 34-44% lower than that for a conventional steel MR joint.

- The FEA of the repairable joints incorporating BRR showed an increase in displacement capacity by a factor of 2 compared with a conventional steel MR beam-column connection. The same lateral strength could also be observed. The initial stiffness of the BRR repairable joint was approximately equal to that for a conventional steel MR joint.

- The FEA showed that the yielding and failure of the joint is limited to the replaceable BRF or BRR for all proposed alternatives, while all other structural components remained in the elastic range. BRF and BRR can be easily replaced after an event, which will significantly reduce the repair time and cost.

Overall, both proposed repairable details were found viable with improved seismic performance compared to conventional MR details. Furthermore, these joins can be quickly repaired after an earthquake through the replacement of the damaged BRF or BRR.

Appendix A: Analytical Studies: System Performance

A.1 Introduction

The present appendix will report the design methodology and analysis of a three-story steel special moment-resisting frame (SMRF). The frame is representative of an office building, located in downtown Los Angeles, California. Upon completion of the design of the conventional frame, pushover analysis was conducted and the response of the structure in terms of base shear versus displacement was recorded. The buckling-restrained fuse (BRF) and buckling-restrained reinforcing (BRR) joints discussed in Chapter 3 were then incorporated to investigate the system performance of the structure. The results were then compared to those from the conventional SMRF.

A.2 Special Moment-Resisting Steel Buildings

ASCE 7-16 (2016) was used to determine the design loads, load combinations, and seismic design criteria for the three-story office building. The risk category of this building was category II, and the seismic importance factor was 1.0, which is based on the building risk category. The soil class considered was site class D, which is indicative of a stiff soil.

A.2.1 Building Geometry

The three-story frame considered for design had four spans in both the longitudinal and transverse directions. For design purposes, only an interior frame was considered, as

shown in Fig. A.1. The story height was 15 ft (4.6 m), and the span length in each

direction was 20 ft (6.1 m). As mentioned, this frame was analyzed in downtown Los

Angeles, CA, with a longitude of 34.0407° and latitude of 118.2468°.
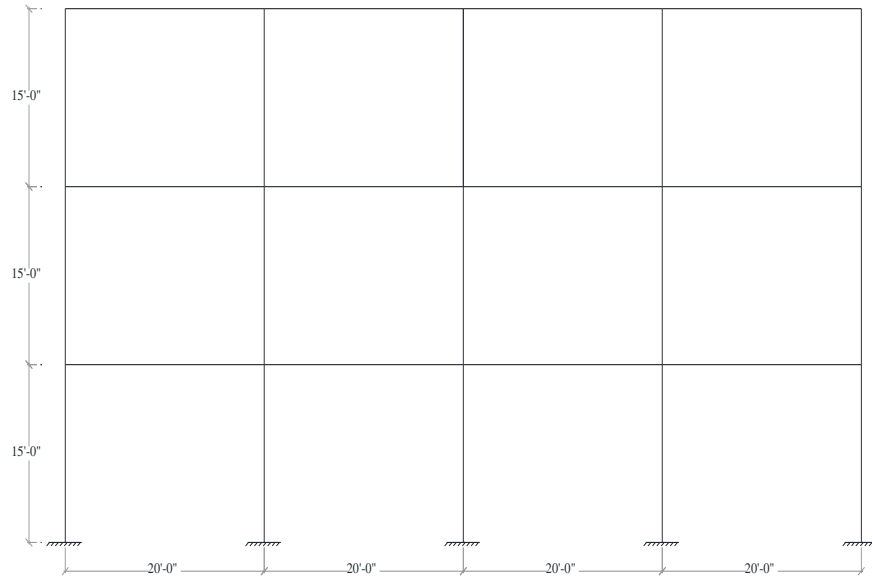
Figure A.1 – Three-story frame located in downtown Los Angeles

A.2.2 Load Combinations

The load combinations taken for strength design were taken directly from ASCE 7-16

(2016) and are as follows:

1. 1.4D

2. $1.2D + 1.6L + 0.5L_r$

3. $1.2D + 1.6L_r + 1.0L$

4. $1.2D + 1.0L + 1.0E$

5. $1.2D + 1.0L - 1.0E$

6. $0.9D + 1.0E$

7. $0.9D - 1.0E$

where D is the dead load, L is the live load, L_r is the roof live load, and E is the earthquake load. The seismic load is applied in both directions as shown in equations 4,5 6 and 7 to account for the uncertainty in direction of the earthquake.

A.2.2.1 Gravity Loads

As mentioned previously, only an interior frame was investigated, and therefore all gravity loads were applied as tributary gravity loads on the beams. The span length in each direction was 20 ft (6.1 m), giving a tributary area of 400 ft^2 (37.2 m^2). Floor dead loads of a typical office building were considered, which consisted of the self-weight of the slab, the floor finish, and the wall loads. The roof dead loads consisted of the self-weight of the slab, the ceiling, and the roof coverings.

For the floor dead load, the slab thickness was assumed to be 5 in (2.0 cm)., producing a slab dead load of 1250 plf (18.2 kn/m). The dead load due to the flooring and wall loads combined was found to be 380 plf (5.6 kn/m). Therefore, the total superimposed dead load on the floor due to all components was determined to me 1470 plf (21.5 kn/m).

For the roof dead load, the slab thickness was the same as the floor, giving a dead load of 1250 plf (18.3 kn/m). Other components that contributed to the roof dead load were the ceiling, covering, sheathing, and deck. Summing all of the aforementioned components produces a dead load of 180 plf (2.6 kn/m), and a total superimposed roof dead load of 1430 plf (20.9 kn/m).

The floor live load for an office building has a code requirement of 50 psf (2.4 kn/m^2), which was not reduced. An additional 15 psf (0.72 kn/m^2) was applied to account for a partition wall, and the total live load per floor beam was 1300 plf (19.0 kn/m).

The roof live load is given by the code as 20 psf (0.96 kn/m^2). This value was not

reduced, and the total roof live load considered for design was 400 plf (5.8 kn/m).

A.2.2.2 Lateral Loads

For the lateral loads, only seismic was considered as part of the design for this frame.

The response spectrum shown in Fig. A.2 was generated using ASCE 7-16 (2016). The

response modification factor (R) for a SMRF is given in the code as 8.
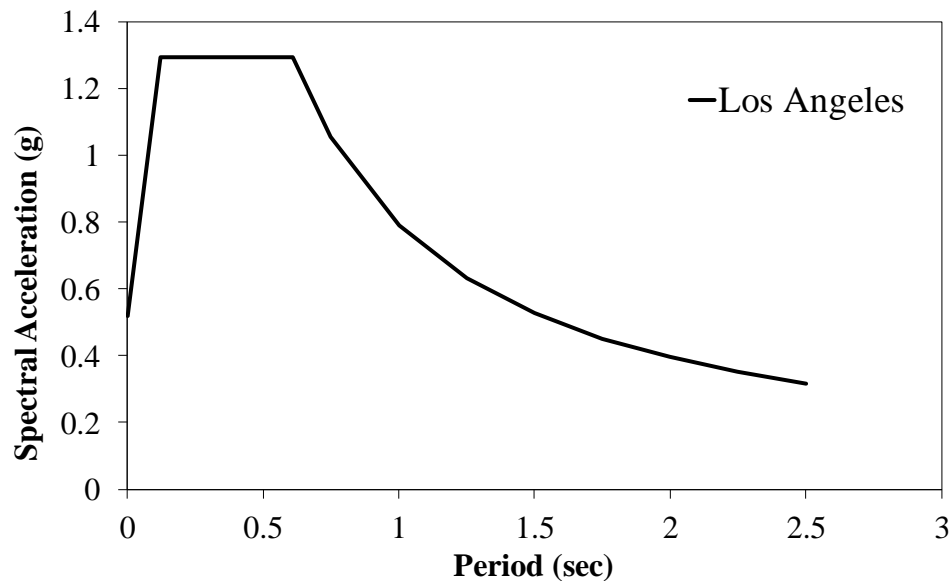
Figure A.2 – Design response spectrum for three-story frame

A.2.3 Software Design

The computer program SAP2000 (2016) was used to design the three-story frame. The

design considered all of the aforementioned building parameters and load combinations in

determining the member sizes. Based on all of the input the most efficient structure

consisted of W14x176 columns and W10x112 columns, as shown in Fig. A.3. The

maximum plastic moment capacity of the W14x176 columns exceeded that of the

W10x112 by over 20% which follows code requirements for special moment frames.
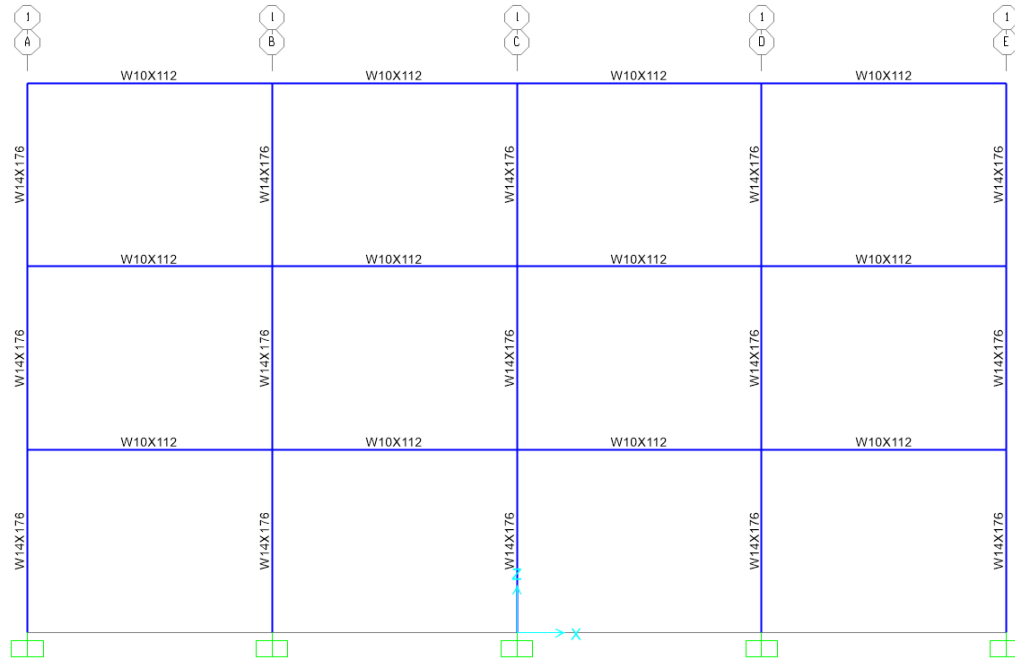
Figure A.3 – Three-story frame design using SAP2000

A.2.4 Output

Based on the designed structure, base shear demands were calculated both by hand and automatically by SAP2000 (2016). Based on the analysis, the maximum base shear obtained from hand-calculations was 69.3 kips (308.3 kN) and the base shear obtained from SAP2000 (2016) was 66.3 kips (294.9 kN). Reasonable correlation between the two methodologies validates the use of the computer program and hand calculations for the calculation of ultimate base shear. Shown in Fig. A.4 is the stress demand to capacity ratio for the three-story frame. It can be observed that all members are adequate in resisting the applied loading and that this frame is sufficient in seismic application.
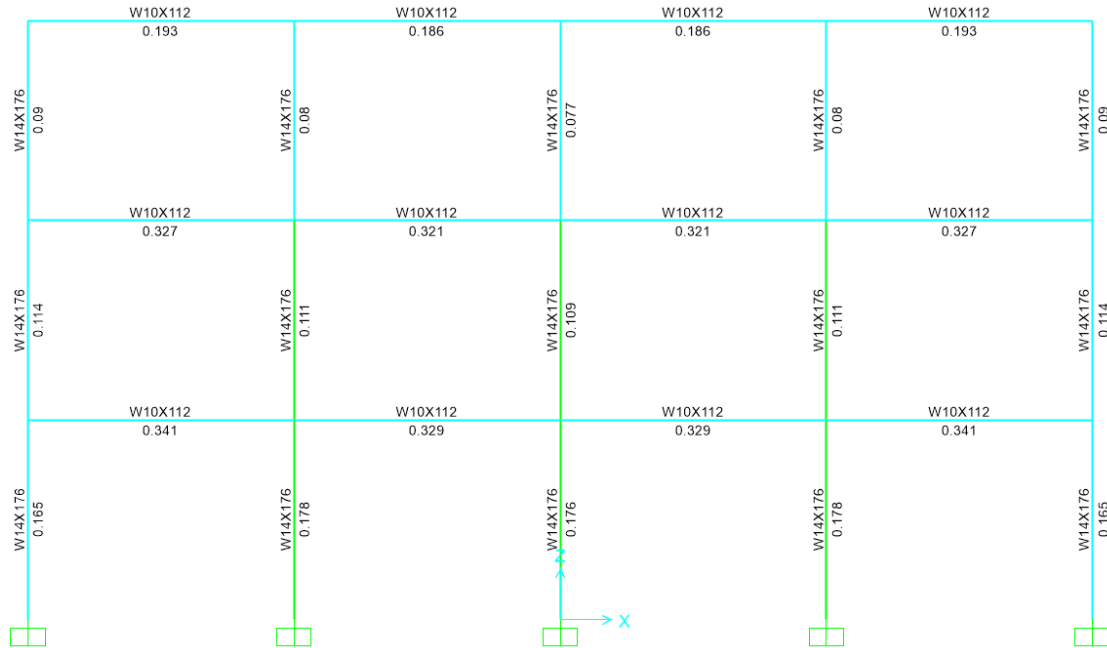
Figure A.4 – Ratio of stress capacity and demand for the three-story SMRF

A.3 Modeling Methods for Conventional Frame

An OpenSees (2013) model was created for both the conventional three-story frame discussed in section A.2, and the same frame with the repairable detailing discussed in Chapter 4. This was done to evaluate the system performance of a structure with the proposed detailing and validate its practicality for usage in seismic applications. Before analyzing the structure using the repairable joint detailing, a model of the conventional three-story frame was created using ANSYS (2017). The results from a pushover analysis from OpenSees (2013) and ANSYS (2017) will now be presented.

A.4.1 Material Models

When analyzed OpenSees (2013), the columns and beams used in the system were of Steel02 material. It should be noted that a reduced strain of 4% was used instead of the specified 9%, as it was found experimentally that the reference beam-column failed at that

value. When the strain was modified in ANSYS (2017) to 4% and the corresponding stress

at that value was used, there was a good match in force-deformation relationship, as

opposed to the overestimation originally observed.

A.3.1 Validation of Models

The results from the pushover analysis using both OpenSees (2013) and ANSYS (2017)

are plotted in Fig. A.5. As demonstrated by the chart, there is good correlation between the

results obtained from each software, which validates the modeling procedure for both

programs for the three-story frame.
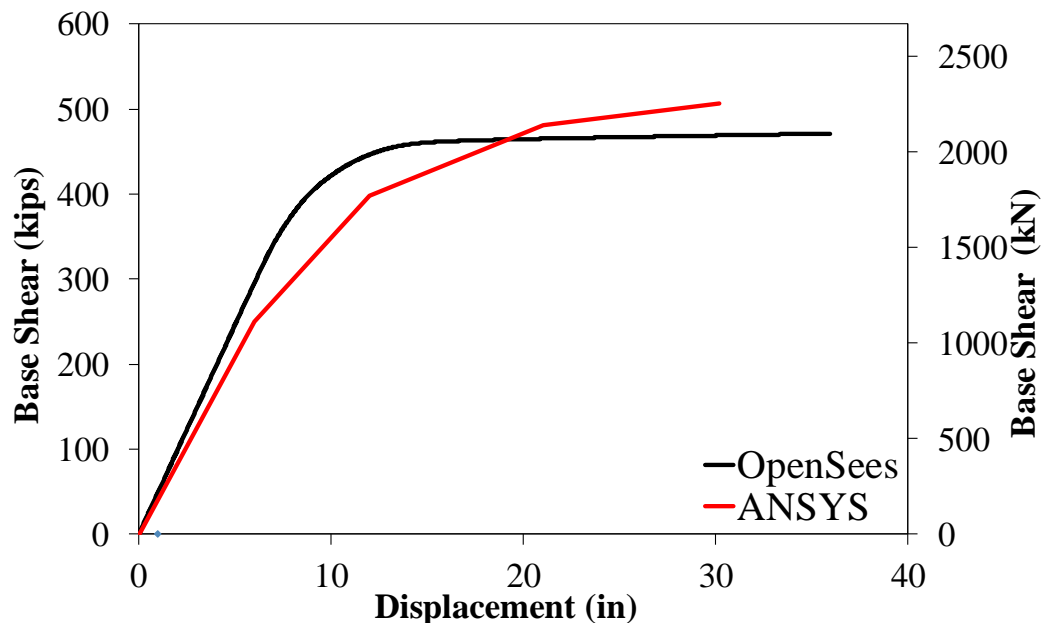
Figure A.5 – Pushover comparison between OpenSees and ANSYS

A.4 Modeling Methods for Repairable Frames

Upon validation of the conventional frame, the proposed joint detailing discussed in

Chapter 3 were incorporated into the system to investigate the performance. The material

models and detailing will be presented in this section, along with the results obtained from

the pushover analysis for each system.

A.4.1 Material Models

The material models used in the frame systems were the same as those presented for the beam-column joint discussed in Chapter 4. Steel02 was again used for the beams and columns in the system. Hysteretic material was used for both the BRF/BRR truss elements.

A.4.2 Detailing of Repairable Joints

Figure A.6 shows a schematic of the frame with the general proposed detailing incorporated, and the parametric detailing for the BRF and BRR joints can be seen in Fig. A.7. Both systems have the same general parameters, but different values associated with them which will be discussed later.
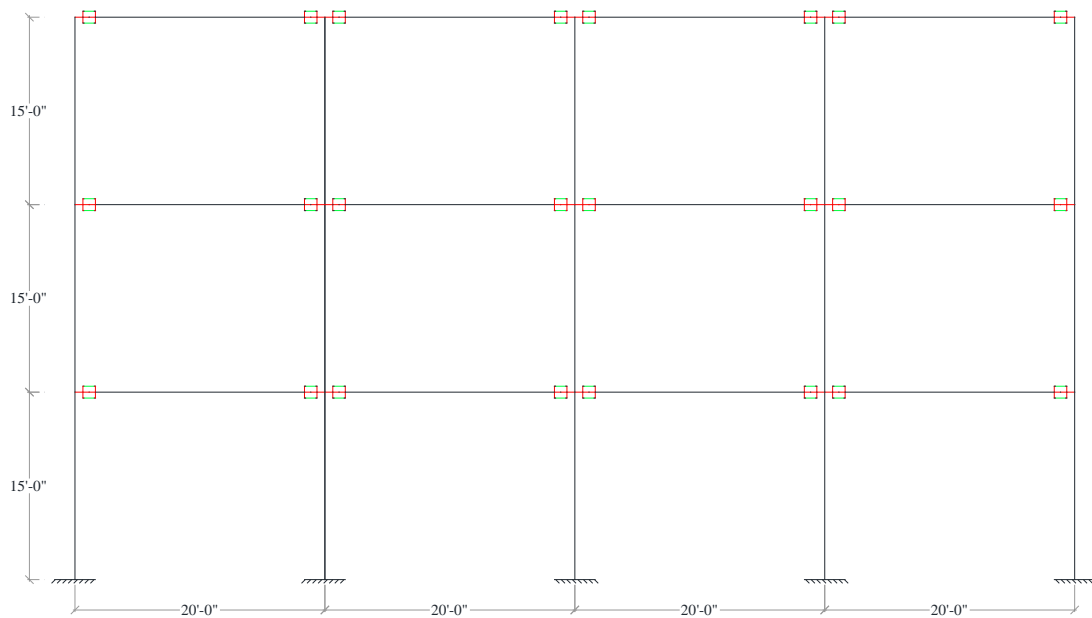
Figure A.6 – Three-story frame with proposed repairable detailing
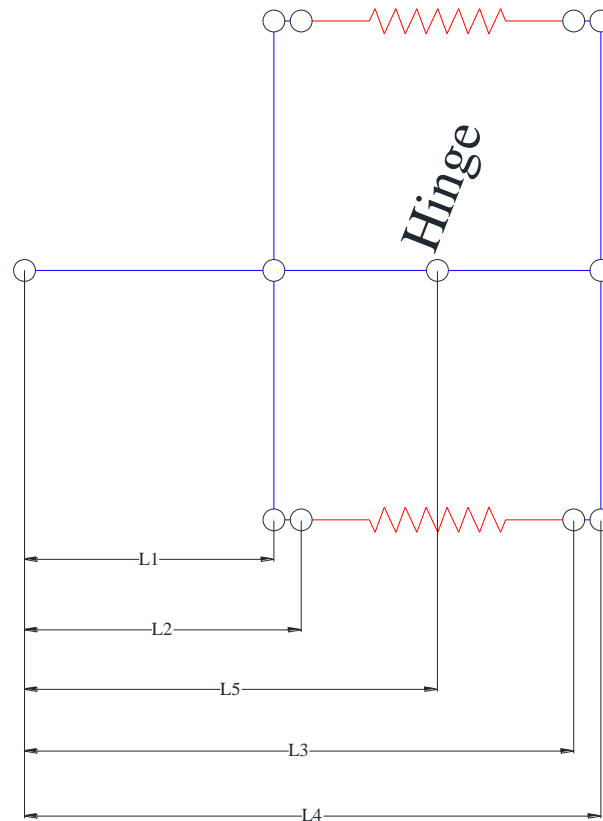
Figure A.7 – Repairable joint detailing

L1 represents the length from the analytical center of the column line to the outside face of the column flange, L2 represents the length associated with the anchorage length of the BRF/BRR plus, L3 represents the length of the fuse, L4 represents the anchorage length of the BRF/BRR, and L5 represents the location of the hinge which in this case is located at the middle. Table A.1 shows the values used in the analysis for the BRF and BRR three-story frame alternatives. It should be noted that the location of the BRF/BRR components in the vertical direction (annotated as H) occur at different elevations. For the BRF, this location corresponds to half of the beam depth plus the half the thickness of the BRF for both the top and bottom components. Regarding the BRR, this location corresponds to the location on the angles bolted to the beam which the BRR passes through. For the BRF and

BRR alternatives, these locations have a value of 6.325 in (16.1 cm) and 3.25 in (8.3 cm)

respectively.

Table A.1 – Specified Material Properties for Repairable Joints Using BRFs

Frame	L1, in (cm)	L2, in (cm)	L3, in (cm)	L4, in (cm)	L5, in (cm)
BRF	7.725	13.725	23.725	29.725	18.725
	(19.623)	(34.862)	(60.262)	(75.502)	(47.5628)
BRR	7.725	8.725	18.725	19.725	13.725
	(19.623)	(22.162)	(47.562)	(50.102)	(34.862)

A.5 Results and Discussion

The results obtained from the pushover analysis for the conventional frame are shown

plotted against the repairable alternatives. As shown, both repairable alternatives showed a

significant increase in displacement capacity, by approximately a factor of 3.5. In terms of

initial stiffness, the BRF closely matched the initial stiffness of the conventional frame,

while the initial stiffness was slightly lower than that obtained from the conventional

frame. In terms of base shear, the BRF outperformed the conventional base shear by a

factor of approximately 1.2. The BRR alternative base shear was approximately 43% of

the base shear obtained from the conventional base shear. It should be noted that the

strength of the repairable frame can be adjusted by altering the core properties. The core

strength was lower in terms of bending moment by 20-25% percent than the w-section.
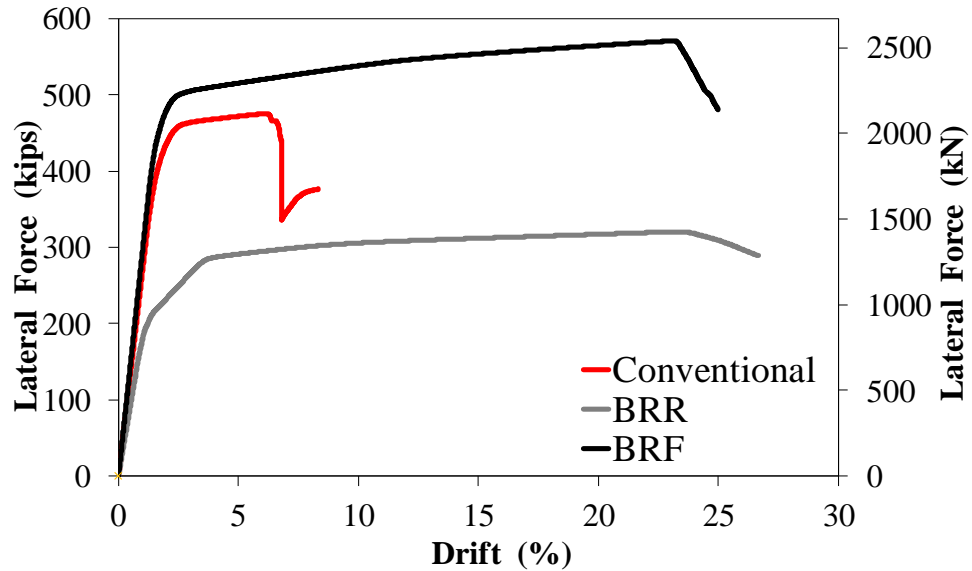
Figure A.8 – Pushover analysis for the three-story frame

A.6 References

AISC. (2011). "Steel Construction manual." 14th Edition., American Institude of Steel
Construction, Chicago, IL.

ANSYS (2017). "Analysis Systems-Workbench," Release 18.2, Canonsburg, PA.

ASCE 7-16 (2016). "Minimum Design Loads for Buildings and Other Structures".
American Society of Civil Engineers.

OpenSees. (2013). "Open System for Earthquake Engineering Simulations," Version 2.4.1,
Berkeley, CA. Available online: http://opensees.berkeley.edu.

SAP2000. Version 18.2.0 Computers and Structures, Inc. Berkeley, CA (2016)

Appendix B: Design and Construction Guidelines

B.1 Introduction

The present appendix will present the design requirements when incorporating

buckling-restrained fuse (BRF) and buckling-restrained reinforcement (BRR) as part of a

moment-resisting (MR) connection. Design methodologies for BRF and BRR joints will

also be discussed. It should be noted that both BRF/BRR core area are determined based

on equations 4.1 and 4.2, so the discussion of the design will focus on the connecting

elements for each alternative.

B.2 Requirements

Regarding both the BRF and BRR joint detailing, the code requires that the maximum

moment of the joint be 20% weaker than that of the maximum plastic moment of the beam.

This requirement is there to ensure linear elastic behavior of the beam and focus all

nonlinearity within the joint connection

B.3 Buckling-Restrained Fuse Design

After determining the fuse geometric properties, the number of slip-critical bolts

required based on the maximum force shall be obtained by the code (AISC Steel

Construction Manual, 2011). When determining the number of slip-critical bolts, the

maximum force is multiplied by a factor of 1.2 so that the strength is 20% stronger than the

ultimate load of the fuse. Code required minimum spacing and edge distances are followed

when determining the spacing of the bolts for the BRF. It should be noted that the area of

any point on the gusset plate portion of the BRF shall never be less than the core area to

ensure that all nonlinear behavior occurs within the fuse of the BRF.

B.4 Buckling-Restrained Reinforcement Design

Regarding the design of the BRR itself, the procedure outlined from Boudaqa (2017)

should be followed. The anchoring angles shall be designed such that they remain linear

elastic as the BRR are deformed. A stiffener shall be incorporated in the angles to reduce

any yielding that may occur due to the BRR tensioned or compressed. The angles are

welded to the beam flange, so general welding requirements such as strength of weld, size

of weld, and length of weld shall be determined by code requirements set by the AISC

Steel Construction Manual (2011).

B.5 References

AISC. (2011). "Steel Construction manual." 14th Edition., American Institude of Steel
    Construction, Chicago, IL.

Boudaqa, A., Tazarv, M., and Tuhin, I. (2017). "Ductility without confinement a new
    design and construction approach for RC bridge columns." International Journal of
    Bridge Engineering, pp. 53–77.